

Aus dem Institut für Transfusionsmedizin und Immunologie
der Medizinischen Fakultät Mannheim
(Direktor: Prof. Dr. med. Harald Klüter)

The immunomodulatory and pro-regenerative capacity of mesenchymal
stromal cells and their therapeutic use for kidney disease

Inauguraldissertation
zur Erlangung des
Doctor scientiarum humanarum (Dr. sc. hum.)
der
Medizinischen Fakultät Mannheim
der Ruprecht-Karls-Universität
zu
Heidelberg

vorgelegt von
Erika

aus
Pati, Indonesien
2023

Dekan: Herr Prof. Dr. med. Sergij Goerd
Referentin: Frau Prof. Dr. rer. nat. Karen Bieback

*For my father,
whose memories shall forever live in me*

Sections/data reported within this dissertation are part of soon to be or already submitted manuscripts.

Introduction chapter comprises material from the published review article: "*Recent advances in understanding mesenchymal stromal cells. F1000Res. 2020 Feb 27;9:F1000 Faculty Rev-156.*"

The first part of this thesis contains material from the published article: "*Harmonised culture procedures minimise but do not eliminate mesenchymal stromal cell donor and tissue variability in a decentralised multicentre manufacturing approach. Stem Cell Res Ther 14, 120 (2023).*"

The second part of this thesis is part of the submitted article: "*Clinical-grade human skin-derived ABCB5+ mesenchymal stromal cells exert modulatory functions on mRNA expression in a cisplatin-induced kidney injury murine model. Submitted to Frontiers in Immunology.*"

The third part of this thesis is part of the submitted article: "*Mesenchymal stromal cells-derived secretome attenuates cisplatin induced inflammation in vitro modifying the interplay between proximal tubular epithelial cells and macrophages.*" Submitted to *Stem Cell Research and Therapy.*

TABLE OF CONTENT

	Page
ABBREVIATIONS	1
1 INTRODUCTION	5
1.1 MSCs and their therapeutic capacity	5
1.2 Tissue Origin and Culture Protocol Affect MSC Phenotypes	20
1.2.1 ABCB5+ MSCs	21
1.3 MSC immunomodulation and its compatibility across species	7
1.3.1 Macrophages are important to player in delivering MSC therapeutic effects	9
1.4 MSC as therapeutic option for Acute Kidney Injury (AKI)	9
1.4.1 Cisplatin is a chemotherapeutic drug with nephrotoxicity side effect	10
1.4.2 Cisplatin promotes proximal tubular epithelial cell death	11
1.4.3 Cisplatin-induced inflammation exaggerates renal damage	14
1.4.4 Macrophages' roles are important in AKI progression	14
2 AIM OF THE STUDY	17
3 MATERIALS AND METHODS	20
3.1 Materials	20
3.1.1 Cells	22
3.1.2 Cell culture products	23
3.1.3 Cell culture medium	26
3.1.4 Magnetic Cell Separation (MACS)	27
3.1.5 Flow Cytometry	27
3.1.6 PCR	29
3.1.7 Immunofluorescence Staining	30
3.1.8 Kits	30
3.1.9 Other Solutions	31
3.1.10 Consumable Laboratory Material	31
3.1.11 Laboratory Equipment	33

3.1.12	Software for Data Analysis	35
3.2	Methods.....	36
3.2.1	Part 1: Assessment of inter-laboratories and tissue of origin in MSC profile	36
3.2.2	Part 2: The immunomodulatory capacity of MSCs in xenogeneic setting	41
3.2.3	Part 3	50
3.2.4	ELISA	62
3.2.5	Statistical Analysis	63
4	RESULTS.....	64
Part 1:	Inter-laboratory and tissue source comparison of MSC culture	64
4.1.1	Harmonization of MSC seeding density	64
4.1.2	Despite inevitable inter-laboratory discrepancies, culture harmonisation preserved tissue-specific signature on growth kinetics	65
4.1.3	Adipogenic and osteogenic differentiation of MSCs were highly influenced by inter-laboratory, tissue source, and donor variation.....	69
4.1.4	Immunophenotypes of MSCs for negative markers differed across the centres	70
4.1.5	A-MSCs exerted the highest inhibitory activity on PBMC proliferation	71
4.2	Part 2: Inter-species Immuno-Compatibility Study.....	74
4.2.1	h- and r-MSCs suppressed TNF- α production of LPS-stimulated macrophage despite xenogeneic setting	76
4.2.2	A-MSC promoted human and rat macrophages but the mediators differed	77
4.3	Part 3: MSCs role in ciPTECs and macrophages crosstalk in <i>in vitro</i> cisplatin injury	80
4.3.1	Development of <i>in-vitro</i> cisplatin-induced AKI	80
4.3.2	Direct effect of MSC CM on cisplatin-treated ciPTECs	81
4.3.3	Immunomodulation of CM on cisplatin-treated macrophage.....	91
4.3.4	Modification of ciPTEC-macrophage interaction by CM.....	93
5	DISCUSSION	104
5.1	Part 1: Inter-laboratory and tissue source comparison of MSC culture.....	104
5.2	Part 2: Inter-species Immuno-Compatibility Study.....	107
5.3	Part 3: Part 3: MSCs role in ciPTECs and macrophages crosstalk in <i>in vitro</i> cisplatin injury.....	108

5.3.1	How CM affect cisplatin-induced toxicity on ciPTECs?	109
5.3.2	What is the mediator of CM anti-apoptotic effect on ciPTECs?	109
5.3.3	How do CM and cisplatin affect macrophage phenotype and function? 111	
5.3.4	How does CM and cisplatin modulate ciPTEC and macrophage crosstalk?	113
6	SUMMARY	117
7	REFERENCES	119
8	CURRICULUM VITAE	131
9	SCIENTIFIC OUTPUTS.....	133
9.1	Publication	133
9.2	Posters or Oral Presentations	133
10	ACKNOWLEDGEMENTS.....	135

ABBREVIATIONS

A	
A	Adipose
ABCB5	ATP-binding cassette member B5
AKI	Acute kidney disease
ATF-3	Activating transcription factor-3
ATMP	Advanced therapeutic medicinal product
ATP	Adenosine triphosphate
B	
Bcl	B-cell lymphoma
BM	Bone marrow
BSA	Bovine serum albumin
BUN	Blood urea nitrogen
C	
CCM	Complete culture media
CCR	CC chemokine receptors
CD	Cluster of differentiation
CDKN1a	Cyclin dependent kinase inhibitor 1a
ciPTEC	Conditionally immortalized proximal tubular epithelial cell
ciPTECs	Conditionally immortalized proximal tubular epithelial cells
Cis	Cisplatin
CKD	Chronic kidney disease
CM	Conditioned Media
CM-FT	Cm flow-through
CPD	Cumulative population doublings
Ctrl	Human copper transporter 1
CTRL	Control
CX-43	Connexin-43
D	
DAMPs	Danger-associated molecular patterns
DAPI	4',6-diamidino-2-phenylindole
DMEM	Dulbecco's Modified Eagle Medium
DMEM HAM's F12	Dulbecco's modified eagle's medium/nutrient mixture f-12 ham
DMSO	Dimethyl sulfoxide
DPBS	Dulbecco's phosphate-buffered saline
E	
ECM	Extracellular matrix
EDTA	Ethylenediaminetetraacetic acid
EGF	Epidermal growth factor
ER	Endoplasmic reticulum
ESRD	End-stage renal disease
EU	European Union
EVs	Extracellular vesicles
F	

FACSs	Fluorescence activated cell sorting
FasL	Fas ligand
FBS	Fetal bovine serum
FGF-2	Fibroblast growth factor-2
G	
GADD45a	Growth arrest and dna damage inducible alpha
GAPDH	Glyceraldehyde 3-phosphate dehydrogenase
G-CSF	Granulocyte-CSF
GM-CSF	Granulocyte-macrophage colony-stimulating factor
GMP	Good manufacturing practice
GRP78	Glucose binding protein 78
GSH	Glutathione reductase
GST	Glutathione-S-transferase
GvHD	Graft-versus-host disease
H	
H2DCFDA	2',7'-dichlorodihydrofluorescein diacetate
HBSS	Hanks' balanced salt solution
HGF	Hepatocyte growth factor
HLA	Human leukocyte antigen
h-Mac	Human macrophages
HMOX-1	Heme-oxygenase-1
hMSCs	Human mesenchymal stromal cells
hPBMCs	Human peripheral blood mononuclear cells
HSP60	Heat shock protein 60
h-TNF- α	Human tumor necrosis factor- α
I	
I3	Triiodothyronine
IDO	Indoleamine 2,3-dioxagenase
IFN- β	Interferron-B
IGF	Insulin-like growth factor
IL	Interleukin
IL-1RA	IL-1 receptor antagonist
ip	Intraperitoneal
IP-10	IFN- γ Inducible Protein-10
IRI	Ischemic-reperfusion injury
ISCT	International Society for Cell and Gene Therapy
IST	Insulin-transferrin-sodium selenite
ITN	Innovative Training Network
iv	intravenous
J	
K	
Kyn	Kynurenine
L	
L-DOPA	Levodopa
M	
MACS	Microbeads and magnetic activated cell sorting

MAPK	Mitogen-activated protein kinase
MATE	Multidrug and toxin extrusion
MCP-1	Monocyte chemoattractant protein 1
M-CSF	Macrophage colony-stimulating factor
MEM- α	Minimum essential medium alpha
MFI	Mean fluorescence intensity
MHC	Major histocompatibility complex
miRNA	Micro-RNA
MLKL	Mixed lineage kinase domain-like protein
MMP	Matrix metalloproteinase
MoA	Mechanism of action
mRNA	Messenger RNA
MSC	Mesenchymal stromal cell
MSCA	Mesenchymal stem cell antigen
MSCs	Mesenchymal stromal cells
N	
NO	Nitric oxide
NOS	Nitric oxide synthase
NTA	Nanoparticle tracking analysis
NUIG	National University of Ireland, Galway
O	
OCT2	Organic cation transporter2
OD	Optical density
P	
PBMC	Peripheral blood mononuclear cell
PBMCs	Peripheral blood mononuclear cells
PBS	Phosphate buffer saline
PCR	Polymerase chain reaction
PD	Population doublings
PD-1	Programmed cell death 1
PDGF-BB	Platelet-derived growth factor-bb
PD-L1	Programmed death-ligand 1
PDT	Population doubling time
PFA	Paraformaldehyde
PGE-2	Prostaglandin-2
PHA	Phytohemagglutinin-L
PRDX	Peroxiredoxin
PTEC	Proximal tubular epithelial cell
PTECs	Proximal tubular epithelial cells
Q	
R	
RIP	Receptor-interacting protein
r-Mac	Rat macrophages
r-MSC	Rat mesenchymal stromal cell
rMSCs	Rat mesenchymal stromal cells
ROI	Region of Interest

ROS	Reactive oxygen species
r-PBMCs	Rat peripheral blood mononuclear cells
RPMI	Roswell Park Memorial Institute Medium
r-TNF- α	Rat tumor necrosis factor- α
S	
SD	Standard deviation
SFM	Serum-free medium
SN	Supernatant
SOD	Superoxide dismutase
SSEA	Stage-specific embryonic antigen
SVF	Stromal vascular fraction
T	
TGF- β 1	Transforming growth factor beta 1
TIMP-1	Tissue inhibitor of metalloproteinase-1
TLR	Toll-like receptors
TNAP	Tissue non-specific alkaline phosphatase
TNF- α	Tumour necrosis factor- α
U	
UC	Umbilical cord
UHEI	University of Heidelberg
UOL	University of Liverpool
UT	Untreated
V	
VCAM-1	Vascular cell adhesion molecule 1
VEGF	Vascular endothelial growth factor
W	
WJ	Wharton's jelly
X	
Y	
Z	

1 INTRODUCTION

1.1 MSCs and their therapeutic capacity

Mesenchymal stromal cells (MSCs) have been studied extensively over the past decade as a potential advanced therapeutic medicinal product (ATMP) for a wide range of degenerative diseases¹⁻⁴. Currently, there are 529 clinical studies investigating MSC therapy registered in ClinicalTrials.gov as of March 2023; 33 out of those are phase III/IV trials, mostly conducted on patients with Graft-vs-Host Disease (GvHD) while the rest are still early phase I/II trials (<https://clinicaltrials.gov/ct2/home>). The growing interest of MSCs is driven by their therapeutic capacity, which consists of angiogenic, anti-apoptotic, immunomodulatory, and anti-oxidative features⁵. According to The International Society for Cell and Gene Therapy, MSCs must fulfil the following criteria⁶: (1) adherence to plastic culture vessel; (2) positivity for CD105, CD73, and CD90, while being negative for CD45, CD34, CD14, CD11b, CD79a, CD19, and HLA class I; (3) capability to differentiate into osteoblast, adipocytes, and chondroblasts *in vitro*. Although MSCs were first isolated from bone marrow, nowadays they can be cultivated from various tissue including adipose tissue, umbilical cord tissue and blood, dental pulp, placenta, and amniotic fluids, among other tissues⁶⁻⁸.

Initially, the underlying mechanisms by which MSCs promote the regeneration of injured tissue were considered to include the homing of transplanted MSCs to the site of injury, the differentiation of MSCs into the cell types needed for tissue repair, and the active factors they secrete^{8,9}. However, recent studies have proven that MSC homing and differentiation following transplantation do not contribute to MSC therapeutic potency as it has become evident that paracrine factors are the key mechanism of action for MSC therapy^{10,11}. Administering the cells has led to some concerns regarding the safety and logistics of the therapy. Immune rejection, tumorigenicity, and transmission of infections are some safety concerns that arise from MSC transplantation. Meanwhile, logistical complications, such as the cell expansion in obtaining enough cell numbers (without the cells entering senescence or genetic modification) as well as the short shelf life of the MSC product, are also hindering the application of MSC therapy^{11,12}. Due to these difficulties, the focus to harnessing the therapeutic benefits of MSC has

been shifted towards factors released by these cells, or collectively named MSC secretome¹³.

MSC secretome comprises a variety of serum proteins, growth factors, angiogenic factors, hormones, ECM proteins, proteases, cytokines, chemokines, anti-oxidants, lipid mediators and genetic material. MSC secretome is mainly categorized into^{8,13}: (1) soluble factors consisting of growth factors, cytokines, chemokines, hormones and other proteins; and (2) extracellular vesicles (EVs) which comprise exosomes (25-200 nm of diameter) and microvesicles (100-1000 nm) (Figure 1). EVs carry proteins, DNA, RNA and lipids to exert their effect on target cells. These factors have been shown to be biologically active and contribute to tissue homeostasis, cell signalling, immunomodulation, angiogenesis, cell survival and ECM modulation¹⁴.

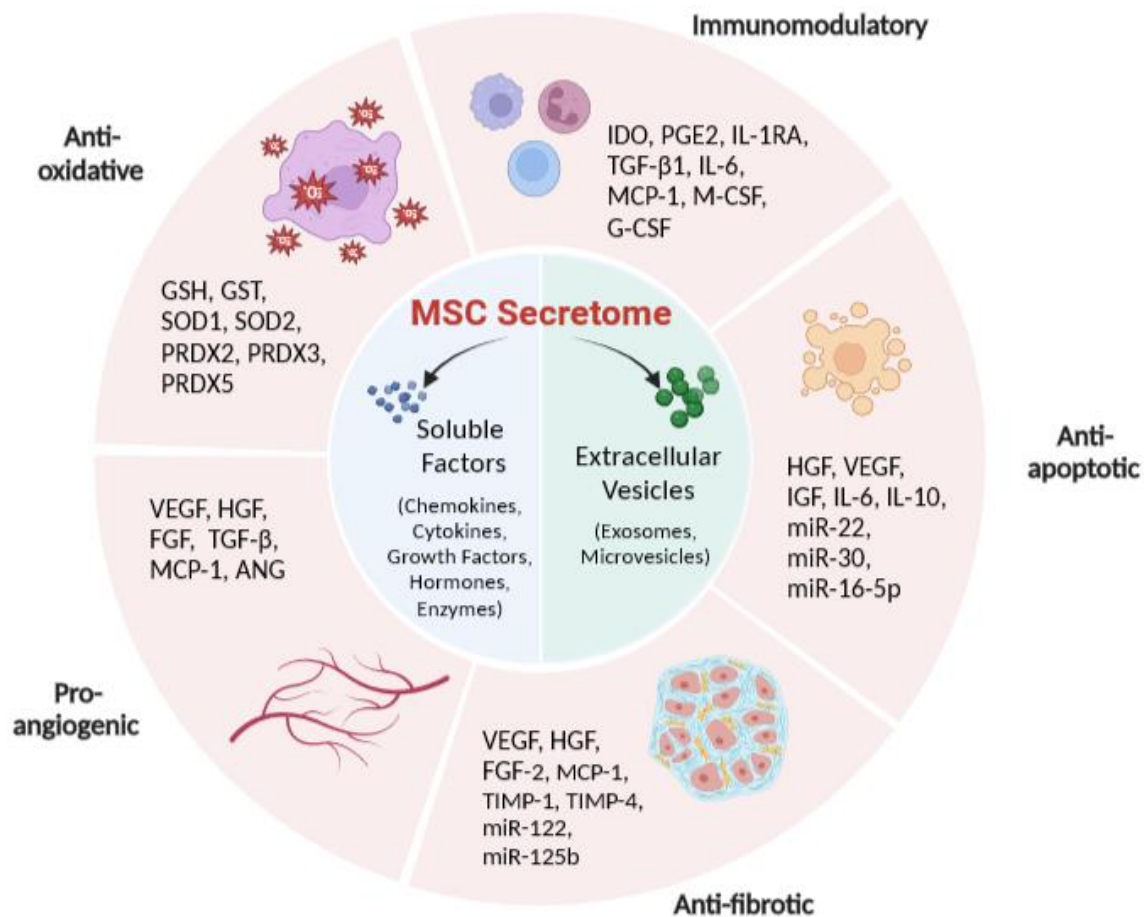


Figure 1. MSC secretome is biologically active and capable of modulating various cellular processes.

MSC secretome contains growth factors, chemokines, cytokines, hormones, and enzymes that are mostly soluble, but also insoluble extracellular vesicles (including exosome and microvesicles) that

can carry a variety of serum proteins and genetic material e.g. DNA and RNA, amongst other factors. MSC secretome has been shown to be immunomodulatory, anti-apoptotic, anti-fibrotic, pro-angiogenic, and anti-oxidative. MSC: mesenchymal stromal cell; IDO; PGE2: prostaglandin 2; IL-6 and 10: interleukin-6 and 10; IL-1RA: IL-1 receptor antagonist; TGF- β 1: transforming growth factor- β 1; MCP-1: monocyte chemoattractant protein-1; M-CSF: macrophage- colony stimulating factor; G-CSF: granulocyte-CSF; HGF: hepatocyte growth factor; VEGF: vascular endothelial growth factor; IGF: insulin-like growth factor; miR: micro RNAs; FGF-2: fibroblast growth factor-2; TIMP-1/4: tissue inhibitors of metalloproteinase-1/4; PDGF: ; GSH: glutathione reductase; GST: glutathione-S-transferase; SOD-1 and -2: superoxide dismutase-1 and 2; PRDX-2, -3, and -5: peroxiredoxin-2, -3, and -5. This image was created using BioRender.

Despite the high enthusiasm for these cells in the last decade and the encouraging outcomes from pre-clinical studies, there are multiple obstacles that need to be tackled to implement MSC therapy in clinical setting. Firstly, the high variability of MSCs used in numerous clinical trials makes it difficult to interpret the efficacy of the cells. This high variation of MSC characteristics and functionality stems from both the tissue of origin from which the cells are isolated as well as from lack of standardization in MSC manufacturing¹⁵. The extrapolation of the outcome from pre-clinical into clinical trials should also be examined critically as the discrepancy of immune system between human and animal models, mostly rodents, might result in misleading conclusion. The mechanism of action (MoA) by which MSCs deliver their therapeutic benefits is not completely understood and might even be specific to the type of disease they shall target. Unravelling how MSCs function is particularly important for the establishment of MoA-based potency assays to ensure the quality of the manufactured MSCs¹⁶.

1.2 MSC immunomodulation and its compatibility across species

In vitro and pre-clinical studies have demonstrated that not only MSCs are able to alleviate the immune response that has gone off the rails^{31,32}, but they can also influence the immune cells to support the repair of damaged tissue³³. Because of these, clinical trials of MSC therapy are done for immune-related disease such as GvHD³⁴⁻³⁶. However, despite the positive results obtained in animal studies, the outcomes from clinical trials are rather disappointing³⁷ indicating that there is a translational hurdle between pre-clinical and clinical studies.

Indeed, human MSCs (h-MSCs) must be tested in animal models first as a pre-requisite demanded by the regulatory authorities to ensure both safety and efficacy of the

cells before progressing into clinical trials in patients. Indeed, MSCs are considered as immune privileged as they show low levels of HLA-I and no expression of HLA-II or other costimulatory factors such as CD80 and CD86³⁷, which is regarded to allow xenogeneic transplantation without the risk of rejection. However, the incompatibility of xenogeneic transplantation of h-MSCs, especially in regulation of T cell proliferation, seemed to hamper MSC efficacy. Lohan and colleagues showed that h-MSCs transplantation in a rat corneal transplantation model did not influence the allograft survival due to their inability to modulate the rats' immune cells. It turned out that rat cytokines were not able to stimulate h-MSCs, leading to the lack of nitrite oxide (NO) and IDO upregulation and subsequent failure in inhibition of rat T cell proliferation³⁸.

In line with the aforementioned study, a previous study in our lab by Torres-Crigna has proven that while human A-MSCs were able to inhibit human PBMC (h-PBMC) proliferation in a direct co-culture system, the inhibition was completely missing in rat PBMCs (r-PBMCs)²² (and Rendra et al., revised manuscript submitted). On the other hand, rat-derived MSCs (r-MSCs) were able to inhibit PBMC proliferation isolated from both human and rat. Interestingly, unlike human A-MSCs, ABCB5+ MSCs were able of inhibiting PBMC proliferation from both species, even though to lesser extent than A-MSCs and r-MSCs. Further experiments then revealed that A-MSCs employed IDO to exert their inhibitory effect on h-PBMCs, while r-MSCs made use of nitrite on both species of PBMCs. This is in concordance to what has described before that according to their ability in inhibiting T cell proliferation, MSCs can be categorized as IDO and NO utilizers. MSCs from monkey, pig, and human employ IDO, meanwhile those from rodents (mouse, rabbit, rat and hamster) make rather use of NO³⁹.

Indeed, inhibition of stimulated PBMC proliferation is one of the most robust and used immunological assay to test MSC benefits, however, a growing body of evidence suggests that MSC immunomodulation also affects other immune cells^{14,40}. Therefore, the interspecies immune-compatibility assessment should also be extended to other type of immune cells.

1.2.1 Macrophages are important to player in delivering MSC therapeutic effects

Macrophages are infiltrating and tissue-resident innate immune cells, that are specialized in phagocytosis, and play an important role in mediating the induction and resolution of sterile inflammation⁴¹. Macrophages exhibit high plasticity in term of their phenotypes which are classified into classically activated or M1 and alternatively activated or M2 macrophages. Classically activated or M1 macrophages are responsible for bacteria removal through cytotoxicity and, hence, pro-inflammatory phenotype. *In vitro* M1 polarization is induced by IFN- γ and lipopolysaccharide^{42,43}. Alternatively activated or M2 macrophages are characterized by enhanced phagocytosis and are able of immunosuppression and tissue repair⁴⁴. M2 macrophages are stimulated *in vitro* by IL-4, IL-10 and IL-13. It is important to note that this M1/M2 polarization is only a theoretical and oversimplified concept. *In vivo* macrophages are able to switch from one activation state to another, which makes their complex phenotype to be more of a continuous spectrum, rather than a rigid dichotomy⁴²⁻⁴⁴.

Macrophages play key roles in mediating the MSC therapeutical benefit⁴⁵. In fact, Giri et al., postulated that macrophages are essential for MSC therapy in colitis mouse model. Adoptive transfer of MSCs modulated host macrophages via CCL2-CXCL12 into IL-10 producing macrophages which subsequently induced more IL-10 secretion by bystander immune cells (T- and B cells)³². Moreover, MSCs also stimulated the release of amphiregulin in macrophages which contribute to epithelial homeostasis *in vitro* and in mice suffering from autoimmune uveoretinitis, an autoimmune inflammation in retina³³. Given the importance of macrophages in the maintenance of tissue homeostasis, the compatibility of between MSCs and macrophages across species should be interrogated to assess the relevance of pre-clinical model in translating MSC therapy.

1.3 MSC as therapeutic option for Acute Kidney Injury (AKI)

Understanding how MSC therapy works for certain diseases (mechanism of action, MoA) is pivotal when aiming at clinical purposes. Without having a comprehensive idea on MSC MoA, development of a reliable potency assay to select the best MSCs (tissue of origin and donors) will be difficult to achieve. Within the European Union-funded International Training Network, RenalToolBox, the focus was to understand the MSC MoA specifically in acute kidney disease. We focused on deepening our understanding

on the interaction between renal cells and innate immune cells, particularly macrophages in a cisplatin-injury setting.

1.3.1 Cisplatin is a chemotherapeutic drug with nephrotoxicity side effect

Cisplatin (cis-diamminedichloroplatinum II) is a chemotherapeutic drug used to treat a broad range of malignancies, such as head and neck, breast, testicular, small cell lung, cervical and bladder cancer ^{46,47}. It has been even used as a combination therapy with other anti-cancer drugs to treat high grade cancers including soft-tissue cancer and osteosarcoma. Cisplatin is considered as the most potent anti-cancer chemotherapy to date. Cisplatin promotes cancer cell death by inducing DNA damage. Here, Cisplatin is able to trigger 1-2 intra- and 1-3 inter-strand crosslink by binding to purine bases of the DNA strand, which eventually activates the DNA repair system ^{46,47}. However, since the cancer cells actively proliferate the rate of DNA damage inevitably exceeds the DNA repair capacity of cancer cells, leading to the accumulation of cross-linking, cell cycle arrest, built up of intracellular reactive oxygen species and, ultimately, cell death. It has been also reported that some cancer cell can develop cisplatin resistance by increasing their DNA repair system to accommodate cisplatin-induced DNA damage. Nevertheless, cisplatin treatment results in not only the cancer cell death, but also a myriad of side effects, including allergic reaction, gastrotoxicity ⁴⁸, ototoxicity, neurotoxicity and nephrotoxicity ⁴⁹. Amongst these adverse effects, nephrotoxicity is the most prevalent and debilitating one: 20-30% of patients receiving cisplatin treatment develop kidney injury, even from the beginning of cisplatin treatment. In fact, cisplatin-induced acute kidney injury accounts up to 60% of hospital-acquired kidney injury, which comes with high mortality and morbidity ⁵⁰. It is no surprise that nephrotoxicity has become the dose-limiting factor for cisplatin treatment.

Cisplatin-induced acute kidney injury (AKI) was first studied in 1971 in which histopathological changes of acute tubular necrosis and azotemia were observed ⁴⁷. The decline of renal function normally started several days after cisplatin treatment, as indicated by elevated levels of plasma creatinine and urea nitrogen. Pathology of cisplatin-induced AKI comprises renal vasoconstriction, reduced flow of kidney plasma and decreased glomerular filtration rate. The urine output also decreases and often contains glucose or protein implying proximal tubule injury, which, in fact, is the hallmark of cisplatin nephrotoxicity. On top of that, proximal tubule injury is accompanied by inflammatory responses that further exaggerate kidney injury. It is also noteworthy that

the vasoconstriction in the kidney vasculature eventually reduces the blood flow causing ischemic injury. These pathological events ultimately lead to acute kidney failure⁵⁰. Some measures to prevent this have been applied including diuretics and adequate hydration, and the renal function can recover within 2-4 weeks, or even longer. However, the lack of renal recovery has also been reported and its prevalence remains high.

1.3.2 Cisplatin promotes proximal tubular epithelial cell death

The kidney is responsible to clear out cisplatin from the body through glomerular filtration as well as tubular secretion. However, the concentration of cisplatin in the kidney of patients with AKI is higher than that in the blood, implying that there is cisplatin retention in the kidney^{46,51}. Previous studies have shown that proximal tubular epithelial cells (PTECs) are responsible for this accumulation by actively uptaking cisplatin from the basolateral side, mainly through copper transporter 1 (Ctr1), organic cation transporter 2 (OCT2), and multidrug and toxin extrusion proteins (MATEs)^{52,53}. Once inside the cells, cisplatin promotes PTEC injury and cell death through multiple pathway. First, cisplatin has been reported to cause DNA damage in PTEC in the similar fashion as in cancer cells, which results in apoptosis (**Figure 2**)^{53,54}. However, since PTECs are not as proliferative as cancer cells and given the high mitochondrial content of PTECs, cisplatin exerts its cytotoxicity mainly through mitochondrial dysfunction^{46,55} (**Figure 2B**). Cisplatin disrupts mitochondrial functions by promoting mitochondrial DNA damage, blocking the electron transport chain and compromising the function of other proteins in the mitochondria. This mitochondrial dysfunction triggers the production of reactive oxygen species (ROS) and release of cytochrome C, which eventually initiates the downstream intrinsic apoptotic pathway⁵⁵. The exacerbated ROS also negatively affect the endoplasmic reticulum (ER) (**Figure 2C**), marked by elevated levels of glucose binding protein 78 (GRP78), a major chaperone protein in ER, that also serves as an indicator of ER stress⁵⁶. Such ER stress response is initiated as an anti apoptotic attempt to restore proteostasis that is disrupted by accumulation of unfolded protein. However, overly prolonged proteostasis restoration upon cisplatin treatment can trigger the apoptosis pathway by the activation of pro-caspase-12 in PTECs⁵⁶.

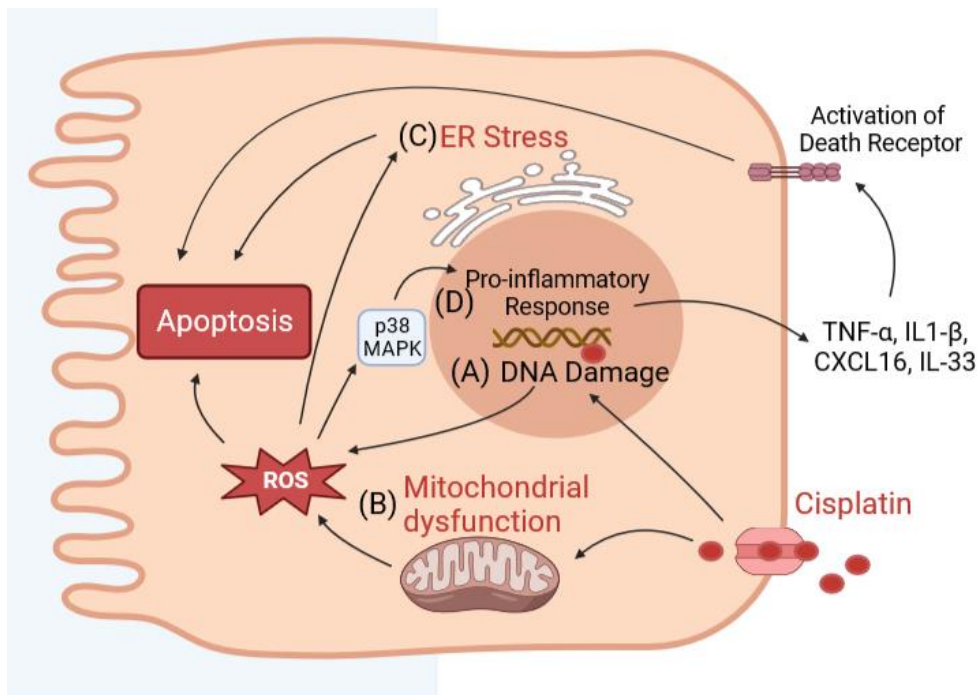


Figure 2. The mechanism of action by which cisplatin promote PTEC apoptosis.

Upon being absorbed by PTECs, cisplatin promotes PTEC apoptosis by multiple ways: by causing DNA damage (A) and inducing mitochondrial dysfunction (B), both of which cause ROS accumulation. The exacerbated level of ROS then leads to ER stress, adding up to the activation of apoptosis (C). p38-MAPK is also activated by the oxidative stress resulting to the production of various cytokines, including TNF- α , which in turn bind to the death receptor and subsequently inducing apoptosis via extrinsic pathway (D). PTEC: proximal tubular epithelial cell; ROS: reactive oxidative species; ER: endoplasmic reticulum; p38-MAPK: p38-mitogen-activated protein kinase; TNF- α : tumour necrosis factor- α . Image was created using BioRender.

Lastly, cisplatin can also cause PTEC death by activating death receptors triggering the extrinsic apoptotic pathway (**Figure 1D**). Cisplatin induces the extrinsic pathway through elevated release of pro-inflammatory cytokines, tumour necrosis factor- α (TNF- α), by PTEC and promoting the shedding of fas ligand (FasL). TNF- α has been well established to exaggerate cisplatin-induced apoptosis as the knockout of TNF-R1 in mice can improve the resistance of cisplatin-induced AKI. It also has been shown that the elevated production of TNF- α by PTECs results from ROS generation and the subsequent phosphorylation of p38 and mitogen-activated protein kinase (MAPK)⁵⁷. The inhibition of P38-MAPK leads to decreased secretion of TNF- α *in vivo* and in turn is protective against cisplatin-induced AKI⁵⁸. Interestingly, treating PTEC with hydroxyl scavenger to suppress oxidative stress also hampers p38-MAPK activation, resulting in amelioration of AKI⁵⁷. Similar to TNF- α , cisplatin-induced ROS also triggers the

shedding of FasL into the urine of mice as indicated by 4-fold increase of FasL concentration. Accordingly, the inhibition of FasL/Fas attenuates PTEC death *in vitro*. Likewise, ROS suppression by intracellular free radical scavenger in mice, TEMPOL, ameliorates AKI-associated biomarkers and normalizes FasL level in urine ⁵⁹.

In addition to apoptosis, in high concentrations cisplatin also promotes necrotic-like cell death of PTECs ^{52,60}. Higher concentration of cisplatin in HK2 cells, a human PTEC line, triggers the activation of apoptotic machinery, however the downstream process is then aborted due to cisplatin-induced inhibition of effector caspases. This blockage of apoptosis inevitably results in the cell death that resembles necrosis, which characterized by swollen cell, plasma membrane rupture and organelle loss. This pro-necrotic cisplatin concentration also promotes unidentified B-cell lymphoma-2 (Bcl-2) and mitochondria-independent pathway that are missing in low and pro-apoptotic concentration of cisplatin ⁶⁰. Yanfang et al., on the other hand, reported that the cell death induced by high concentration of cisplatin is not exactly necrosis, but rather programmed necrosis which is also known as necroptosis. They showed that inhibition of necroptosis protein effectors in mice, such as receptor-interacting protein 1 (RIP1) and 3 (RIP3), and mixed lineage kinase domain-like protein (MLKL), abrogated proximal tubule damage. Interestingly, this necroptosis can be recapitulated *in vitro* by treatment of cisplatin and a combination of pro-inflammatory cytokines implicated in cisplatin nephrotoxicity, for instance TNF- α , TNF-related weak inducer of apoptosis, and IFN- γ . Furthermore, RIP-3 and MLKL-deficient mice that were treated with cisplatin showed decreased level of pro-inflammatory cytokines, suggesting that there was positive loop between necroptosis and pro-inflammatory cytokines in cisplatin-induced AKI ⁶¹.

All in all, the cytotoxic effect of cisplatin on PTECs is heavily linked to ROS accumulation which activates intrinsic and extrinsic apoptotic pathway, as well as, necroptosis in higher concentration. These pathogenic events also involve in the recruitment of immune cells supporting the inflammation in the kidney and further augment the cisplatin-induced tubule damage ⁵⁵, which will be discussed in the next section.

1.3.3 Cisplatin-induced inflammation exaggerates renal damage

Inflammatory reaction has been postulated to play a big role in cisplatin-induced AKI. The involvement of inflammation is induced by the release of danger associated molecular patterns (DAMPs) by injured PTECs which in turn activate toll-like receptors (TLR) ⁵⁵. Some TLRs that are implicated in cisplatin nephrotoxicity include TLR2, TLR4 and TLR9. While TLR2 and TLR9 are shown to be protective by supporting autophagy and Tregs-recruitment, respectively, TLR4 promotes injury even further. TLR4 deficiency in mice significantly reduced renal injury 72h after cisplatin treatment as reflected in decreased BUN, serum creatinine and less histological changes. TLR4 deficiency also suppresses the concentration of cytokine and chemokine in serum, kidney, and urine, including TNF- α , IL-1 β , IL-6, IL-2, IL-10, CCL-5, MCP-10, and IP-10. Furthermore, phosphorylation of P38-MAPK and JNK is also reduced by TLR-4 deficiency in cisplatin-induced AKI, implying that TLR-4 plays a significant role in the inflammation response of cisplatin-induced AKI ^{62,63}.

In addition to TLR4, cisplatin also stimulates a range of cytokine production in PTECs allowing immune reaction in the kidney. As mentioned before, TNF- α plays a central role in the inflammation triggered by cisplatin ⁶⁴. Previous studies have shown that inhibition of TNF- α , by both GM-6001, a TNF- α antagonist, and TNF- α silencing, resulted in the amelioration of kidney injury and preserved kidney functions ⁶⁵. TNF- α also augments the activation of NF κ B, emphasizing the importance of TNF- α in mediating cisplatin-induced inflammation in the kidney ⁴⁶. In addition to TNF- α , other cytokines and chemokines also orchestrate in recruiting and activating immune cells such as IL-6, IL-33, CXCL16, CXCL1, and IL-10. Prompted by the release of the DAMPs, cytokines, and chemokines, innate and adaptive immune cells eventually infiltrate the kidney parenchyma ⁴⁶. A wide range of immune cells has been implicated in disease including neutrophils, dendritic cells, macrophages, helper, and cytotoxic T-cells ⁴⁷. Amongst these immune cells, macrophages significantly affect the progression of kidney disease in general, and have been implicated a lot in renal ischemic-reperfusion injury (IRI) ⁴³.

1.3.4 Macrophages' roles are important in AKI progression

Macrophages are the predominant leukocytes in the kidney during both physiological and pathological settings ⁶⁶. The high number of macrophages in the kidney seems to

be the result of CSF-1 and IL-34 secreted by renal tubular epithelial cells. Resident macrophages in the kidney are derived from both the yolk sac and hematopoietic progenitor during organogenesis, and are able to self-renew themselves throughout the lifetime⁶⁷. Unlike resident macrophage, monocyte-derived macrophages arise from infiltrating monocytes that undergo differentiation in the kidney and turn over every 14 days. Monocyte-derived macrophages do not replace the resident macrophages, except when the niches of kidney-resident macrophages is vacant^{42,43,68}. Interestingly, regardless the origin, tissue macrophages show tissue-specific transcriptional programming, implying the tissue specific regulation on their phenotype⁴³. Nevertheless, both are present in resting and injured kidney, and show tissue specific transcriptional characteristics, implying that they are programmed to the specific needs of the tissue they reside in in order to maintain tissue homeostasis^{42,43}.

Even though the role of macrophages in cisplatin-induced AKI is not yet as widely studied as in IRI models, these cells seem to contribute in the progression of the cisplatin-induced AKI. Nakagawa et al reported the composition of macrophages population in cisplatin-treated rats changed throughout the 20 days of observation⁶⁹. They noticed that CD68-expressing M1 population increased abruptly on day 5, peaked on day 9, and decreased thereafter. Meanwhile, CD163-expressing M2 macrophages number also increase after the day of cisplatin administration on day 5 and peaked on day 12. Although the level of M2 macrophages tended to decrease; it showed a more stable trend than that of M1 macrophages. On later phase of the injury, on day 12, 15 and 20, 62 to 78% of macrophages expressing CD68 concomitantly expressed CD163. This might be caused by M1 macrophages switching their phenotype towards M2. Interestingly, despite the increase of M2 in this later stage of injury, the macrophages expressing MHC class II were also abruptly elevated starting from day 9 and remained high until day 20. Of note, MHC class II expression is one of M1 phenotypes, implying that both M1 and M2 macrophages are present and involved in the progression of AKI⁶⁹.

Indeed, fine-tuning the balance between M1 and M2 macrophages throughout the phase of kidney injury is a crucial factor that determines tissue repair or fibrosis⁷⁰⁻⁷². AKI models such as IRI and glycerol injection elicit faster response in macrophages. Monocyte infiltration promoted by CCR2 and CX3CR1 takes place within the first 48h

and stops on day 3 in renal IRI mouse model. Interestingly the peak of tubular injury also occurs simultaneously with the peak of infiltrating monocytes^{73,74}. The infiltrating monocytes are skewed towards M1 polarization by the injured tubular milieu and in turn secrete pro-inflammatory cytokines (e.g. TNF- α , IL-12, IL-6) and NO⁷⁵. The presence of M1 macrophages also subsides on day 3 following IRI as M2 macrophages start to predominate the kidney parenchyma as a result of MCSF, GM-CSF, retinoic acid and DAMPs secreted by tubular epithelial cells⁷⁶. The M2 macrophages contribute to tissue repair by phagocytosing the apoptotic cells and intraluminal debris, and secreting anti-inflammatory and pro-regenerative factors such as IL-22, Wnt 7b, breast regression protein 39 and IL-10^{42,43,75}.

Despite M2 macrophages contribution in tissue repair, a growing body of evidence has shown that they are also the key player of renal fibrosis by secreting pro-fibrotic factor TGF- β 1⁷¹. This is particularly true when the severe injury and prolonged inflammation take place. Interestingly, previous studies showed that depleting M2 on later phase (starting from day 3) does not always result in positive outcome. Some studies indeed reported positive outcome, but more studies showed increased fibrosis, enhanced fibrosis, decreased glomerular filtration rate and failed tubule regeneration⁴². In contrast to M2, M1 depletion using chlodronate before IRI treatment consistently leads to reduced tubular necrosis and suppressed inflammation, implying that suppressing M1 macrophages in early phase of AKI is more beneficial than inhibiting M2 macrophages in late phase^{42,76}. Furthermore, Cao et al postulated that fibrosis is a result of M1 macrophages that are carried from early into the late phase of injury and co-exist with the M2 macrophages, which gives rise to incomplete inflammation resolution and fibrosis progression⁷⁷. Given the implication of macrophage phenotype, it is important to take the macrophages and PTEC interaction into consideration in exploring MSC therapy to treat cisplatin-induced AKI.

2 AIM OF THE STUDY

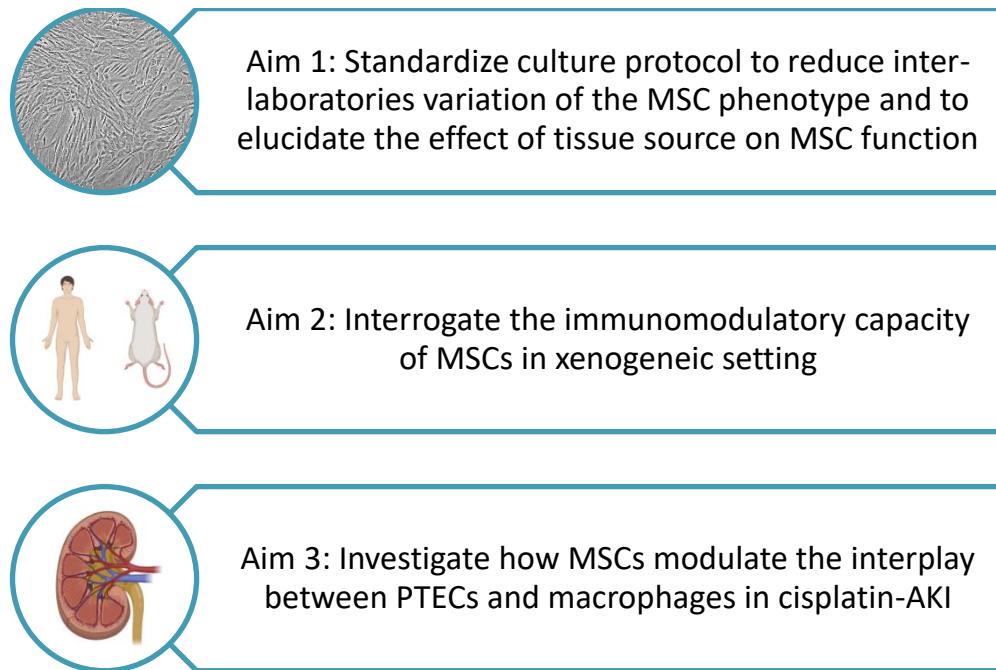


Figure 3. Aims of the study

This image was created using BioRender.

Aim 1: Standardize culture protocol to reduce inter-laboratories variation of the MSC phenotype and to elucidate the effect of tissue source on MSC function

Despite the growing body of studies reporting the therapeutic potential of MSCs, the clinical translation of MSC therapy is still hampered by multiple factors. The lack of standardized protocols across laboratories on how to culture MSCs that are used for clinical trials has been a major issue, given the fact that MSC functionality is greatly affected by the culturing method. This, along with the difference of tissues from which the cells were isolated, has rendered it difficult to interpret the conflicting clinical trial results because the fitness and functionality of the MSCs highly differed from one trial to another. Aim 1 thus was to standardize culture protocols to reduce inter-laboratories variation of the MSC phenotype and to elucidate the effect of tissue source on MSC function (**Figure 3**).

We hypothesized that the variations of MSC phenotypes after being cultured in different centres could be minimized by standardizing the culture protocols. To do this, we have collaborated with different MSC laboratories within our graduate school,

RenalToolBox, in Liverpool and Galway to establish a harmonised MSC culture protocol, encompassing the sera, seeding density, and basal medium. The MSCs were isolated from BM, UC and adipose, each of them was isolated in different centers before internationally sent to the other centres. The basic characteristics of those MSCs were compared between the tissue sources and across the three centres. Furthermore, the influence of tissue source on MSC immunomodulatory on T cell proliferation was evaluated using a mitogen-driven PBMC proliferation assay. Of note, this work has been published in *Stem Cell Research and Therapy*⁷⁸.

Aim 2: Interrogate the immunomodulatory capacity of MSCs in a xenogeneic setting

Next, another issue we are trying to address in present study is the immune compatibility of xenogeneic transplantation. Given the fact that the regulation of immune system varies across species, the immunomodulatory potential of MSCs in xenogeneic transplantation should be assessed critically, too. Indeed, a preclinical study in animal model is necessary to interrogate the safety and efficacy of MSCs therapy, thus a preliminary study on the relevance of the data obtained in animal model to human application in term of immune response is imperative. Although it has been reported that inter-species immune incompatibility affected MSC ability in modulating T cell proliferation, whether it also influences MSC modulatory effect on macrophages is not yet elucidated.

Given that there were some discrepancies by which immune system was regulated across species, we expected there were some immune barriers or incompatibilities which hampered MSCs effects on macrophages in xenogeneic transplantation between human (A-MSCs and ABCB5+ MSCs) and rat (BM-MSCs). Firstly, we harnessed the MSC secretome in their conditioned medium (CM) from human and rat MSCs. We also established the culture of rat macrophages isolated from healthy rats' bone marrow. We then compared how MSCs modulated macrophage phenotype across species and if they employed the same mediator in exerting their effect. This work is part of collaborative project with the working group of Prof. Norbert Gretz and RheaCell/TICEBA (manuscript in preparation)

Aim 3: Investigate how MSCs modulate the interplay between PTECs and macrophages in cisplatin-AKI

Lastly, understanding the MoA by which MSCs exert their protective effect is of importance for clinical development of MSC therapy. Within the framework of RenalToolBox, an EU-funded ITN, the study was focused in elucidating the underlying mechanism of MSCs in ameliorating kidney injury caused by cisplatin, a chemotherapeutic drug. It has been shown that the interaction between PTECs and macrophages plays a pivotal role in determining the fate of the injury progression and resolution. Despite the pro-regenerative capacity of MSCs, little is known on how MSCs orchestrate the PTEC-macrophage interaction in *in vitro* cisplatin-induced injury model.

We hypothesized that MSCs could orchestrate the crosstalk between PTECs and macrophages which in turn would further improve reno-protective effect of MSCs against cisplatin-induced injury. To prove this hypothesis, the protective effect in MSC secretome in CM was first tested separately on conditionally immortalized PTECs (ciPTECs) and monocyte-derived macrophages treated with cisplatin. The possible MoA and mediator by which CM elicited its effect were also elucidated. Next, we established co-culture system which allows ciPTECs and macrophages crosstalk in the presence of cisplatin injury. How cisplatin and CM modulated ciPTECs and macrophages were evaluated using confocal and live-cell imaging as well as Luminex assay.

3 MATERIALS AND METHODS

3.1 Tissue Origin and Culture Protocol Affect MSC Phenotypes

Although MSCs isolated from different tissues might fulfil all the criteria determined by ISCT, they still display tissue-specific characteristics and, hence, differ in their therapeutic capacity. To date the predominant tissues from which MSCs are isolated for clinical trials are bone marrow (BM), adipose tissue (A), umbilical cord (blood (UC), and Wharton's Jelly (WJ)). Morphologically, umbilical cord-derived MSCs (UC-MSCs) exhibit smaller cell size, faster proliferation rate and lower senescence rates than bone marrow- (BM-MSCs) and adipose-derived MSCs (A-MSCs). The ability of trilineage differentiation also varies amongst these MSCs depending their tissue origins: A-MSCs possess more ability for adipogenic differentiation; UC-MSCs chondrogenic differentiation; meanwhile BM-MSCs osteogenic and chondrogenic differentiation¹⁷. Furthermore, their expression of CD146, an adhesion molecule, also varies between the tissue of origin; in which UC- and WJ-MSCs showing a more prominent expression than those of BM-MSCs and A-MSCs^{17,18}.

Previous study by Medrano-Trochez¹⁹ revealed that despite their high heterogeneity, out-of-thaw BM-MSCs and WJ-MSCs differ in gene expression. While BM-MSCs showed enrichment in genes associated with lipids and lipo-protein metabolism, mitochondrial translation and metabolic pathways, WJ-MSCs exhibited enrichment in ECM organization, signal transduction and biosynthesis of collagen. Of note, each BM- and WJ-MSCs showed two major clusters of donor profiles which varied in their immune signalling, cell-cycle related transcripts, cell surface markers, and metabolic pathway. Interestingly, the discrepancies of transcriptomic profile between those clusters were not consistent between both the tissues of origin. It is also noteworthy that the observed discrepancies due to donor-to-donor variation are relatively inferior compared to the differences caused by the tissue of origin¹⁹.

The tissue of origin also affects MSC therapeutic capacity in modulating angiogenesis and immune cells. A-MSCs were shown to express higher level of insulin-like growth factor-1 (IGF-1), vascular endothelial growth factor-D (VEGF-D) and interleukin-8 (IL-8), as compared to MSCs isolated from bone marrow and skin tissue. This is in line with the superior A-MSCs' ability to induce tubulogenesis of endothelial cells, which

was attributed with VEGF-A and VEGF-D ²⁰. In contrast to this, Kehl and colleagues showed that A-MSCs exhibit the least pro-angiogenic support (lowest paracrine factors and least endothelial stimulation), whilst Wharton's jelly-derived MSCs (WJ-MSCs) the highest, followed by BM-MSCs ²¹. Similarly, in terms of immunomodulation, the difference between the tissues of origin can be observed in several studies although consistent patterns are still lacking. Based on the previous study in our lab, A-MSCs demonstrated a superior ability in inhibiting PBMC proliferation as compared to BM- and UC-MSCs, which was associated with A-MSCs' secretion of IDO upon IFN- γ stimulation ²². However, another study revealed that BM-MSCs inhibited PBMC proliferation more effectively than A-MSCs and WJ-MSCs ¹⁸. Other clinical efficacy that differs due to the tissue origins are their ability in controlling blood glucose level and lipid metabolism in diabetic mice ²³; inducing platelet activation ²⁴; and supporting neurites outgrowth ¹⁸.

The distinct results reported across those studies might also be caused by the variation of the manufacturing protocols in which MSCs were grown. As MSCs secrete their factors according to the environmental stimuli, the composition of MSC secretome in each and every study might differ from one to another depending of the culture condition ⁸. This, of course, adds another layer of complexity in translating the MSC therapy since reproducibility and consistent product quality of the cells as well as the secretome is essential to minimise the variability of clinical outcome ²⁵. A study by Stroncek et al., has shown that the variation in manufacturing protocols for MSC cultivations in five independent laboratories resulted in the distinct functional and molecular characteristic of harvested MSCs to a higher degree than did the source of material itself ²⁶. The differences in culture protocols include amongst others the sera (the source and concentration), basal medium (the type and composition), and seeding density ²⁶. Therefore, it is imperative to establish a standardized culture protocol, which is scalable and time- and cost- efficient, to ensure the quality of MSCs, especially for clinical purposes.

3.1.1 ABCB5+ MSCs

In addition to the MSCs mentioned above, a sub-population of skin-derived MSCs expressing ATP-binding cassette subfamily B member 5 (ABCB5+) have been described. These are already commercially exploited, received a manufacturing licence by the Paul Ehrlich Institute and are used as an off-the-shelf ATMP in clinical trials, e.g. for

wound healing ^{27,28}. These cells are isolated from surgical discard skin tissue. Upon the isolation, the ABCB5+ cells enrichment is performed in three steps: plastic adherence, cell expansion in proprietary medium and immunomagnetic selection ²⁷. ABCB5 transporter is first identified in a CD133+ human epidermal melanocyte progenitor cells and functions as chemoresistance-conferring drug efflux transporter. In normal cells, ABCB5 plays role in the elimination of harmful xenobiotics and metabolites and is often found in cells with secretory and excretory functions. Thanks to its function in eliminating toxic xenobiotics, ABCB5 also maintain the stem cell integrity and regulate MSC quiescence. ABCB5+ MSCs are also capable of immunomodulation on macrophages, neutrophil and T-cell by IL-1RA and SOD3 secretion, and through the PD1/PD-L1 axis ²⁹.

Therapeutic benefit of ABCB5+ MSCs has been reported in multiple preclinical and clinical trials showing pro-wound healing capacity. In iron overload and immunodeficient NOD-SCID IL2r-gamma null (NSG) mouse model, ABCB5+ MSCs supported wound healing by releasing the IL-1RA which modulated macrophages polarization towards pro-regenerative macrophages ^{28,30}. In interventional, multi-centre, and single arm phase I/IIa clinical trial on patients with chronic venous ulcer, topical application of ABCB5+ MSCs was safe and well tolerated by the patients. Given the safety profile of these cells, US Food and Drug then granted the permission to conduct a phase III trial for epidermolysis bullosa, while in Germany a permission was obtained to treat refractory chronic venous ulcers ²⁹.

Given the unique characteristic of ABCB5+ MSCs, a head to head comparison with the other more commonly used MSCs would be of interest to elucidate how MSC origin affect their therapeutic capacity.

3.2 Materials

3.2.1 Cells

Cell Type	Source / Manufacturer
Adipose-derived human MSCs (A-MSCs)	Mannheim Ethics Commission II (vote number 2006-192 N-MA);
	Self isolated in laboratory

Bone marrow-derived human MSCs (BM-MSCs)	Provided kindly by Prof. Timothy O'Brien, National University of Ireland, Galway;
	Obtained from Lonza (Basel, Switzerland)
Umbilical cord blood-derived human MSCs (UC-MSCs)	Provided kindly by Prof. Patricia Murray, University of Liverpool;
	Isolated and obtained from NHS Blood and Transplant in accordance to Declaration of Helsinki, before being transferred to University of Liverpool
ABCB5+ MSCs	Provided kindly by Ticeba-RHEACELL GmbH & Co. (Heidelberg, Germany) as a collaboration.
Human peripheral blood mononuclear cells (PBMCs)	Provided kindly by the German Red Cross Blood Donor Service in Mannheim, Germany. Leukapheresis samples: Mannheim Ethics Commission II (vote number 2018-594N-MA);
	Previously isolated from leukapheresis samples.
Monocyte-derived human macrophages (hMac)	Provided kindly by the German Red Cross Blood Donor Service in Mannheim, Germany;
	Self isolated in laboratory from buffy coats
Monocyte-derived rat macrophages	Provided kindly by Prof. Benito Yard from control experiments of licensed animal experimentations
	Self isolated in laboratory from healthy rat bone marrows
Conditionally immortalized proximal tubular epithelial cells	Commercially purchased from Cell4Pharma.

3.2.2 Cell culture products

Product	Company	Catalog No.
NB6 GMP grade collagenase	SERVA Electrophoresis	17458
α -MEM	Gibco	2561029
MSC Adipogenic Differentiation Medium	Promocell	C-28016

MSC Osteogenic Differentiation Medium		C-28013
Supplement mix Adipogenic Differentiation Medium		C-39816
Supplement mix Osteogenic Differentiation Medium		C-39813
Hoechst 33342	Invitrogen	917368
Adipored Assay Reagent	Lonza	PT-7009
Human allogeneic serum pooled from healthy AB donors (AB serum)	German Red Cross Blood Donor Service, Institute Mannheim	
Fetal Bovine Serum (FBS serum)	Gibco	10270-106 (Lot 2Q7096K)
Penicillin/Streptomycin	PAN-Biotech	P06-07100
L-glutamine		P04-80100
Trypsin/EDTA		P10-024100
DMEM		P04-01500
EDTA	Applichem	A3145,0500
DPBS 1X	Gibco	14190-094
Dymethylsuphoxide (DMSO)	Wak-chemie Medical GmbH	WAK-DMSO-10
Ficoll-Paque™ Premium	GE Healthcare Bio-science AB	17-5442-03
RPMI 1640	Lonza	12-918F
IL-2 human recombinant	Promokine	C-61240
Phytoemagglutinin-L (PHA)	Merck Millipore	M5030
Interferron- γ human recombinant	R&D Systems	285-IF
Ham's F-10 media		

Supplement stem cell media	Proprietary formulation TICEBA	
X-Vivo 10	Lonza	BE04-380Q
M-CSF human recombinant	Peprotech	300-25
M-CSF murine recombinant	Peprotech	
Lipopolysaccharide	Sigma Aldrich	
Sarilumab	R&D Systems	MAB10346-SP
GW788388	Cayman Chemical	Cay16255-1
L-161,982		Cay10011565-1
Bindarit		Cay11479-1
DMEM-F12	ThermoFisher	11039047
HBSS	Sigma-Aldrich	H8264
Accutase		
Insulin-Transferrin-Sodium Selenite Supplement (ITS)		11074547001
Epidermal Growth Factor (EGF) human recombinant		E9644
Hydrocortisone		H0135
Triiodothyronine (I3):		T5516
PrestoBlue™ HS	Invitrogen	P50200
Apotracker	Biologend	427401
H ₂ DCFDA	Invitrogen	D399
IncuCyte® pHrodo® Green <i>E. coli</i> Bioparticles®	Essen BioScience	4616
Levodopa (L-DOPA)	Sigma Aldrich	D9628
Collagen Type IV	Sigma Aldrich	C6745

Albumin fraction V (bovine serum albumin)	Carl Roth	8076.2
-------------------------------------------	-----------	--------

3.2.3 Cell culture medium

Media	Composition
MSC Growth Media (Part 1)	500 ml α -MEM
	100,000 U/ml penicillin and 10 mg/ml streptomycin
	4 mM L-glutamine
	10% FBS
MSC Growth Media (Part 2 and 3)	500 ml DMEM
	100,000 U/ml penicillin and 10 mg/ml streptomycin
	4 mM L-glutamine
	10% AB serum
PBMC Media	500 ml RPMI
	100,000 U/ml penicillin and 10 mg/ml streptomycin
	4 mM L-glutamine
	10% FBS
Human Macrophage Media	X-Vivo 10
	25 ng/ml hM-CSF
Rat Macrophage Media	X-Vivo 10
	25 ng/ml mM-CSF
ciPTEC Complete Culture Media (CCM)	500 ml DMEM-F12
	5 μ g/ml Insulin, 5 μ g/ml Transferrin, 5 ng/ml Sodium Selenite
	10 ng/ml EGF
	36 ng/ml Hydrocortisone
	40 pg/ml I3
	10% FBS
	500 ml DMEM-F12

ciPTEC Serum Free Media (SFM)	5 µg/ml Insulin, 5 µg/ml Transferrin, 5 ng/ml Sodium Selenite
	10 ng/ml EGF
	36 ng/ml Hydrocortisone
	40 pg/ml I3
ABCB5+ MSC Media	Ham's F-10 media plus stem cell supplement

3.2.4 Magnetic Cell Separation (MACS)

3.2.4.1 MACS Beads

Products	Company	Catalog Number
Anti- human CD14 microbeads	Miltenyi Biotech	130-050-201
Anti-PE MicroBeads		130-048-801
PE- conjugated human CD11b/c		130-124-893

3.2.4.2 MACS Solutions

Name	Composition
MACS Buffer	500 ml DPBS
	0.5 % BSA
	2 mM EDTA
10X Red Blood Cell Lysis Buffer	Distilled water
	0.1 mM NH ₄ HCO ₃
	1.55 mM NH ₄ Cl
	1 mM EDTA

3.2.5 Flow Cytometry

3.2.5.1 Flow Cytometry Solutions

Name	Composition
FACS Buffer	1 L DPBS
	0.4 % BSA
	0.02 % NaN ₃
	Adjust pH to 7.4

3.2.5.2 Flow Cytometry Antibodies

Antibody	Fluorochrome	Clone	Company	Cat.-No.
Anti-IDO	PE	eyedio	eBioscience	12-9477-42

Anti-STAT3	PE	49/p-Stat3	BD	558557
Extended Human MSC Characterization				
Anti-CD202b	AF488	33.1	BioLegend	334208
Anti-CD31	FITC	WM59	BD	555445
Anti-NG-2	AF488	9.2.27	eBioscience	53-6504-82
Anti-HLA-ABC	PE Vio770	REA230	Miltenyi	130-101-460
Anti-CD49a	AF647	TS2/7	AbD Serotec	MCA1133A647
Anti-CD49b	FITC	P1E6-C5	Biolegend	359306
Anti-CD44	APC Cy7	IM7	Biolegend	103028
Anti-CD90	APC	5E10	BD	559869
Anti-CD73	PE	AD2	Biolegend	344004
Anti-CD45	PE-Cy7	HI30	Biolegend	304016
Anti-CD146	PE	TEA1/34	Beckman Coulter	A07483
Anti-CD34	APC	581	BD	555824
Anti-CD13	APC Cy7	WM15	Biolegend	301710
Anti-CD105	PE Cy7	SN6	eBioscience	25-1057-42
Anti-CD140b	APC	18A2	BioLegend	323608
Anti-CD140a	PE	16A1	BioLegend	323506
Anti-CD248	AF647	B1/35	BD	564994
Anti-CD106	FITC	51-10C9	BD	551146
Anti-HLA-DR	APC Cy7	L243	BioLegend	307618
Anti-CD29	AF488	TS2/16	BioLegend	303016
Anti-CD49f	PE	GoH3	Biolegend	313612
Anti-Integrin β 7	APC	FIB504	Biolegend	321208
Anti-CD49e	PE	NKI-SAM-1	Biolegend	328010
Anti-CD49d	PE Cy7	9F10	Biolegend	304314
Rat MSC Characterization				
Anti-CD90	PE	OX-7	BD	551401
CD44	APC	12K35	LSBio	LS-C182786
Anti-MHCII	VioGreen	REA510	Miltenyi	130-107-870
Anti-CD45	PE Vio770	REA504	Miltenyi	130-124-890
Anti-CD31	FITC	REA396	Miltenyi	130-126-036
Human Macrophage Characterization				

Anti-CD206	PE	19.2	BD	555954
Anti-CD163	BV510	GHI/61	BioLegend	333628
Anti-HLA-DR	PE-Cy7	L243	BioLegend	307616
Anti-CD86	BV421	IT2.2	BioLegend	305426
Anti-CD38	APC Cy7	HB-7	BioLegend	356616
Rat Macrophage Characterization				
Anti-CD11b/c	PE	REA325	Miltenyi	130-124-893
Anti-CD68	APC	REA237	Miltenyi	130-102-725
Anti-CD45	PE Vio770	REA504	Miltenyi	130-124-890
Anti-MHCII	VioGreen	REA510	Miltenyi	130-107-870
Anti-CD31	FITC	REA396	Miltenyi	130-126-036
Anti-CD86	APC Vio770	24F	Miltenyi	130-109-179

3.2.5.3 Flow Cytometry Reagents

Product	Company	Catalog Number
Cell Wash	BD Bioscience	349524
IC Fixation Buffer	eBioscience	00-8222-49
Permeabilization Buffer	Invitrogen	00-8333-56
Cytotell Green	ATT Bioquest	22253
Sytox Blue	Invitrogen	S34857
FcR Blocking reagen (human)	Miltenyi	130-059-901
Fixable Viability Dye eFluor450	Invitrogen	65-0863-14
BD Cytotfix™ Fixation Buffer	BD Bioscience	554655
BD™ Phosflow Perm Buffer III	BD Bioscience	558050*

3.2.6 PCR

3.2.6.1 PCR Array Kits and Reagent

Product	Company	Catalog Number
miRNeasy Kit	Qiagen	217084
RT ² First Strand Kit		330401
RT ² Profiler PCR Array for Nephrotoxicity		330231
RT ² SYBR Green Mastermix		330502

3.2.6.2 qPCR Kits and Reagent

Product	Company	Catalog Number
RNeasy® Mini Kit	Qiagen	74104
SensiFAST™ cDNA Synthesis Kit	Bioline	BIO-65054
SensiFAST™ SYBR® No-ROX Kit	Bioline	BIO-98005
QIAzol Lysis Reagent	Qiagen	79306

3.2.6.3 qPCR Primers

Gene	Primer Sequence (5'-3')	
GADD45A	F	GCTCAACGTAATCCACATTC
	R	GAGATTAATCACTGGAACCC
CDKN1A	F	CAGCATGACAGATTTCTACC
	R	CAGGGTATGTACATGAGGAG
HMOX1	F	CAACAAAGTGCAAGATTCTG
	R	TGCATTCACATGGCATAAAG
ATF3	F	AGAAAGAGTCGGAGAAGC
	R	TGAAGGTTGAGCATGTATATC
GAPDH	F	TCCACTGGCGTCTTCACC
	R	GGCAGAGATGATGACCCTTTT

3.2.7 Immunofluorescence Staining

Product	Company	Catalog Number
Rabbit anti-human connexin-43 Ab	Sigma	C6219
Goat anti-rabbit Ab AF568	Life Technologies	A-11011
DAPI	SantaCruz	SC-300415
Apotracker	Biologend	427401
Mounting medium	Sigma Aldrich	23,472-9
Paraformaldehyde (PFA)	Roth	0335.3

3.2.8 Kits

Kit	Company	Catalog Number
-----	---------	----------------

BD Biosciences StemFlow Human MSC Analysis Kit	BD Biosciences	562245
human TNF- α DuoSet ELISA	R&D Systems	DY210
Rat TNF- α DuoSet ELISA	R&D Systems	DY510
Human IL-6 DuoSet ELISA	R&D Systems	DY206
Human IL-8/CXCL8 DuoSet ELISA	R&D Systems	DY208
CellTiter-Glo® Luminescent Cell Viability Assay	Promega	G7570
Thiol Quantification Assay kit	Abcam	ab112158
ProcartaPlex 22-plex panel	Thermo Fisher Scientific	PPX-22
LEGENDplex™ Human Growth Factor Panel	Biolegend	741061

3.2.9 Other Solutions

Solutions	Composition
Freezing media	FBS
	10 % FBS
PFA 4%	50 ml DPBS
	4% PFA
Tris Buffer	Distilled Water
	10mM Tris Base
	Adjust pH to 8.5
Blocking Solution	10 ml DPBS
	10 % FBS
	0.15 % Triton-X
PBS/EDTA	500 ml DPBS
	2 mM EDTA

3.2.10 Consumable Laboratory Material

Product	Company	Catalog Number
ImageLock 96 well plates	Essen BioScience	4379

Wound maker	Essen BioScience	4563
Transwell inserts 0.4 µm Transparent PET Membrane	Falcon	353095
24-well plate	Falcon	353504
Cell Scraper	VWR	734-2603
20 G needle	Sterican	4657519
Petri dish	Corning	353803
25 cm ² cell culture flasks	Thermo Fisher	156367
75 cm ² cell culture flasks	Thermo Fisher	156499
175 cm ² cell culture flasks	Thermo Fisher	159910
6-well cell culture plate	Thermo Fisher	140675
12-well cell culture plate	Thermo Fisher	150628
24-well cell culture plate	Thermo Fisher	142475
96-well cell culture plate	Eppendorf	0030 790.119
96-well black cell culture plate	Perkin Elmer	6005550
15 ml Cell star tubes	Greiner Bio-one	188271
50 ml Cell star tubes	Greiner Bio-one	227261
10-20 µl sterile filter tips	Star Lab	S1120-3710
200 µl sterile filter tips	SurPhob	VT0243X
1000 µl sterile filter tips	SurPhob	VT0263X
1.25 ml Precision Dispenser (PD) sterile tips	Brand	702386
2.5 ml PD sterile tips	Brand	702388
5 ml PD sterile tips	Brand	702390
10 ml PD sterile tips	Brand	631060
5 ml serological sterile pipettes	Star Lab	180806-069
10 ml serological sterile pipettes	Star Lab	180720-070
25 ml serological sterile pipettes	Star Lab	190105-071
Cell strainer, 70µm	Sarstedt	83.3945.070
Cell strainer, 100µm	Sarstedt	83.3945.100
50 ml syringe	Dispomed	21050
10 ml syringe	Dispomed	20010
5 ml syringe	Braun	4606051

1 ml syringe	BD Biosciences	300013
Rotilabo syringe filters 0.22 µm	Carl Roth	SE2M035I07
Syringe filters 0.45µm	NeoLab	3-1904
0.2 ml thin-walled tubes with flat caps	Thermo Fisher	AB0622
Cryopreservation tubes	Greiner Bio-one	122278
1.5 ml tubes	Eppendorf	0030 125.150
1.6 ml tubes (Low binding, DNA-DNase, RNase free)	Biozym Scientific	710176
5 ml Polystyrene round bottom FACS tubes	Corning	352052
CASY cup	OMNI Life Science	5651794
Gloves	Hartmann	3538071
Pursept A Xpress	Schülke	SMH 230131
Scalpels	Braun	10567364
5 ml Polystyrene round FACS bottom tubes	Corning	352052
PCR plate	Axon	27994
ELISA Plate	RnD Systems	DY990
V-Bottom 96 well plate	Greiner	651201

3.2.11 Laboratory Equipment

Product	Model	Manufacturer
Luminex 200 Multiplex Bead Array		Merck - Millipore
Live Cell Imaging Device	Incucyte SX5	Essen BioScience, Ltd.
Live imaging microscope	IncuCyte Zoom	Essen BioScience, Ltd.
Confocal Microscope	LSM 800	Zeiss
Thermal Cycler	PTC0200	Bio-Rad Laboratories GmbH
Light Cycler	LightCycler® 480	Roche
Centrifuge	ROTINA 420	Hettich Zentrifugen
Centrifuge	ROTINA 420R	Hettich Zentrifugen
Centrifuge	5415R	Eppendorf

Small Centrifuge	Minispin	Eppendorf
Cell counter	CASY	OMNI Life Science
Cell counter	Nucleo Counter	Chemometec
Microscope	Axiovert 100	ZEISS
Microscope	Axiovert 40C	ZEISS
Microscope Camera	AxioCam M Rc	ZEISS
Live imaging microscope	IncuCyte Zoom live imaging device	Essen BioScience, Ltd.
Sterile laminar flow hood	Hera safe	Thermo Fisher Electron Cooperation
Chemical flow hood	Airflow-Control EN14175	Caspar and Co. Labora
Cell culture incubator	CB210	Binder
Cell culture pump	Vacunsafe Comfort	Integra Biosciences
Cell culture shaker	Lab Dancer	IKA
Water bath	WNE 7	Memmert
Magnet stirrer	MR Hei-Standard	Heidolph Instruments
pH-Meter	pH 211	Hanna Instruments
Microplate reader	TECAN infinite M200PRO	TECAN
Thermal cycler	DNA Engine Cycler	BioRad
Flow cytometer	BD FACS Canto II	BD Biosciences
Flow cytometer	FACS Aria IIu	BD Biosciences
Chemiluminescent detector	FusionCapt Advanced Solo 4	Vilbert Lourmat
Horizontal shaker	Thermo Mixer C	Eppendorf
Rotator	SB2	Stuart
Chamber shaker	UniHood 650	Edmund Bühler
Precision scale	EW 2200-2NM	Kern & Sohn
Precision scale	ABJ 22-4M	Kern & Sohn
Flow cytometer	BD FACS Canto II	BD
Plate washer	Well wash 4MK2	Thermo Fisher
Cell culture incubator		Binder
Nitrogen tanks	Biosafe UN 1977	Cryotherm
Autoclave	V-150	Systec

Zetaview	PMX 220 ZetaView TWIN Laser	Particle Metrix
----------	--------------------------------	-----------------

3.2.12 Software for Data Analysis

Software	Version	Company
FlowJo	10	FlowJo, LLC, Ashland, OR, USA
GraphPad Prism	9	GraphPad Software Inc. San Diego, USA
FIJI Image-J		NIH
Zen		Zeiss
IncuCyte 2020B Software		Essen BioScience, Ltd.
IncuCyte ZOOM 2018A		Essen BioScience, Ltd.
LEGENDplex™ Data Analysis Software		BioLegend
i-Control	1.10	TECAN
Luminex xPonent	3.1	DiaSorin
GeneGlobe Data Analysis Center		Qiagen

3.3 Methods

The methods are described according to the parts explained in section 2.

3.3.1 Part 1: Assessment of inter-laboratories and tissue of origin in MSC profile

The general workflow of the first part of this thesis can be seen in **Figure 4**. MSCs for adipose tissue, bone marrow, and umbilical cord blood were first isolated in University of Heidelberg (UHEI), National University of Ireland, Galway (NUIG), and the University of Liverpool (UOL), respectively. These MSCs were then expanded in the respective centres, cryopreserved, and internationally shipped to the other centres. Once all the centres received all the MSC types, the inter-laboratory comparison of MSC basic characterization began concomitantly. In addition to the basic characterization, we also compared the immunomodulatory of MSCs across the MSC sources.

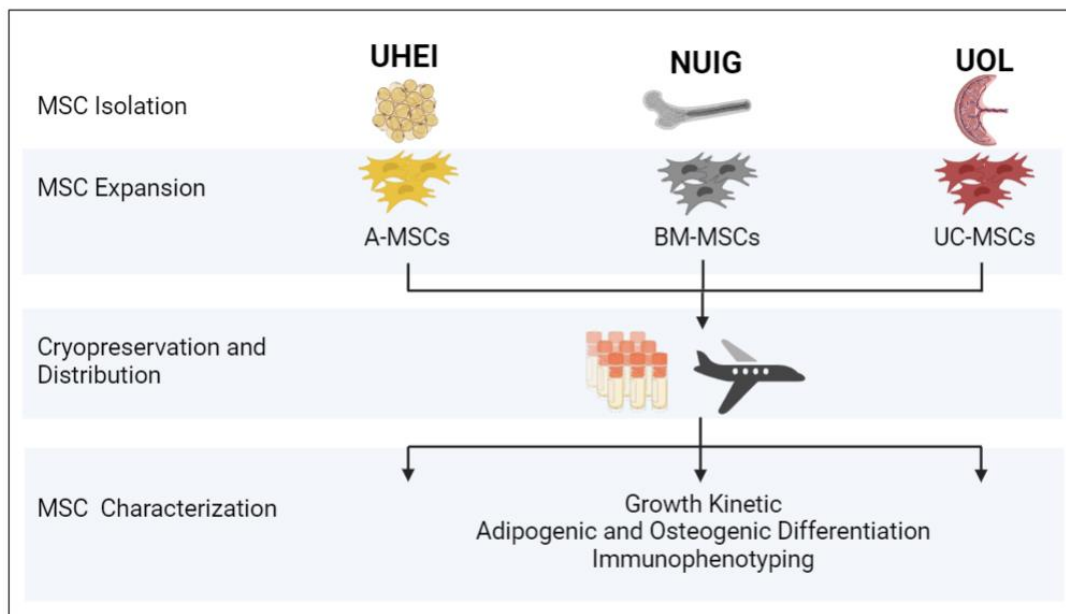


Figure 4. The scheme of inter-laboratory comparison for MSC basic characterization.

A-, BM-, and UC-MSCs were isolated in UHEI, NUIG, and UOL, respectively according to the protocol used in each site. The MSCs were expanded and cryopreserved using standardized protocol and shipped internationally to the rest of the sites. MSC characterization was performed in all centres using the standard protocol to evaluate the growth kinetic, adipogenic and osteogenic differentiation, and immunophenotype of the MSCs. This image was created using BioRender.

3.3.1.1 A-MSCs Isolation and Culture

A-MSCs were isolated from lipoaspirate of healthy donors after informed consent was given ((Mannheim Ethics Commission II; vote numbers 2006-192 N-MA). Raw lipoaspirate was briefly washed using DPBS to remove red blood cells and cellular debris by

centrifugation at 420 xg for 10 minutes. The lipoaspirate was then diluted with DMEM in 1:1 ratio containing NB6 collagenase to a final concentration of 0.15 PZU/ml and left for incubation at 37° C for 50 minutes with gentle agitation. Following the incubation, collagenase was inactivated by adding equal amount of DMEM 10% FBS. The lipoaspirate mixture was then centrifuged at 1200g for 10 minutes to obtain the high-density stromal vascular fraction (SVF). The supernatant was discarded, while the pellet was incubated with red blood cell lysis buffer for 10 minutes at room temperature and centrifuged once more. After the centrifugation, the SVF pellets were resuspended in empty DMEM, filtered through a 100 µm nylon mesh filter, and centrifuged again. The remaining SVF pellet was then resuspended with DMEM AB and transferred to T25 or T75 flask, depending on the pellet size. The SVF was then incubated overnight at 37°C, 5% CO₂, before being subjected to an extensive wash using DPBS the following day, to remove non-adherent red blood cells. The culture was monitored closely and the media was refreshed twice per week until the A-MSC colonies appeared. The resulting growing A-MSC colonies were then harvested and seeded with density of 300 cells/cm² in a fresh culture flask.

Once the A-MSCs reach 70-80% confluence, the cells were detached with Trypsin/EDTA, counted by CASY cell counter and reseeded again with the same density for expansion or used for further experiment.

3.3.1.2 A-MSCs Expansion and Cryopreservation

For the inter-laboratory comparison study, A-MSCs were cultured under α-MEM 10% FBS and expanded up to passage 3 under the same seeding density. Once the culture reached 70-80 % confluence, the cells were harvested with Trypsin/EDTA, resuspended, and cryopreserved in FBS 10% DMSO. The cryovials were then stored in liquid nitrogen before being shipped internationally to the UOL and NUIG in dry ice.

3.3.1.3 A-, BM-, and UC- MSC Basic Characterization

While we isolated and sent A-MSCs to the other institutes, BM- and UC-MSCs were isolated and sent by UOL and NUIG, respectively. Upon receiving all the MSC type, the basic characterization was done simultaneously in each institute. Basic MSC characterization was performed as per the criteria set by ISCT. The characteristics of MSCs were then compared between the centres and between the tissue sources.

3.3.1.3.1 Growth Kinetics

Upon receiving BM- and UC-MSCs, all the MSC types were thawed and seeded in α -MEM 10% FBS for at one passage before calculating their growth kinetic. Once the cells recovered from the cryopreservation, the cells were seeded at 300 cells/cm², for A-MSCs and 3000 cells/cm² for BM- and UC-MSCs. The population doublings (PDs) and population doubling times (PDTs) were calculated by counting the cell number at every passage for three consecutive passages. The PDs and PDTs were then calculated with the following formula:

$$\text{Population Doublings (PDs)} = \frac{\log_{10} (F_{cn}) - \log_{10}(I_{cn})}{\log_{10}(2)}$$

$$\text{Population doubling times (PDTs)} = \frac{\text{culture duration}}{\text{PD}}$$

With F_{cn} and I_{cn} indicated final and initial cell number of each passage, respectively. The morphology of the cells was also monitored closely.

3.3.1.3.2 Adipogenic Differentiation

To assess the MSC capacity to differentiate into adipocytes, the cells were first seeded at a density of 5,700 cells/well in 96-well plate. After 48 hours, the differentiation was induced using Adipogenic Differentiation Medium 2 for 14 days and the medium was refreshed twice per week. MSCs cultured with normal growth medium, α -MEM 10% FBS, served as negative control.

After two weeks, the cells were fixed using 4% of PFA for 30 minutes at room temperature, washed and incubated with 10 mg/ml Hoechst for another 30 minutes in the dark. Hoechst fluorescence was measured using a plate reader (excitation/emission: 354/442 nm) and used to normalize the value obtained from the following AdipoRed Assay. After briefly washed with DPBS, 5 μ l of AdipoRed was added into each well containing 200 μ l of DPBS and incubated for 15 minutes, protected from light. Following the incubation, the fluorescence of AdipoRed was read on microplate reader at excitation/emission: 485/572 nm. The AdipoRed signal was then normalized with Hoechst signal and presented and the fold-change of undifferentiated negative control.

3.3.1.3.3 Osteogenic Differentiation

Osteogenic differentiation of MSCs was performed by seeding the cells in 96-well plate in density of 2,900 cells/well, before the treatment using Osteogenic Differentiation

Medium 48 hours afterwards. The differentiation was done for 14 days and the media was replenished twice per week. The cells cultured under normal α -MEM 10% FBS were used as negative control.

Upon 14 days of differentiation, the cells were fixed and stained with Hoechst as described above. The measurement of osteogenic differentiation was done as per the manufacturer's manual. The cells were first washed briefly with Wash Buffer and incubated with Osteoimage staining solution (1:100 dilution in Staining Reagent Dilution Buffer) for 30 minutes at room temperature. Upon the incubation, the staining solution was discarded and the cells was washed three times, before measuring the fluorescence on a plate reader at excitation/emission: 492/520 nm. The Osteoimage signal was then normalized with Hoechst signal and presented and the fold-change of negative control.

3.3.1.4 Immunophenotypic Characterization

Once the MSCs reach 70-80 % confluency, the cells were harvested and washed once with DPBS. 10^5 of MSCs were transferred into FACS tubes and resuspended with 100 μ l FACS Buffer. 10 μ l of FcR blocking reagent was added into each tube and incubated at 4 $^\circ$ C for 5 minutes. The analysis of MSC immunophenotype was performed using BD Stemflow™ Human MSC Analysis Kit according to the manufacturer's instruction. The cells in the FACS tube was stained with the following antibody: FITC Anti-Human CD90, PE Anti-Human CD44, PerCP-Cy™5.5 Anti-Human CD105, APC Anti-Human CD73, h-MS C Positive Isotype Control Cocktail, PE h-MS C Negative Isotype Control Cocktail, h-MS C Positive Cocktail, PE h-MS C Negative Cocktail. The MSCs were incubated with the antibodies for 30 minutes in the dark before washed twice with Cell Wash and measured on FACS Canto. A total of 10^4 cells were assessed and the obtained .fcs files were then analyzed using FlowJo to generate the percentage of positive cells for given surface markers.

3.3.1.5 MSC Immunomodulatory Analysis

3.3.1.5.1 PBMC Proliferation Assay

For the first part of this dissertation, the immunomodulatory capacity of MSCs was investigated on their ability to inhibit PBMC proliferation in a direct co-culture upon PHA stimulation. 10^4 cells/well of A-, BM-, and UC-MSCs were seeded with α -MEM 10% FBS media in 96-well plate a day prior to the co-culture to allow the cell attachment to the bottom of the well. The next day, cryo-preserved PBMCs, that were previously

isolated from leukapheresis samples from healthy donors, provided by the German Red Cross Blood Service in Mannheim (Mannheim Ethics Commission; vote number 2018-594N-MA), were thawed and washed with DPBS to remove the residual DMSO. The cells were then labelled with proliferation dye Cytotell Green (1:500 dilution of stock solution) and incubated at 37° C for 30 minutes. Afterwards, the cells were washed 3x with DPBS and resuspended in RPMI 10% FBS media in the presence of 200 U/ml IL-2. Once resuspended, 10⁵ PBMCs were added into the well containing pre-seeded MSCs to obtain 1:10 MSCs:PBMCs ratio. To stimulate proliferation, PHA was added to the culture to a final concentration of 4.8 µg/ml. PBMCs cultured alone with and without PHA served as positive and negative control, respectively. The co-cultures were kept for five days at 37°C, 5% CO₂, before the PBMCs were harvested by transferring the non-adherent cells into the FACS tube. Upon washing step with Cell Wash once, the PBMCs were resuspended in FACS Buffer. The proliferation of PBMCs was measured based on the Cytotell Green dye dilution acquired using FACS Canto II. The .fcs files were later on analysed with FlowJo Software.

3.3.1.5.2 IDO measurement of IFN-γ-treated MSCs

Since previous study in our lab has shown that the inhibition of T-cell proliferation by MSCs was mediated through IDO-tryptophan axis (ATC Paper), we sought to evaluate the IDO production of interferon-γ (IFN-γ) stimulated MSCs. All the MSC type were seeded in α-MEM 10% FBS with density of 5000 cells/cm² and left overnight allow cell attachment. The next day, the media was changed with the α-MEM 10% FBS containing 25 ng/ml IFN-γ. The IFN-γ treatment lasted for 24 hours and the cells were harvested thereafter. Of note, MSCs cultured in the absence of IFN-γ served as negative control.

Once MSCs were harvested and washed once with DPBS, the cells were incubated with Fixable Viability dye eF450 (1:4000 final dilution) for 30 minutes at 4°C. The cells were then fixed by incubating them with IC Fixation Buffer for 30 minutes at room temperature, followed by two washing steps with 1X Permeabilisation Buffer. Afterwards, the cells were stained with PE-conjugated anti-IDO antibody in 1X Permeabilisation Buffer for 30 minutes and washed twice. The cells were then subjected to flow cytometry using FACS Canto II and the .fcs files were analysed using FlowJo. The results are presented as both percentage of positive cells and Median Fluorescence Intensity (MFI).

3.3.2 Part 2: The immunomodulatory capacity of MSCs in xenogeneic setting

In the second part of this dissertation, human MSCs (h-MSCs) evaluated included A-MSCs and ABCB5+ MSCs. We deemed it important to include ABCB5+ MSCs in this study because the cells are clinical grade and manufactured under Good Manufacturing Practice (GMP) compliance. Furthermore, ABCB5+ MSCs are currently being tested on multiple clinical trials (Phase I/II and Phase III) (Ref). In addition to h-MSC, r-MSCs, provided were also used as comparison to this study. The immunomodulatory of MSCs were assessed by harnessing their secretome in their conditioned medium (CM) (**Figure 5**). These CM were then used to culture macrophages obtained from human and rat to investigate the macrophage phagocytosis and TNF- α upon LPS stimulation.

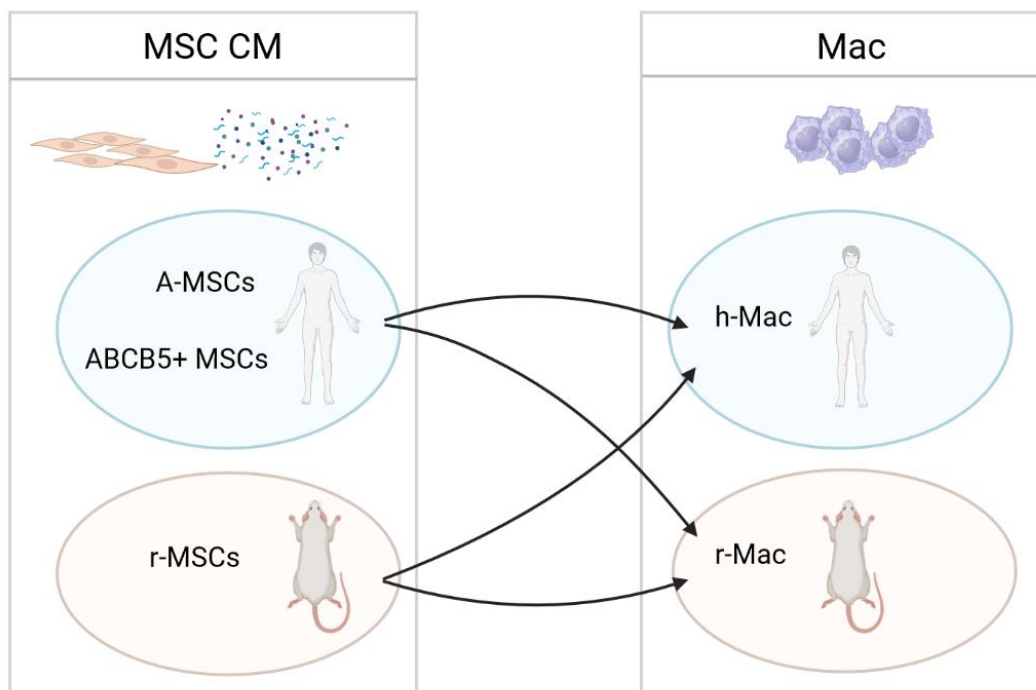


Figure 5. The workflow of immune-compatibility study to investigate MSC-CM on macrophage polarization in xenogeneic setting.

CM from human and rat MSCs were tested upon macrophages from human and rats. This image was created using BioRender.

3.3.2.1 MSC Characterization and CM Production

3.3.2.1.1 A- and ABCB5+ MSC Extended Immunophenotypic Characterization

An extended panel of surface marker characterization was performed to better understand the possible discrepancy between A- and ABCB5+ MSCs. While A-MSCs were harvested from on-going culture, ABCB5+ MSCs were freshly thawed from cryovials

kindly provided by TICEBA/RHEACELL. A long-term culture of ABCB5+ MSCs was not possible since the cells might lose their distinguished characteristic, the ABCB5+ expression on their plasma membrane (Ref). Once the A- and ABCB5+ MSCs were harvested or thawed and washed, the cells were incubated with FcR Blocking solution (1:10 dilution) at 4°C for 5 minutes. The cells were then stained with the following anti-human antibodies: anti-CD31-FITC, anti-HLA-ABC-PE Vio770, anti-CD49a-AF647, anti-CD49b-FITC, anti-CD44-APC Cy7, anti-CD90-PC, anti-CD73-PE, anti-CD45-PE-Cy7, anti-CD146-PE, anti-CD34-APC, anti-CD13-APC Cy7, anti-CD105-PE Cy7, anti-CD140b-APC, anti-CD248-AF647, anti-HLA-DR-APC Cy7, anti-CD49f-PE, anti-CD49e-PE, and anti-CD49d-PE Cy7. The cells were incubated with the antibodies for 20 minutes in the dark at 4°C, before being washed once and resuspended with FACS buffer containing SYTOX blue dead cell stain (1:2000 final dilution). The data from 10⁴ viable cells were acquired with FACS CANTO II. The .fcs data were then analyzed with FlowJo Software to obtain the MFI of each surface marker.

3.3.2.1.2 Production of CM for macrophage culture

Prior to the conditioned media (CM) production, A-MSCs, and r-MSCs between passage 4-6 were cultured in DMEM AB and DMEM 10% FBS, respectively, until they reached 80-90% confluence. The cell monolayer was then washed twice with DPBS and incubated with macrophage basal medium, X-Vivo 10 without any supplement for 24h at 37°C and 5 % CO₂. Following the incubation, the CM was transferred into 50 ml conical tube and centrifuged at 2000 xg, 4°C for 10 minutes and filtered through 0.22 µm PES filter to ensure debris removal. The CM was then aliquoted and stored in -80°C freezer for further use.

For CM production of ABCB5+ MSCs, frozen cells were thawed, and seeded at a density of 2.5 x 10⁴ cells/cm² in ABCB5+ MSC Media and left overnight to allow cell attachment. The adherent cells were washed 2x with DPBS, then the media was replaced or X-Vivo 10. The media was conditioned for 24h and processed as described above.

3.3.2.2 Macrophage Assay

3.3.2.2.1 Human monocyte isolation and culture

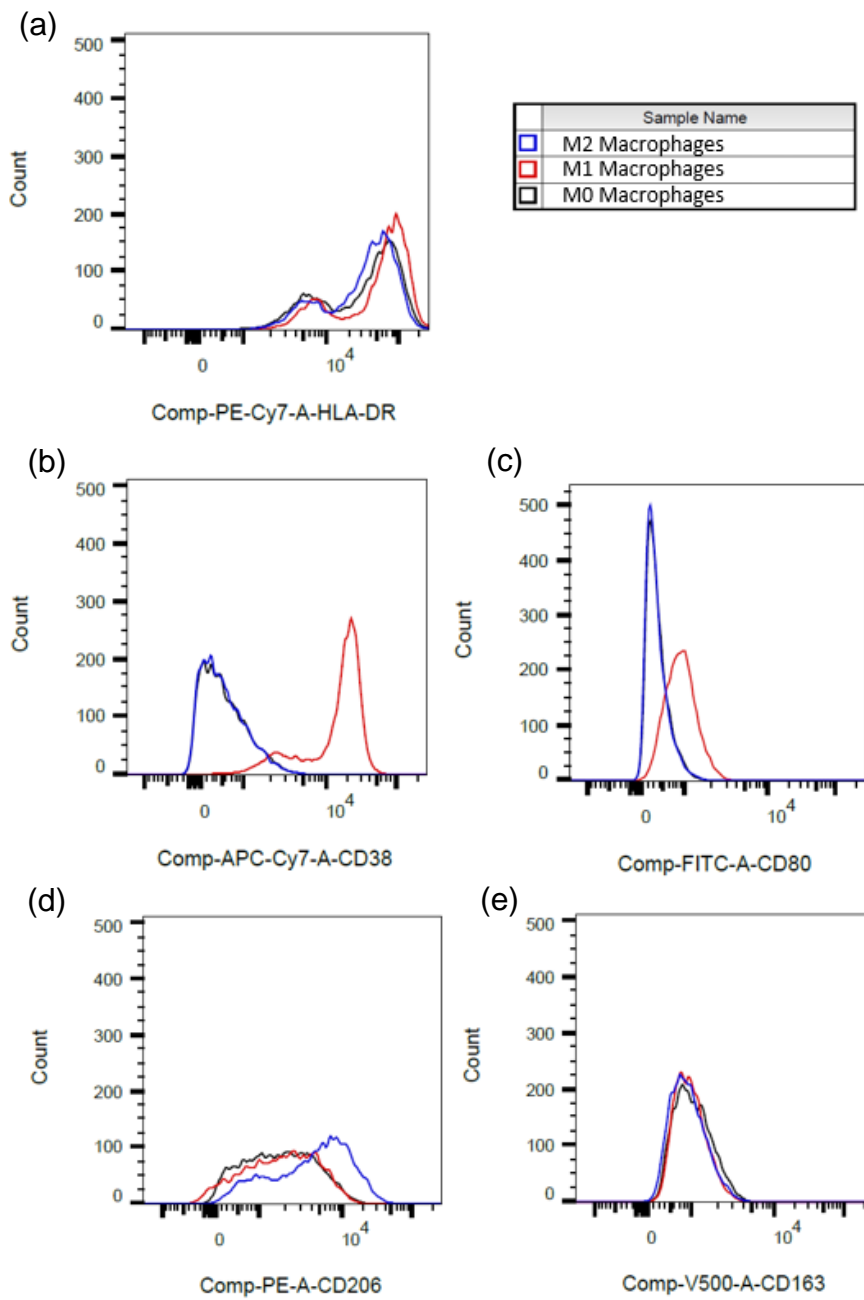
Human monocytes were isolated from buffy coats, provided by German Red Cross Blood Donor Service in Mannheim, Germany, from healthy donors after obtaining informed consent. The buffy coats were first subjected to gradual centrifugation to isolate PBMCs. The buffy coats were diluted in PBS/EDTA with ratio of buffy coat:PBS/EDTA

1:2. 35 ml of buffy coats mixture was then gently overlaid on top of 15 ml Ficoll in 50 ml canonical tube. The tubes were centrifuged in a swing bucket centrifuge for 30 min 420 xg at room temperature with low acceleration and no brake. Once the centrifugation is done, the interface between the plasma and Ficoll phase containing the PBMCs were aspirated and transferred into a fresh tube. The PBMCs were then washed three times with PBS/EDTA, first, by centrifugation in 200 xg for 15 minutes to remove platelets, followed by two more times centrifugation in 420 xg for 10 minutes. The total PBMC number was counted using CASY cell counter.

CD14⁺ monocytes were then isolated from the PBMC preparation using magnetic cell separation (MACS). The cells were first resuspended with 80 µl MACS Buffer and incubated with 20 µl human-anti CD14 microbeads for every 10⁷ PBMCs. The incubation was done at 4° C for 15 minutes with gentle agitation. Following the incubation, the cells were washed with once and resuspended in 1 ml cold MACS buffer. In the meantime, an LS column was placed on the magnetic stand and calibrated with 3 ml MACS Buffer. Once, there was no more MACS buffer dripping from the column, the cell suspension was passed through the column. After the cell suspension has passed through, the column was washed with 3 ml MACS buffer for three times to remove the unlabeled cells. After the buffer stopped dripping, the column was then removed from the magnet by pulling it with laterally and gently. The column was transferred into a fresh 15 ml canonical tube. The CD14⁺ monocytes were recovered from the column by rinsing it with 5 ml of MACS buffer using the plunger. The isolated monocytes were washed with MACS buffer once and counted with CASY cell counter. The monocytes were sampled for purity check using flow cytometry. To obtain unpolarized macrophages, the monocytes were cultured in X-Vivo 10 supplemented with 10 ng/ml human M-CSF in density of 10⁶/ml for 6 days without media change.

As proof of concept, we also check the macrophages' ability to polarize by changing their medium with fresh X-Vivo 10 containing 20 ng/ml IFN-γ or 25 ng/ml IL-4 plus 25 ng/ml M-CSF to induce M1 or M2 polarization. After 24h culture with the polarizing medium, macrophages were harvested and their surface markers were measured using FACS as described in **Section 3.2.3.2.1**. As seen in Figure 6, IFN-γ induced M1 polarization as marked by higher HLA-DR (**Figure 6a**), CD38 (**Figure 6b**), and CD80 (**Figure 6c**), as compared to unpolarized and M2 polarized macrophages. Meanwhile, IL-4 stimulated M2 polarization by increasing CD206 expression (**Figure 6d**), but not CD163 (**Figure 6d**). Nonetheless, macrophages undergoing M2 polarization showed

remarkable increase of phagocytosis (**Figure 6f**). In conclusion, our macrophages have the plasticity to polarize into M1 and M2 macrophages.



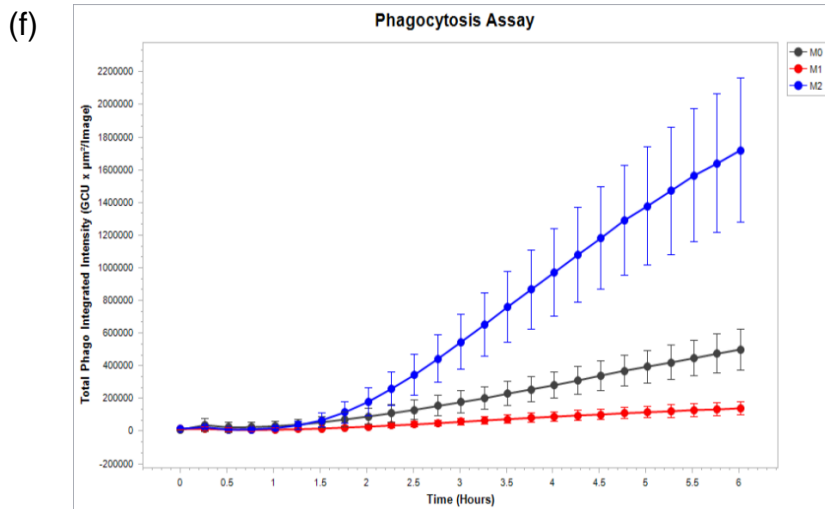


Figure 6. The expression of surface markers and phagocytic capacity of h-Mac after polarization.

Following the isolation, monocytes were seeded in X-Vivo 10 supplemented with 10 ng/ml of M-CSF for 6 days without media change. On the sixth day, the media was changed with fresh X-Vivo 10 containing either 10 ng/ml M-CSF to induce resting macrophage or M0, 20 ng/ml IFN- γ to induce M1 polarization, or 25 ng/ml IL-4 plus 25 ng/ml M-CSF to induce M2 polarization. After 24h of polarization, both adherent and non-adherent cells were harvested and subjected to FACS to measure expression of HLA-DR (a), CD38 (b), CD80 (c), CD206 (d), and CD163 (e). The phagocytosis of these macrophages was monitored for 6 hours after polarization using live cell imaging (f).

3.3.2.2.2 Rat monocyte isolation and culture

The rat monocytes were isolated from bone marrow-derived PBMCs. The rats were kindly provided by Prof. Benito Yard from healthy control animal. After extracting the femurs of the rats, both edges of the bone were cut and the bone marrow was flushed out with PBS/EDTA. The bone marrow suspension was then passed through 100 μ m cell strainer to remove any debris. The suspension was topped up with PBS/EDTA until to 50 ml of volume and centrifuged in 420 xg for 10 minutes at room temperature. After removing the supernatant, the pellet was resuspended in 1x RBC Lysis Buffer and incubated for 10 minutes at room temperature. Following the incubation, the cells were washed three times in PBS/EDTA by centrifugation. The cell number of mononuclear cells were determined using CASY cell counter.

Upon the isolation of bone marrow mononuclear cells, the isolation of CD11b/c⁺ monocytes was performed with MACS. First, the cells were labelled with primary PE-conjugated anti-CD11b/c antibody (10 μ l antibody in 100 μ l MACS buffer for every 10⁷ cells) and incubated for 10 minutes at 4^o C in the dark. Following the incubation, the

unbound antibody was washed by adding 1-2 ml MACS buffer per 10^7 cells and centrifugation at 300 xg for 10 minutes. After discarding the supernatant, the pellet was resuspended in 80 μ l per 10^7 cells. 20 μ l of anti-PE microbeads was added to the cell suspension for every 10^7 cells, followed by another incubation at 4° C in the dark for 15 minutes. Once the incubation finished, the cells were washed with MACS buffer once and the pellet was resuspended in 500 μ l MACS buffer. In the meantime, an LS column was prepared on the magnetic stand and calibrated with 3 ml of MACS buffer. Upon the calibration, the cell suspension was applied onto the column, followed by three time washing with MACS buffer. After ensuring there was no more buffer dripping, the LS column was removed from the magnetic stand and transferred into a new 15 ml canonical tube. Finally, 3 ml of MACS buffer was added to the column and the CD11b/c expressing monocytes were recovered by flushing them out using the plunger. The monocytes were washed once more and counted using CASY cell counter.

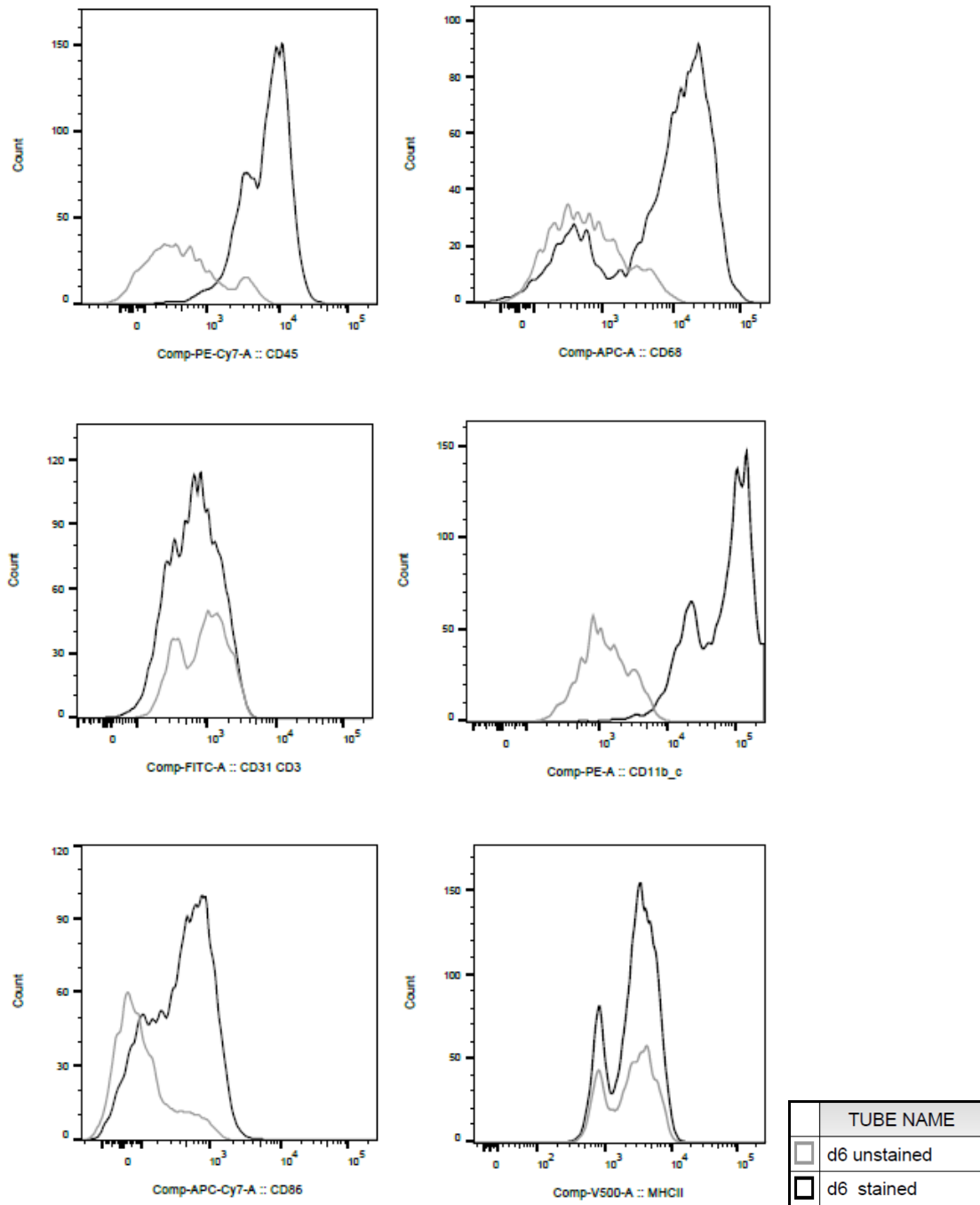


Figure 7. FACS-based characterization of r-Mac after 6 days of culture.

Following monocyte isolation, the cells were cultured for 6 days in X-Vivo 10 supplemented with 25 ng/ml murine M-CSF. Both adherent and non-adherent cells were harvested and subjected to FACS to measure their surface markers.

The purity check was done by flow cytometry, while the rest of the cells were seeded for macrophage culture. Unpolarized macrophages were obtained by culturing monocytes in X-Vivo 10 supplemented with 25 ng/ml murine M-CSF in density of 10^6 /ml for

6 days without media change. After 6 days of culture, the r-Mac were harvested and subjected to FACS to measure their surface markers (**Figure 7**).

3.3.2.2.3 CM treatment of macrophages

The CM obtained from all three, A-, ABCB+, and r-MSCs, each of which from 3 different donors, were used to treat both human (h-MAC) and rat macrophages (r-MAC). The treatment was begun after the monocyte isolation and lasted for the entire maturation of monocyte into macrophages. 10^5 human or rat monocytes were seeded in 96-well plate in CM supplemented with 10 ng/ml or 25 ng/ml human or murine M-CSF, respectively. The monocytes were then cultured for 6 days without media change until they matured into macrophages. Human or rat monocytes cultured in X-Vivo 10 supplemented with 10 ng/ml or 25 ng/ml human or murine M-CSF served as control. Monocytes were plated in three wells per condition.

3.3.2.2.4 LPS treatment of macrophages and SN Isolation

To stimulate pro-inflammatory response of the macrophages, lipopolysaccharides (LPS) from *E. coli* were added into the macrophage culture after 6 days of culture. LPS was added into each well to a final concentration of 100 ng/ml without media change. After 24 hours of LPS stimulation, the culture supernatant (SN) was harvested and centrifuged at 420 xg for 10 min and stored in -80° C for TNF- α measurement using ELISA. The macrophages without LPS stimulation were used as negative controls. Of note, the confluence (%) of the cells after 24 hours of LPS stimulation was determined using Incucyte XS5 and used to normalized the level of TNF- α .

3.3.2.2.5 Phagocytosis Assay

To assess the macrophage phagocytic function after the CM treatment, 5 μ g/ml PHrodo-conjugated *E. coli* bioparticle was added into each well on day 6 after the treatment had begun. Once the bioparticle was added, the plate was gently swirled to ensure that the bioparticles was distributed evenly. The plate was then placed inside a live-cell imaging device, Incucyte XS5, and scanned every 15 min for a total of 6 hours. The integrated intensity of green fluorescence (GCU $\times\mu$ m²/image) representing the cells phagocytosing the bioparticle was normalized by cell confluence (%) and presented as fold change to control group (**Figure 8**).

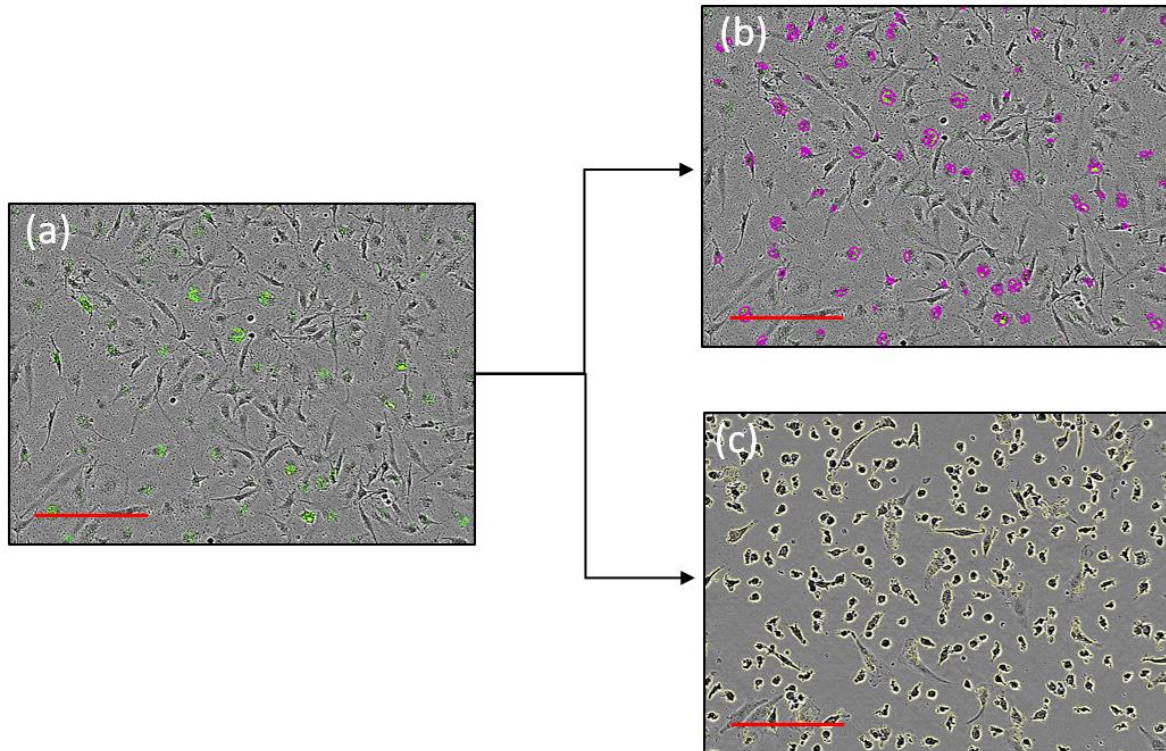


Figure 8. Phagocytosis assay analysis.

Representative image of phagocytosing macrophage, as indicated by green fluorescence, after the addition of pHrodo-labeled *E. coli* bioparticles (a). Representative image of the mask detecting phagocytosis which is used to quantify the integrated intensity of green fluorescence (b). Representative image of the mask detecting cell confluence prior to the addition of bioparticles (c).

3.3.2.2.6 Investigation of Key Mediators in CM

To investigate the key factors by which CM exerts immunomodulatory function on macrophages, we inhibited the known factors that are present in the CM. For this experiment the CM from 3 different donors of each MSC type were pooled. After monocyte isolation, the cells were seeded in the presence of absence of CM containing the inhibitors and cultured for the entire maturation process (6 days). The inhibitors and their concentration used in this experiment are listed in Table 1 below.

Table 1. Inhibitors of MSC factors on macrophages used in this study

Inhibitor	Inhibited Factor	Concentration
Anti-Interleukin-6 (IL-6) receptor- α antibody Sarilumab	IL-6	0.4 μ g/ml
GW788388	Transforming Growth Factor- β 1 (TGF- β 1)	2.5 μ M

L-161,982	Prostaglandin E ₂ (PGE-2)	20 µM
Bindarit	Monocyte Chemoattractant Protein-1 (MCP-1)	18.75 µM

The macrophages cultured without the inhibitor in the absence and presence of CM were used as controls. After the inhibition treatment for 6 days, the phagocytosis of h- and r-MAC was assessed.

3.3.3 Part 3

3.3.3.1 Pro-regenerative effect of A-MSC-CM on cisplatin-treated ciPTECs

3.3.3.1.1 ciPTEC culture

Conditionally immortalized proximal tubular epithelial cells 14.4 (ciPTECs) were purchased from Cell4Pharma and cultured as described previously⁷⁹. ciPTECs were grown in complete culture medium (CCM) with seeding density of 1×10^4 – 1.5×10^4 cells/cm² and kept in 33 °C and 5% (v/v) CO₂ incubator. The media was replenished twice every week. ciPTECs up to passage 50 were used for experiments.

When used for experiments, confluent culture of ciPTECs were detached and harvested using accutase and seeded in 48,000 cell/cm² density. The seeded ciPTECs were then returned to 33 °C and 5% (v/v) CO₂ incubator overnight to allow cell attachment, before being moved to 37 °C with 5% (v/v) CO₂ incubator for maturation. The media was change twice per week. After seven days of maturation, ciPTECs were ready for treatments.

3.3.3.1.2 Development of *in vitro* injury model using ciPTECs using cisplatin

To establish an *in vitro* model of cisplatin-induced AKI, we first treated matured ciPTECs with cisplatin in the concentration ranging from 15 – 250 µM in serum-free medium (SFM) for 24 hours. After 24 hours, ciPTECs viability, ATP content, and migratory capacity were assessed as described on the following sections.

3.3.3.1.3 Viability Assay (Presto Blue)

Viability of ciPTECs was assessed by measuring the conversion of resazurin to fluorescent resorufin using PrestoBlue probe. The assay was done as per the manufacturer's instruction. After cisplatin treatment, 10 µl of PrestoBlue was added into each well containing 100 µl of media. The cells were incubated at 37 °C for 10 minutes and the fluorescence was measured using microplate reader Tecan at excitation/emission:

560/590 nm. The results are presented as the fold-change to the healthy untreated ciPTECs.

3.3.3.1.4 ATP Assay

The intracellular ATP content of ciPTECs was also measured to determine the toxicity of cisplatin. The ATP measurement was assessed using CellTiter-Glow® as per the manufacturer's instruction. CellTiter-Glow® substrate was first reconstituted with CellTiter-Glow® buffer to obtain the CellTiter-Glow® reagent. Before the assay started, the CellTiter-Glow® reagent and the cell culture plate were equilibrated at room temperature for at least 30 minutes. Next, the CellTiter-Glow® reagent was added into the cell culture with the same volume as the media in each well. The plate was placed on an orbital shaker for 2 minutes to induce cell lysis. Then the plate was kept at room temperature for 10 minutes to stabilize the luminescent signal. The luminescence was then measured using a Tecan microplate reader. The results are presented as the fold-change to the healthy untreated ciPTECs.

3.3.3.1.5 Wound Scratch Assay

The effect of cisplatin and CM treatment on ciPTEC migratory capacity was assessed by wound scratch assay. After 24 hours of cisplatin treatment, ciPTEC monolayer seeded in ImageLock 96-well plate was scratch using wound maker. The old medium were then immediately aspirated and the cells were washed once with HBSS. After the washing step, 100 µl fresh ciPTEC SFM was then added into each well. The plate was then placed using live-cell imaging, Incucyte ZOOM and the migration of ciPTECs to close the scratch was monitored for the next 3 days with 3 hours of scan interval. The closing of the wound is presented in relative wound density.

3.3.3.1.6 Cisplatin and CM Treatment on ciPTECs

Once the cisplatin-induced injury model was established, we proceeded by testing whether or not CM can ameliorate cisplatin toxicity on ciPTECs. First, ciPTECs were incubated with 15 µM cisplatin in SFM for 1 hour, following media change CM containing 15 µM cisplatin. The cells were then cultured for additional 23 hours. ciPTECs cultured in SFM in the absence and presence of cisplatin served as untreated (UT-CTRL) and cisplatin-treated control (cis-CTRL). After a total of 24 hours after the cisplatin treatment started, the cells were subjected for further assessment.

3.3.3.1.7 Apoptosis Assay

Apoptosis assay started after 24 hours of cisplatin treatment and lasted for another 3 days following the cisplatin removal from the medium. First, cisplatin-containing media was discarded and the cells were washed once with HBSS. Upon washing, the CTRL and CM medium containing 40 nM Apotracker was added into each well. The apoptosis of the cells was monitored for 3 days after the cisplatin-containing medium was discarded using live-cell imaging, Incucyte SX5. Total integrated intensity of green fluorescence ($\text{GCU} \times \mu\text{m}^2/\text{image}$) representing apoptotic ciPTECs was then normalized by cell confluence (%) and presented as relative value to cisplatin-treated ciPTEC in SFM (cis-CTRL) (**Figure 9**).

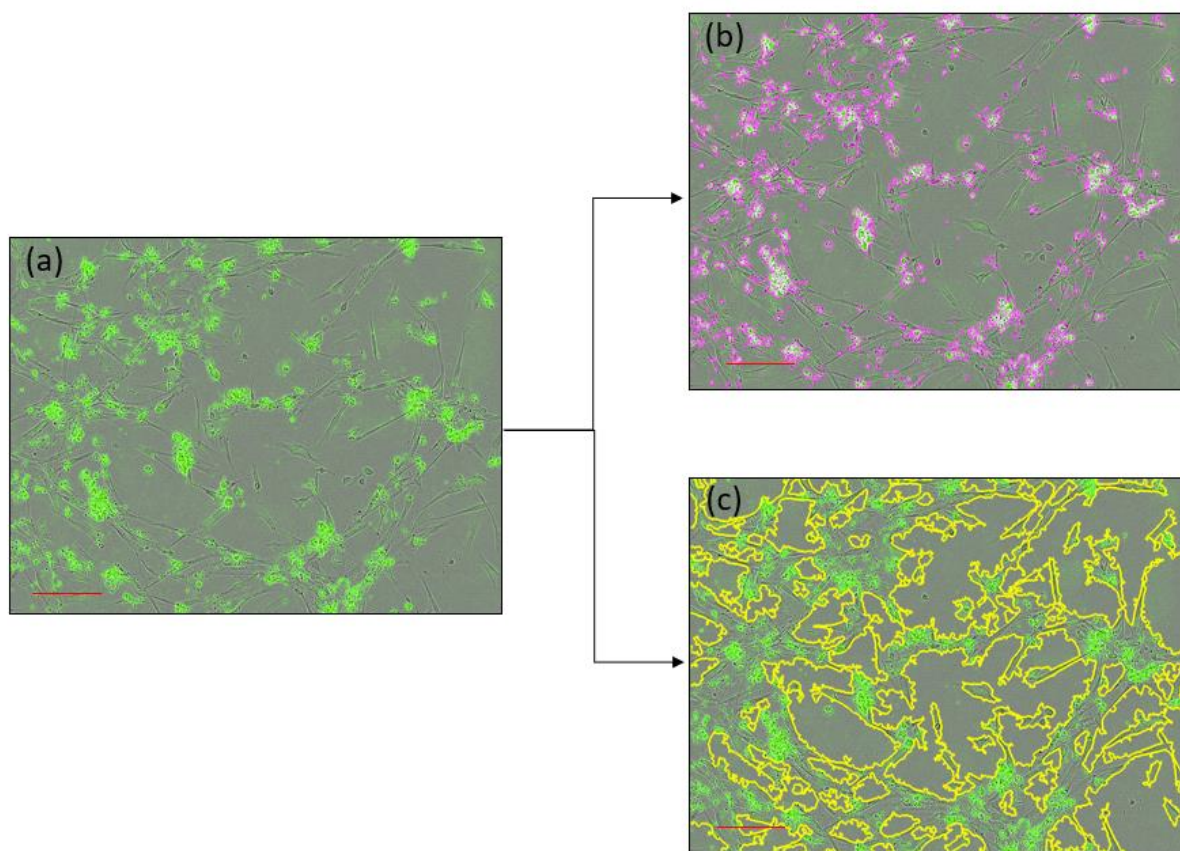


Figure 9. The analysis of apoptosis assay.

Representative image of apoptotic cells, as indicated by green fluorescence (a). Representative image of the mask detecting apoptotic cells which is used to quantify the integrated intensity of green fluorescence (b). Representative image of the mask detecting cell confluence (c).

3.3.3.1.8 RNA Isolation for PCR Array

To ensure the purity of mRNA for PCR array, miRNeasy Mini Kit was used to isolate total RNA of ciPTECs after cisplatin treatment with or without CM. ciPTECs treated in

6-well plate was lysed using 350 μ l QIAzol and homogenized by resuspension. The cell lysate as than incubated for 5 minutes at room temperature, before 70 μ l chloroform was added and mixed vigorously for 15 seconds. Subsequently the lysate was incubated at room temperature for 3 minutes and centrifuged at 4°C at 12,000 xg for 15 minutes. Following the centrifugation, the upper aqueous phase was carefully collected and transferred into a new tube, making sure that the interphase was not pipetted. Next, 1.5x volume of 100 % ethanol was added into the tube and resuspended thoroughly. The samples were then transferred into RNeasy® Mini column in a 2 ml collection tube and centrifuged at 8000 xg for 15 seconds at room temperature. Once the centrifuge finished the flow through in the collection tube was discarded and 700 μ l RWT buffer was added onto the upper column followed by another centrifugation at 8000 xg for 15 seconds at room temperature. After discarding the flow through, 500 μ l RPE buffer was added onto the column and centrifuged again. The washing step with RPE buffer was performed once again with longer centrifugation time, 2 minutes. Finally, the total RNA as eluted by with 30 μ l RNase-free water and centrifugation at 8000 xg for 1 minute at room temperature.

The concentration of RNA was then measured using NanoQuant Plate™ and microplate reader, Tecan. The ratio of absorbance at 260 nm and 280 nm was also calculated. Samples with ratio ~2.0 were used for further analysis.

3.3.3.1.9 cDNA synthesis for PCR Array

The synthesis of cDNA was performed with RT² First Strand Kit as per the manufacturer's instruction. First, genomic DNA was removed from the RNA samples by mixing the samples with genomic DNA elimination mix as shown at the **Table 2**. The genomic DNA elimination mix was incubated at 42° C for 5 minutes and then immediately transferred on ice for at least 1 minute.

Table 2. Component of Genomic DNA Elimination Mix

Component	Amount
RNA sample	750 ng
Buffer GE	2 μ l
RNse-free water	variable
Total volume	10 μ l

After the elimination of genomic DNA, the mix for reverse-transcription was prepared as shown on **Table 3** below.

Table 3. Component of Reverse-Transcription Mix

Component	Volume per reaction
5x Buffer BC3	4 μ l
Control P2	1 μ l
RE3 Reverse Transcriptase Mix	2 μ l
RNase-free water	3 μ l
Total Volume	10 μ l

Into a fresh PCR tube, 10 μ l genomic DNA elimination mix containing the RNA samples was added, followed by 10 μ l reverse-transcription mix. Both mixtures were mixed thoroughly by pipetting up and down and incubated at 42° C for 15 minutes. To stop the reaction, the tubes were then incubated at 95° C for 5 minutes. The samples were then stored in -80° C freezer for PCR Array.

3.3.3.1.10 PCR Array for Nephrotoxicity

Once the cDNA of ciPTECs ready the expression of gene related with nephrotoxicity was evaluated using RT² Profiler PCR Arrays for Nephrotoxicity in combination with RT² SYBR® Green Mastermixes, as recommended in the manufacturer's instruction. The PCR master mix was prepared as described on **Table 4** below.

Table 4. Composition of PCR Array Master Mix

Component	Volume
2x RT ² SYBR® Green Mastermix	1350 μ l
cDNA sample (from previous section)	102 μ l
RNase-free water	1248 μ l
Total volume	2700 μ l

25 μ l/well master mix was then dispensed into the 96-well RT² Profiler PCR Arrays using multi-channel pipettor and sealed tightly with optical adhesive film. The arrays were centrifuged at 1000 xg for 1 minute at room temperature to ensure bubble removal. The PCR was run using Roche LightCycle 480 with the following cycles: 1 cy-

cles of polymerase activation at 95⁰ C for 10 minutes, followed by 45 cycles of fluorescence data collection at 95⁰ C for 15 seconds and 60⁰ C for 1 minute. Absolute quantification was selected to calculate the threshold cycle (C_T) of each well. The C_T values obtained from the PCR were then analysed using the GeneGlobe Data Analysis Center (<https://geneglobe.qiagen.com/us/analyze>). The data was shown as relative value to healthy untreated ciPTECs cultured with SFM (UT-CTRL).

3.3.3.1.11 mRNA Isolation for qPCR

For qPCR, RNA of ciPTECs was isolated with RNeasy® Mini Kit as per the manufacturer's manual. First, treated ciPTECs in 6-well plate was lysed using 350 µl RLT lysis buffer and carefully homogenized to ensure complete lysis of the cells. The cell lysates were transferred into fresh 1.5 ml microtubes, before adding 1 volume of 70 % ethanol (350 µl). After mixing by pipetting up and down, up to 700 µl of the samples were added onto RNeasy Mini spin column placed in a 2 ml collection tube and centrifuged for 15 seconds at 8000 xg at room temperature. The flow through in the collection tube was then discarded and 700 µl RW1 buffer was added onto the column, centrifuged with the same speed and duration. After discarding the flow through, 500 µl RPE buffer was next added onto the column, followed by another centrifugation. The column was then washed once more with RPE buffer and centrifuged for two more minutes. The RNA was then eluted using 30 µl RNase-free water and centrifugation for 1 minute. Obtained RNA was then measured as described before and store at -80⁰ C freezer until further analysis.

3.3.3.1.12 cDNA synthesis and qPCR

cDNA synthesis for qPCR analysis was done using SensiFAST™ cDNA Synthesis Kit. The preparation of the master mix was done on ice. Up to 1 µg total RNA was mixed with 4 µl 5x TransAmp Buffer and 1 µl Reverse Transcriptase. The volume was adjusted using RNase-free water to reach final volume of 20 µl per well. The tubes were then placed on Thermal cycler with the following cycles: 25⁰ C for 10 minutes, 42⁰ C for 15 minutes, 85⁰ C for 5 minutes, and 4⁰ C hold. cDNA samples were then stored at -20⁰ C freezer for qPCR analysis.

Gene expressions of growth arrest and DNA damage inducible alpha (GADD45a), cyclin dependent kinase inhibitor 1A (CDKN1a), activating transcription factor-3 (ATF-3), heme-oxygenase-1 (HMOX-1) were assessed using SensiFAST™ SYBR® No-ROX Kit. The master mix was prepared as the following **Table 5**:

Table 5. Component of qPCR per Reaction

Component	Volume
2x SensiFAST SYBR® No-ROX Mix	10 µl
2 µM Forward and Reverse Primer Mix	2 µl
cDNA Template (25-50 ng)	Up to 8 µl
Distilled water	variable
Total Volume	20 µl

The qPCR was run using Roche LightCycle 480 with the following cycles: 1 cycles of polymerase activation at 95⁰ C for 2 minutes, followed by 40 cycles of denaturation at 95⁰ C for 5 seconds, annealing at 60-65⁰ C for 10 seconds, and extension at 72⁰ C for 20 seconds. Glyceraldehyde 3-phosphate dehydrogenase (GAPDH) served as reference gene. Relative value of the target genes was analyzed using 2^{-ddCt} method and normalized against the reference gene. The results were then presented as relative value to the UT-CTRL.

3.3.3.1.13 Analysis of CM key mediator in ciPTEC

Once we established the protective effect of CM on cisplatin-treated ciPTECs, we sought to investigate the key mediator responsible for this effect. Therefore, we interrogated the role of EV and free thiols on ciPTECs.

3.3.3.1.13.1 EV Depletion by Ultrafiltration

EV depletion from CM was performed as previously described⁸⁰. 100 kDa Amicon Ultra-15 centrifugal filter devices was first pre-coated with 1 % (w/v) BSA in PBS to reduce the possible entrapment of soluble factors in the membrane, hence increasing their recovery in the flow through (FT). First, the 100 kDa centrifugal filter devices were washed with EV-grade water as per the manufacturer's manual. Then, 12 mL of 1 % (w/v) BSA in PBS was added into the upper compartment of the device and incubated undisturbed for 2.5 hours in room temperature. Following the incubation, the upper compartment was washed 4x with 15 mL PBS without centrifugation and 1x with centrifugation in swing rotor at 4000 xg, 10 min, 4 °C. After the washing step, 15 mL of CM was added into the upper compartment of the device and centrifuged until all the CM was filtered (dead stop). ciPTEC SFM was also subjected to the ultra-filtration as CM and served as CTRL and CTRL-FT. The original CM (without filtration) and CM-FT,

along with CTRL and CTRL-FT were then subjected to nanoparticle tracking analysis (NTA) to determine the concentration of particles or EVs of the medium.

3.3.3.1.13.2 EVs Measurement with Nanoparticle tracking analysis (NTA)

The number of particles of EVs (≥ 100 nm) were assessed with light scattering technology, NTA. For the measurement, 10 μ l of medium was diluted with 0.22 μ m sterile-filtered PBS to obtain a 1:100 dilution. The EVs were then visualized using ZetaView (Particle Metrix) with 80 % sensitivity and 100 shutters. A total of 11 positions and 2 cycles of measurement was performed for each sample. The EV concentrations (≥ 100 nm) were then further analyzed with GraphPad Prism software.

3.3.3.1.13.3 pSTAT3 Measurement

To measure the phosphorylation of STAT3 following the CM treatment, ciPTECs were first treated with cisplatin in SFM for 1 hour as described before. After 1 hour of cisplatin treatment, the medium was changed with CM or SFM with or without cisplatin and incubated for 20 minutes at 37 °C, 5 % CO₂. Since the culture supplements present in SFM might also induce phosphorylated STAT3 (pSTAT3), healthy ciPTECs incubated with basal medium DMEM:F12 were used as the control. After the incubation time finished, ciPTECs were harvested and washed once. The cell pellet was then fixed immediately using 500 μ L BD Cytifix™ Fixation Buffer to preserve the phosphorylation state by vortexing and incubating them at 37 °C for 10 minutes. The cell suspension was then centrifuged at 300 xg for 10 minutes. The pelleted cells were then permeabilized by adding 500 μ L BD™ Phosflow Perm Buffer III drop by drop while vortexing them. The cells were then incubated on ice for 30 minutes, followed by washing step with FACS buffer twice. After the washing steps, the cells were resuspended in 100 μ L FACS buffer containing 10 μ L of anti-pSTAT3 antibodies and incubated in room temperature for 30 minutes in the dark. Following the staining, the excess antibody was removed by washing the cells twice with FACS buffer. The cells were finally resuspended in 500 μ L of FACS buffer and the data were acquired using FACS CANTO II. The .fcs data were then analyzed with FlowJo Software.

3.3.3.1.13.4 Free Thiol Measurement

Free thiols are sulfhydryl groups (R-SH) that can be found in peptides and proteins and are very sensitive to ROS. Therefore, free thiols not only serve as a redox switch in the cells but also act as a ROS scavenger^{81,82}. Given their roles in cellular redox state, next we measure the concentrations of free thiols in our CM to predict its anti-oxidative

capacity using Thiol Quantification Assay kit. The standard and the thiol green indicator solution were prepared according to the manufacturer's manual. 50 μ L of standard solution or CM (equilibrated to room temperature and centrifuged to remove any debris) were incubated with 50 μ L of thiol green indicator solution for 10 min in the dark. The fluorescence was read using microplate reader (TECAN, M200) at ex/em: 490/520 nm.

3.3.3.1.13.5 ROS Assay

Intracellular reactive oxygen species (ROS) of ciPTECs were measured using 2',7'-dichlorodihydrofluorescein diacetate (H₂DCFDA). ciPTECs seeded in 96-well plate were first loaded with 10 μ M H₂DCFDA in HBSS for 10 min, followed by two washing steps with HBSS. Then, the cells were incubated with their normal growth media for 30-45 min at 37 °C, 5 % CO₂ to allow for cell recovery. Once the cells recovered, they were treated with cisplatin for one hour, and the media was changed with CM containing cisplatin. Four hours later, H₂DCFDA fluorescence representing intracellular ROS level was measured using microplate reader, TECAN, at excitation/emission: 495/520 nm. ciPTECs treated with 1 μ M H₂O₂ in ciPTEC SFM served as positive control. The ROS level was calculated presented as relative value to UT-CTRL.

3.3.3.2 CM effect on cisplatin treated macrophages

How cisplatin and CM affected macrophage phenotype was elucidated with the same treatment scheme as ciPTECs. The macrophages were obtained by maturation of PBMC-derived monocytes isolated with the same methods as previously described in Section 3.2.2.2.1. Following isolation, monocytes were cultured in X-Vivo 10 supplemented with 10 ng/ml M-CSF for 6 days without media change. After the 6 days of culture, macrophages were treated with 15 μ M cisplatin in X-Vivo 10 containing and incubated for one hour. Next, the media was changed with CM containing 15 μ M cisplatin plus 10 ng/ml M-CSF and the cells were incubated for another 23 hours. Of note, both the non-adherent and adherent macrophages were included in the treatment. The adherent cells in the SN were collected and centrifuged each time the media was changed and the cell pellet were resuspended into their corresponding wells. After a total of 24 hours since cisplatin treatment started, macrophages were subjected to surface marker and phagocytosis (as described in Section 3.2.2.2.6) analysis. The macrophages cultured in X-Vivo 10 supplemented with 10 ng/ml M-CSF in the absence and presence of cisplatin served as UT- and Cis-CTRL, respectively.

3.3.3.2.1 Evaluation of macrophage immunophenotype

Immunophenotyping of macrophages was done by flow cytometry upon cisplatin and CM treatment. The un-adherent macrophages were first collected in FACS tube, while the adherent ones were detached using accutase for 10 minutes at 37⁰ C. After the incubation, the adherent cells were then gently scraped using cell scraper and transferred into the corresponding FACS tube containing the non-adherent macrophages. The cells were then washed once with PBS/EDTA by centrifuging them at 420 xg for 10 minutes. Following the washing step, the cells were resuspended in 100 µl FACS buffer and 10 µl FcR Blocking reagent was added. The cells were incubated for 5 minutes at 4⁰ C, followed by subsequent staining at 4⁰ C for 20 minutes with the following antibodies: anti-HLA-DR-PE-Cy7, anti-CD86-BV421, anti-CD206-PE, anti-CD38-APC C7, and anti-CD163-BV510. The volume of each antibody added was properly optimized by titration. Once the staining finished, the cells were washed twice with Cell Wash solution and resuspended in FACS buffer containing Sytox Blue (1:2000 dilution). The fluorescence of the antibodies were then acquired using FACS Canto II and the .fcs data were analyzed with FlowJo 10 software.

3.3.3.3 CM Effect on ciPTEC-macrophage co-culture

3.3.3.3.1 ciPTEC seeding on transwell insert prior to co-culture

Before seeding ciPTECs on transwell membrane, transwell inserts 0.4 µm Transparent PET Membrane for 24 well plates were coated with L-DOPA and human collagen type IV. First, 200 µl 2 mg/mL L-DOPA was added onto the apical side of the membrane and incubated for 4 hour at 37°C. After the incubation, the L-DOPA solution turned rather dark which indicated polymerization. The L-DOPA was then removed and the membrane was washed with 300 µl once, before adding 50 µl 25 µg/mL of human collagen IV. The membrane was incubated again for one hour at 37°C, followed by three times washing with 300 µl HBSS. Once the membranes were coated, ciPTECs were harvested and seeded on top of the membrane with seeding density of 4 x 10⁴ ciPTECs /transwell. 300 µL and 700 µL of ciPTEC growth medium were added to the apical and basolateral side, respectively. The ciPTECs were then kept at 33 °C to allow adherence and growth, before being moved to 37 °C for maturation for an additional 7 days. The ciPTEC medium was refreshed periodically.

3.3.3.3.2 Macrophage seeding prior to co-culture

During the maturation of ciPTECs, monocytes were isolated and seeded in a 24-well plate at a density of 2×10^5 cells/well to obtain ciPTEC:macrophage ratio of 1:5. The monocytes were cultured in X-Vivo-10 supplemented with 10 ng/mL M-CSF at 37 °C for 6 days without media change until matured into macrophages.

3.3.3.3.3 Cisplatin and CM treatment on ciPTEC-macrophage co-culture

Once ciPTECs and macrophages were matured, the cisplatin and CM treatment began. First, ciPTECs and macrophages were treated separately with 30 μ M cisplatin in ciPTEC SFM and X-Vivo, respectively, for one hour, as depicted in **Figure 10**. After one hour, ciPTECs transwells were transferred to the well plates containing the macrophages. The co-cultures were then treated with either CM (pooled from 3 different donors) or control medium (in ciPTEC SFM and X-Vivo-10 supplemented with 10 ng/ml M-CSF, for apical and basolateral side, respectively) with or without 30 μ M cisplatin for another 23 hours. As a control, ciPTECs and macrophages were cultured alone and treated in the same manner as the co-culture.

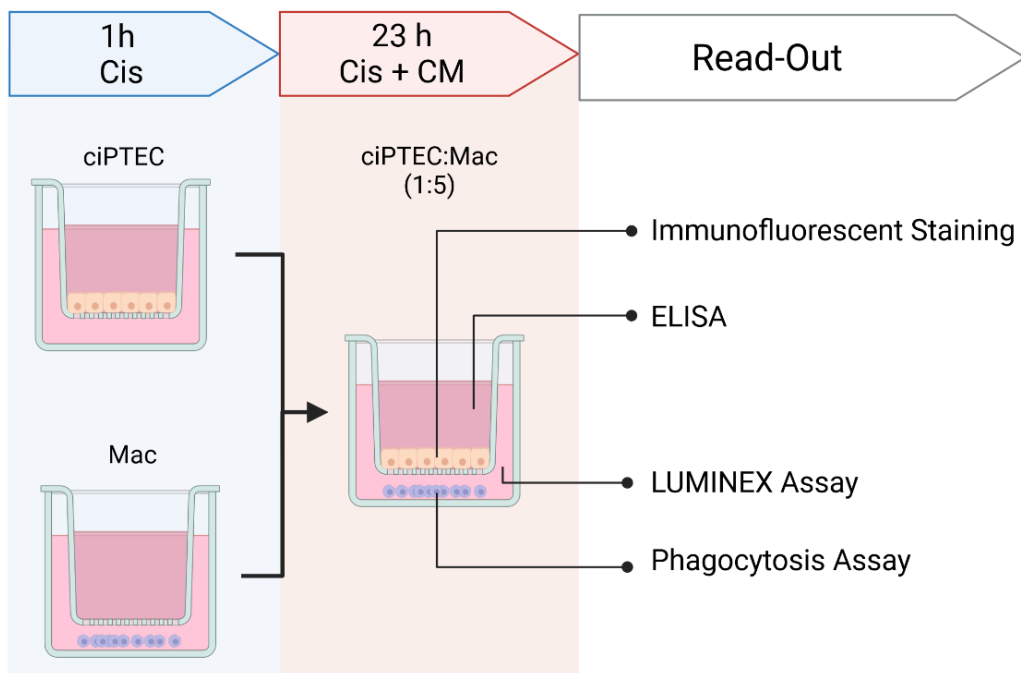


Figure 10. The workflow of ciPTEC and macrophage co-culture treated with cisplatin and CM.

After a total of 24 hours of cisplatin treatment, culture SN from the apical and basolateral side was collected, centrifuged at 420 xg for 10 minutes to remove cell debris, and cryopreserved at -80 °C. The ciPTECs on the transwell membrane were subjected to staining (see below), while the macrophages were subjected to phagocytosis assay as previously described. This image is created using BioRender.

3.3.3.3.4 Immunofluorescence Staining of ciPTECs

After the co-culture treatment, ciPTEC transwells were transferred to a new 24-well plate and washed with HBSS once. The apoptotic cells were stained by incubating the cells with 150 nM Apotracker in HBSS at 37 °C for 20 minutes, followed by two washing step with HBSS to remove excess Apotracker. Next, the cells were fixed with 4% paraformaldehyde (PFA) for 10 minutes at room temperature. Once fixed, the cells were washed once with DPBS and the membranes were carefully cut from the insert using a 24 G needle and transferred back into the wells. The membranes were washed again DPBS twice to remove remaining PFA, and blocked with blocking solution for one hour at room temperature in the dark. The membranes were then stained with rabbit anti-human connexin-43 (CX43) primary Ab in blocking solution (1:1000 dilution) overnight in the dark at 4° C. The next day, the membrane was washed three times with DPBS with 5 minutes incubation per wash, before incubating with the goat anti-rabbit secondary Ab AF568 for 30 min in the dark. Following three washing steps with DPBS, the membranes were stained with 300 nM DAPI in DPBS for 5 minutes and washed again three more times, before being mounted in a microscope slide.

The images of the ciPTECs were acquired using Zeiss LSM 800. The fluorescence intensity of CX-43, the number of Apotracker spots (using Plugin TrackMate7⁸³), and the number of nuclei fragments, fragmented and intact nuclei were analyzed with ImageJ Fiji. The results of fluorescence intensity of CX-43, the number of apotracker spots, nuclei fragments, and fragmented nuclei were normalized against the number of intact nuclei and presented as the relative value of the untreated ciPTEC cultured alone.

3.3.3.3.5 Luminex Assay

A ProcartaPlex 22-plex panel was employed to measure the following secreted factors within the SN harvested from the basolateral side of the co-culture:: Arginase-1, Fractalkine (CX3CL1), Granulocyte-macrophage colony-stimulating factor (GM-CSF), Hepatocyte growth factor (HGF), Heat shock protein 60 (HSP60), Interferon- β (IFN- β), Interleukin-1 β (IL-1 β), IL-1RA, IL-8 (CXCL8), IL-10, IL-13, IL-33, IFN- γ inducible protein-10 (IP-10), M-CSF, Matrix metalloproteinase 9 (MMP-9), Platelet-derived growth factor-BB (PDGF-BB), Chemokine (C-C motif) ligand 5 (CCL5), S100A8/A9, Survivin (BIRC5), Tissue inhibitor of metalloproteinase-1 (TIMP-1), TNF- α , and VA-MSCular cell adhesion molecule 1 (VCAM-1). The kit was first equilibrated to room temperature. The dilution of the standard solution and the loading of the beads and SN were done

as per the manufacturer's manual. The intensity of each marker in the samples was then acquired using Luminex 200 Multiplex Bead Array (Merck-Millipore) and Luminex xPonent Version 3.1 software. The standards calibration was done with the Logistics 5P Weighted method. This work has been done in the Proteomics Core Facility, Core Facility Platform Mannheim.

3.3.3.4 Legendplex Human Growth Factor Panel

To measure the concentration of growth factors in the CM, we analysed the CM with Legendplex Human Growth Factor Panel. Both CM produced in ciPTEC SFM and X-Vivo 10 to treat ciPTECs and macrophages, respectively were subjected to this assay along with the control ciPTEC SFM and X-Vivo 10 as the baseline. The CM from four MSC donors were analysed.

Firstly, the standards were reconstituted and diluted with a factor dilution of 4 in Assay Buffer. 8-points of standard curved were obtained. 25 µl/well of samples and standards were added into V-bottom plate, followed by the addition of 25 µl/well of Assay Buffer, resulting in 1:1 dilution in each well. 25 µl/well of Premixed Beads were then added to each well and the plate was sealed and incubated at room temperature for 2 hours with 500 rpm agitation. Upon the incubation, the wells were washed with 150 µl Wash Buffer and centrifuged at 250 xg for 5 minutes. The plate was decanted and blotted on tissue paper to remove excess liquid, followed by another washing step. After the washing step, 25 µl/well Detection Antibody was added, followed by incubation room temperature for 1 hour with 500 rpm agitation. 25 µl/well of SA-PE was added and the plate was incubated 30 minutes at room temperature with 500 rpm agitation. Lastly, the plate was washed twice, followed by resuspension of the content with 150 µl of Wash Buffer. Each probe from each well was then transferred in FACS tube and the data were acquired with BD FACS Canto II with acquisition rate limit of 300 beads/analyte. The data were then analysed with the LEGENDplex™ Data Analysis Software according to the manufacturer's instructions.

3.3.4 ELISA

The concentrations of TNF- α , IL-8, and IL-6 of macrophage SN and CM were analysed with ELISA (Duo Set, R&D systems). After cell debris removal by centrifugation, the SN and CM were ready for ELISA, which was done as per the manufacturer's instruction.

The day before the ELISA measurement, a 96-well plate was coated with Capture antibody diluted in DPBS as indicated in the manuals at room temperatures overnight. The following day, the coated wells were washed three times with Wash Buffer and blocked with Reagent Diluent for 1 hour at room temperature. Afterwards, the plate was washed again three times before 100 µl samples and standards were added to the wells. The plate was incubated again for 2 hours at room temperature, before being subjected to three washing steps. Streptavidin-HRP was then added, followed by 20 minutes incubation prior to the addition of substrate solution, which comprised color reagent A and B (1:1). 20 minutes after the addition of substrate solution, the stop solution (2N H₂SO₄) was finally added to the wells. The OD of the wells was then acquired using microplate reader set to 450 nm with wavelength correction at 570 nm. The best fitting standard curves ($0.90 \leq R \leq 1$) and the concentration of each sample were analysed with GraphPad Prism.

3.3.5 Statistical Analysis

The statistical analysis was done using GraphPad Prism 9.2.0 software (GraphPad Software). N refers to the biological replicates for each donor per cell type and n indicates the independent technical replicates. The statistical analyses run for each data set and the number of replicates is indicated in the figure legends. Statistical significance is indicated as the following: $p < 0.5$, $**p < 0.01$, $***p < 0.001$, $****p < 0.0001$.

4 RESULTS

Part 1: Inter-laboratory and tissue source comparison of MSC culture

Before we started with the evaluation of MSC profiles between laboratories and tissue sources, the standardized culture protocol had to be established. The standardization of the MSC culture protocol comprised the use of the identical basal medium, namely MEM- α , one batch of FBS and a fixed seeding density. Since the quality of FBS has a critical influence on MSC profile⁸⁴, the FBS suitable to support MSC growth and multilineage differentiation was carefully selected by our collaborator in NUIG. The full report on the FBS testing can be found in⁷⁸.

4.1.1 Harmonization of MSC seeding density

Once the culture medium was established, the seeding density of MSCs was evaluated. The optimization of seeding density is particularly important as it can greatly affect the proliferation kinetics of primary cell culture such as MSCs whose growth potential is limited^{84,85}. The evaluation of the seeding density for A-, BM-, and UC-MSCs was done in UHEI, NUIG, and UOL, respectively. Two seeding densities were tested in all the three types of MSCs for two passages: 300 and 3,000 cells/cm². As shown in **Figure 101a-b**, at higher seeding density, cumulative population doublings (CPD) of A- and BM-MSCs decreased over time, resulting in prolonged expansion time (**Figure 11d**). On the contrary, UC-MSCs cultured at higher seeding density exhibited higher CPD implying in decreased doubling times (**Figure 11d**).

In addition to growth kinetic, the seeding density also affected MSC morphology (**Figure 11e**). The morphology of UC-MSCs expanded at 300 cells/cm² lost their spindle-shaped structure and tended to clump and form colonies, as compared to the cells cultured at 3,000 cells/cm². Similarly, BM-MSCs at lower seeding density showed flatter and extended cytoplasm. Interestingly, in contrast to both UC- and BM-MSCs, A-MSCs exhibited a more elongated, spindle-shaped morphology at 300 cells/cm². Since we aimed to perform the comparison with MSCs cultured in their optimum seeding density, it was decided that BM- and UC-MSCs were expanded at 3,000 cells/cm², while A-MSCs at 300 cells/cm².

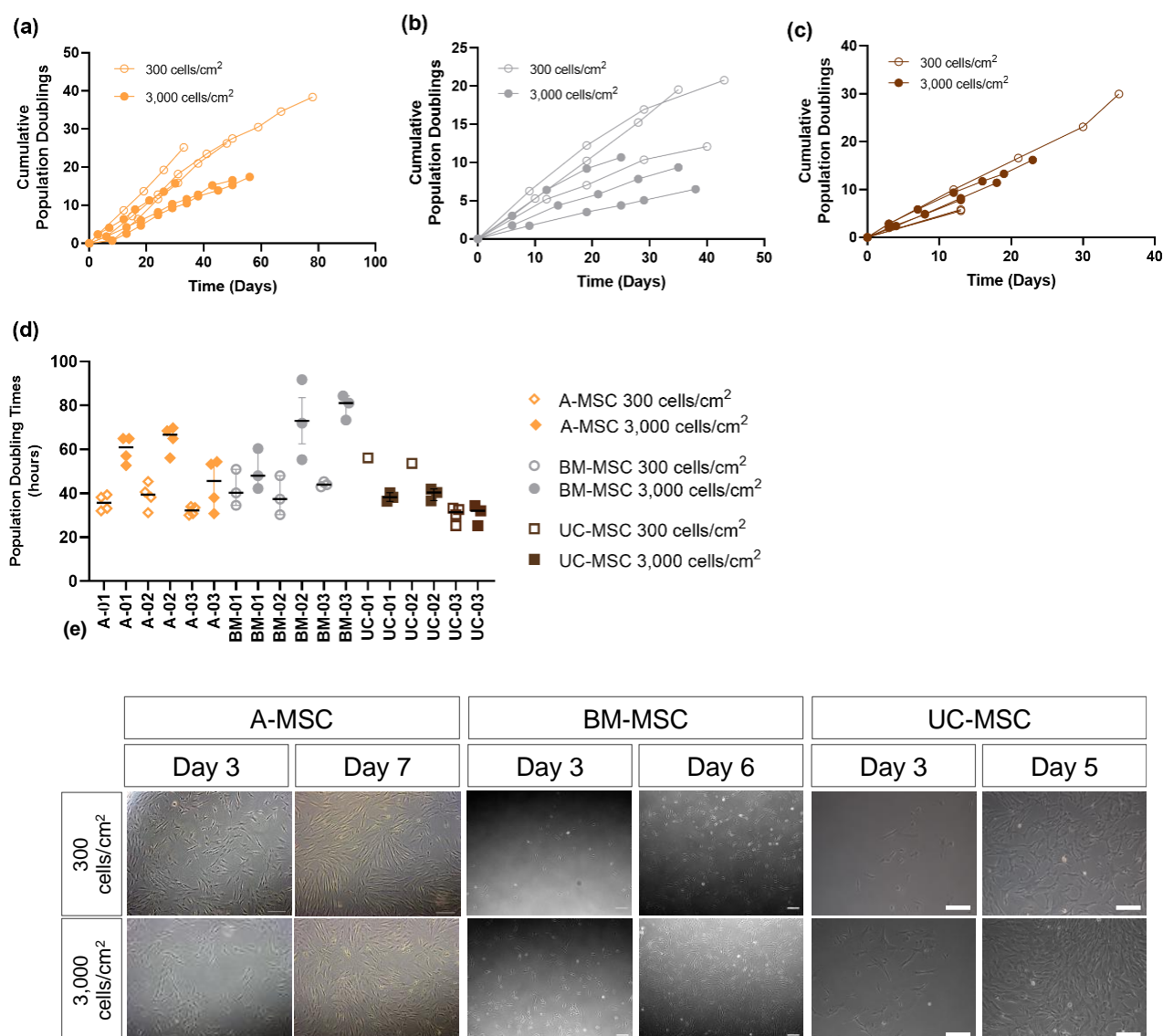


Figure 11. Tissue source influences the MSC growth under different seeding density.

Cumulative population doublings of A- (a), BM- (b), and UC-MSCs (c) seeded at 300 (empty symbols) and 3,000 (filled symbols) cells/cm². Population doubling time of all the MSCs cultured in those two seeding densities (d). Representative images of MSCs (e). All graphs: N=3. Pictures taken at 40X. [85]

4.1.2 Despite inevitable inter-laboratory discrepancies, culture harmonisation preserved tissue-specific signature on growth kinetics

After the culture protocol was harmonized, all MSCs were cultured according to this standardized protocol for the rest of the study. A-, BM-, and UC-MSCs were expanded and cryopreserved in UHEI, NUIG, and UOL, respectively, before being shipped internationally to the all the sites. Once each site obtained all the MSC types, the cells were

subjected to MSC characterization to be compared between the tissue sources and laboratories.

The first MSC characteristic being compared was the growth kinetics that were obtained by culturing all the MSCs for three consecutive passages. The population doublings and doubling time from the different cell sources and sites of culture are depicted in **Figure 12a and b**, respectively. It is noteworthy that the tissue source of MSCs affected their growth kinetics resulting in the trends of doubling times shown in **Figure 12a**. Despite being cryopreserved and shipped internationally, the trends of MSC growth kinetics remained consistent across the centres. BM-MSCs consistently exhibit the longest doubling time in all sites (90.81 ± 10.57 hours, 66.78 ± 16.32 hours, 95.72 ± 28.02 hours in UHEI, NUIG and UOL, respectively). Meanwhile, doubling times of A- (43.17 ± 3.84 hours, 37.25 ± 1.64 hours, 51.10 ± 1.25 hours in UHEI, NUIG and UOL, respectively) and UC-MSCs (68.07 ± 9.11 hours, 38.06 ± 1.04 hours, 46.06 ± 9.47 hours in UHEI, NUIG and UOL, respectively) are more comparable to each other.

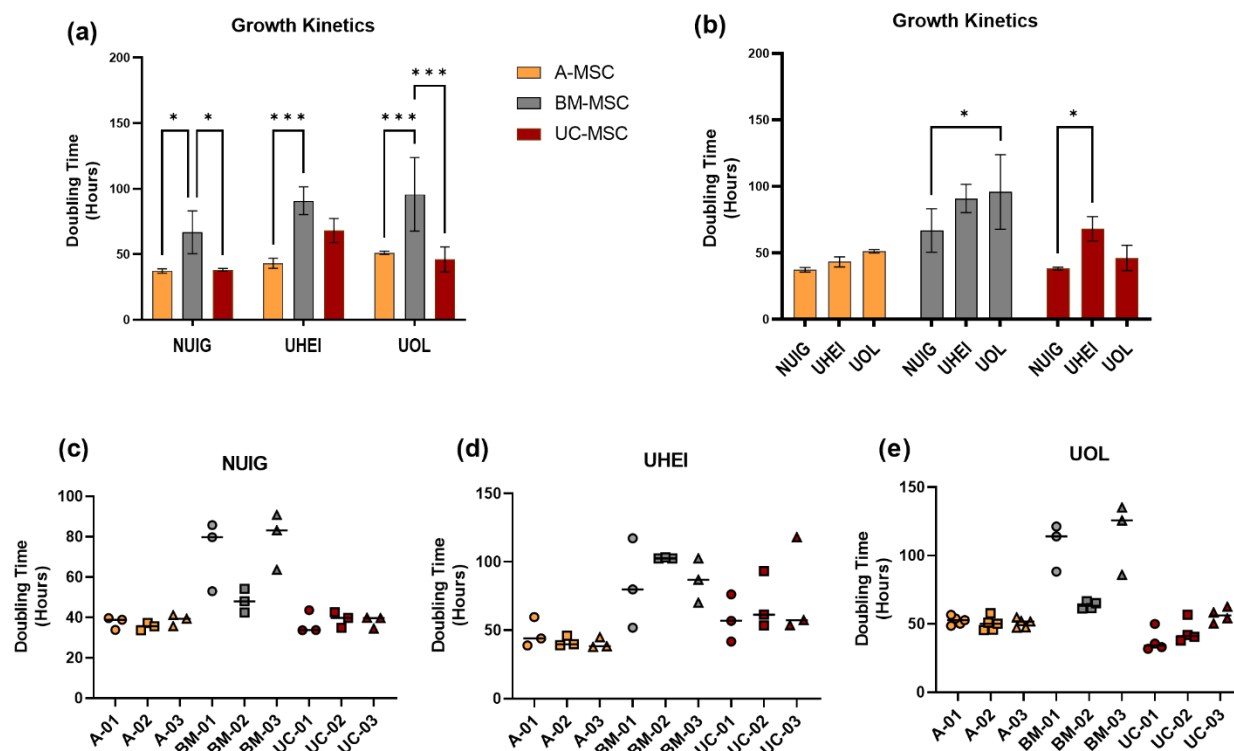


Figure 12. Culture harmonisation could reduce inter-laboratory variation and preserve tissue source signature on growth kinetic across all centres.

The comparison of MSC doubling times between tissue sources within each centre (a). The comparison of doubling times between the three centres per MSC tissue source (b). Donor per donor breakdown of

doubling times in NUIG (c), UHEI (d), and UOL (e). Two-way ANOVA with Tukey's multiple comparison test. All graphs: N=3. ⁷⁸

As expected, some discrepancies in doubling time due to site-to-site variation were also observed (**Figure 12b**) although the culture was done with a standardized protocol. Representative phase contrast images can be found in **Figure 13**. While growth kinetics of A-MSCs tended to differ slightly across the centres, a significant site-to-site discrepancy was found in BM- and UC-MSCs. When looking at the individual donor of each MSC type, A-MSCs appeared to be the most stable MSCs as they demonstrated the least variations between the donors and passages in all centres (**Figure 12c-e**, each dot within represents the doubling time of a passage). In contrast to A-MSCs, BM-MSCs consistently showed high donor-to-donor and passage-to-passage variations across all the centres. UC-MSCs also demonstrated relatively stable growth kinetics except in UHEI where differences between passages were notably higher than the other two centres.

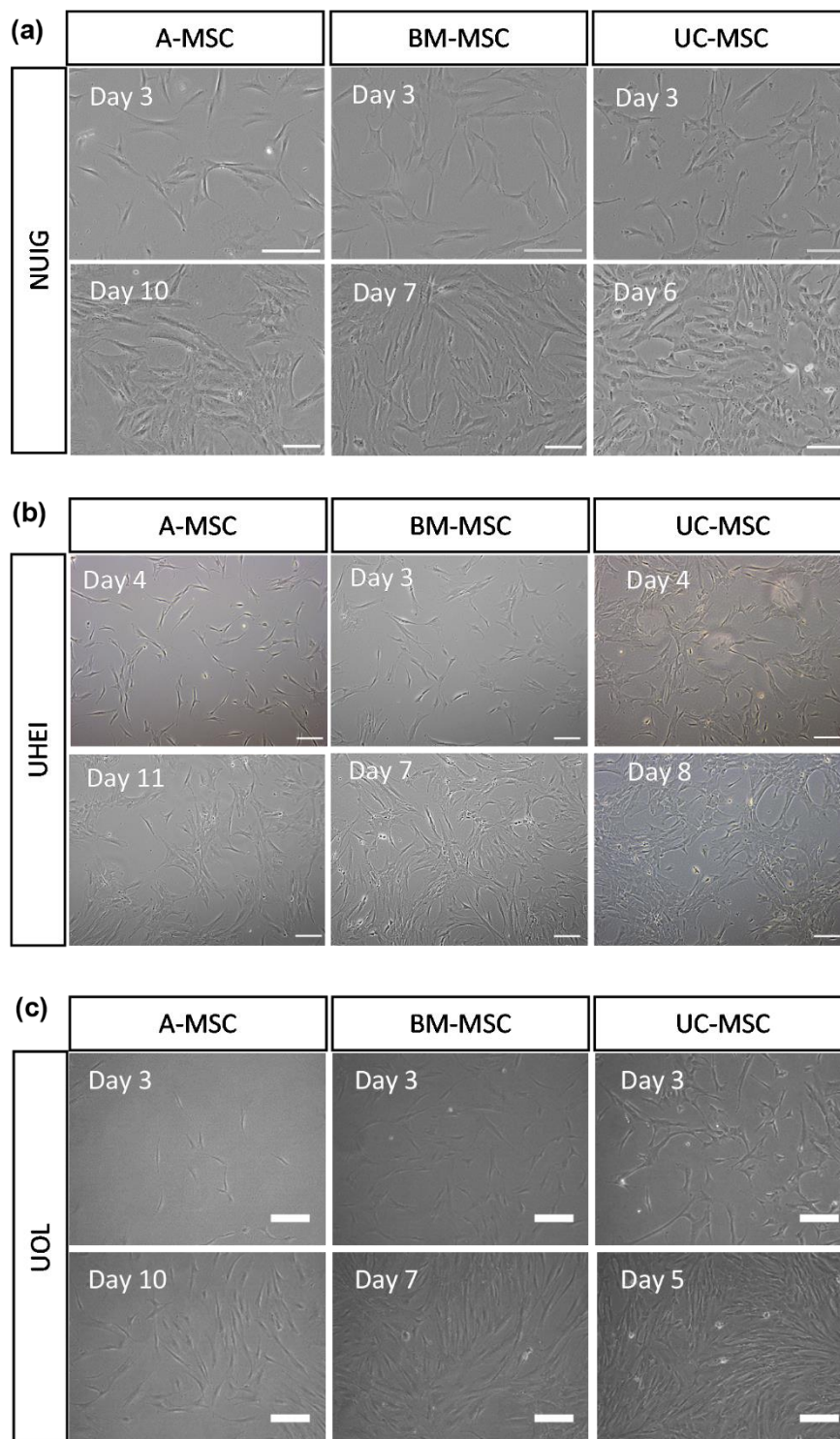


Figure 13. Morphology of A-, BM-, and UC-MSCs during the culture.

Representative images of MSCs cultured in NUIG (a), UHEI (b), and UOL (c). Scale bars indicate 200 μm.

4.1.3 Adipogenic and osteogenic differentiation of MSCs were highly influenced by inter-laboratory, tissue source, and donor variation

Analysing their differentiation capacity, high levels of variability were obvious, which are attributed to the discrepancies in culture handling between the centres, the characteristic of the tissue of origin, and the donor intrinsic factors (**Figure 14a-d**). In spite of apparent differences between sites, A- and BM-MSCs displayed higher tendency of adipogenic and osteogenic differentiation, as compared to UC-MSCs which showed negligible level of both differentiations (**Figure 14a-b**). Amongst all the MSC type, BM-MSCs exhibited the highest differentiation capacity for both lineages, but with relatively high centre-to-centre and donor-to-donor variabilities. In comparison to BM-MSCs, A-MSCs demonstrated lower variabilities between centres and donors in their differentiation ability with an exception of one donor showing superior induction abilities in UHEI (**Figure 14c-d**). Furthermore, it is noteworthy that the differentiation range resulted in each centre also remarkably differed. While A- and BM-MSCs possessed considerably greater capacities for adipogenic and osteogenic differentiations in UHEI and UOL, the differentiation of all MSC types in NUIG remained modest. Likewise, the variations due to donor-to-donor difference was also higher in UHEI and UOL for all tissue sources, as compared to those in NUIG (**Figure 14c-d**).

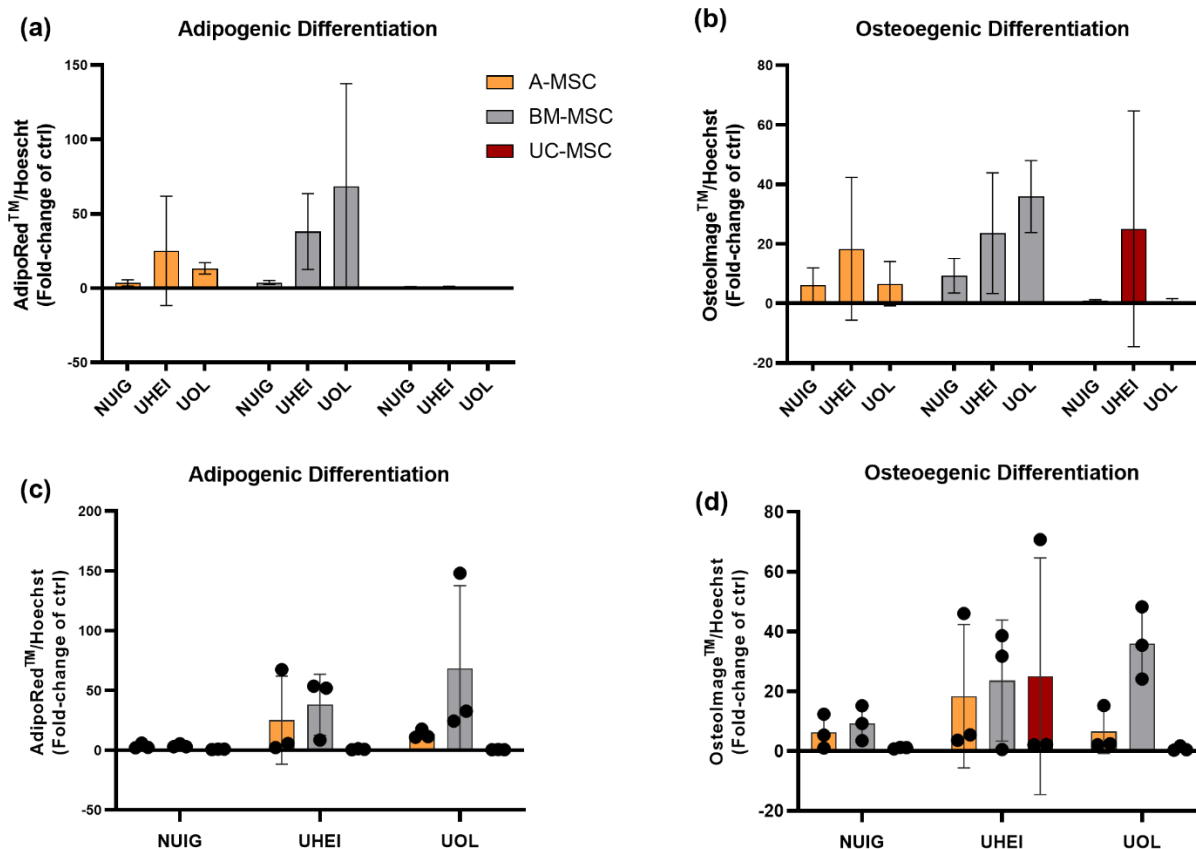


Figure 14. MSCs' ability to differentiation into adipocytes and osteocytes was greatly affected by centre-to-centre and tissue variation

Comparison of adipogenic (a) and osteogenic differentiation (b) across the laboratories per tissue source. The comparison of adipogenic (c) and osteogenic differentiation (d) between the three centres per MSC tissue source. Two-way ANOVA with Tukey's multiple comparison test. All graphs: N=3. ⁷⁸

4.1.4 Immunophenotypes of MSCs for negative markers differed across the centres

In respect of their immunophenotype, all MSC sources showed consistently high levels (> 95%) of positive marker of MSCs, including CD73, CD90 and CD105 across all three centres (**Figure 15a-c**). In UHEI and UOL, A-MSCs showed some positivity of negative surface markers that are normally found in hematopoietic stem cells such as CD34 ($10.21 \pm 12.96\%$ in UHEI and $18.40 \pm 11.69\%$ in UOL) and CD45 ($10.81 \pm 7.77\%$ in UOL) (Figure 9b-c). Moreover, in UOL and UHEI BM-MSCs also expressed appreciable levels of HLA-DR ($3.70 \pm 3.36\%$ and $7.33 \pm 6.51\%$ in UHEI and UOL, respectively), which remained negative in NUIG.

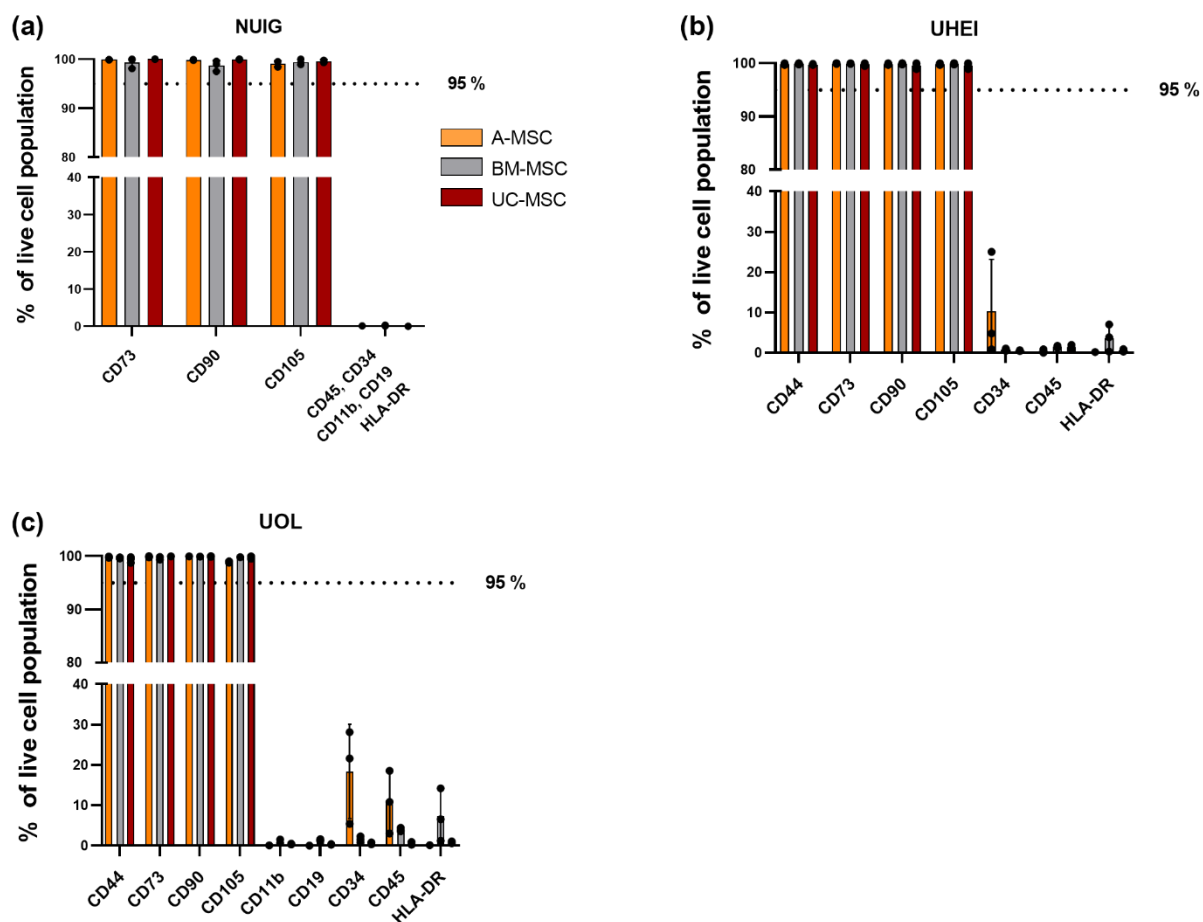


Figure 15. Immunophenotype of MSCs for positive marker

Analysis of the immunophenotype by flow cytometry in NUIG (a), UHEI (b), and UOL (c). One-Way ANOVA with Tukey's multiple comparison corrections. All graph: N=3. ⁷⁸

4.1.5 A-MSCs exerted the highest inhibitory activity on PBMC proliferation

Since immunomodulation is one of the key therapeutic benefits of MSC therapy ⁷, we next sought to investigate the capacity of MSC from the three different tissue sources to inhibit stimulated PBMC proliferation. The abilities of MSCs in inhibiting PBMC proliferation was interrogated in a direct co-culture setting upon PHA stimulation. Figure 16a shows that all MSCs were, to some degree, able to suppress PBMC proliferation, as indicated by a reduction in the number of proliferating PBMCs co-cultured with MSCs than those cultured alone. A-MSCs exhibited the highest degree of proliferation inhibition (0.17 ± 0.52 proliferation relative to positive control), followed by BM- (0.52 ± 0.07 proliferation relative to positive control) and UC-MSCs (0.61 ± 0.21 proliferation relative to positive control).

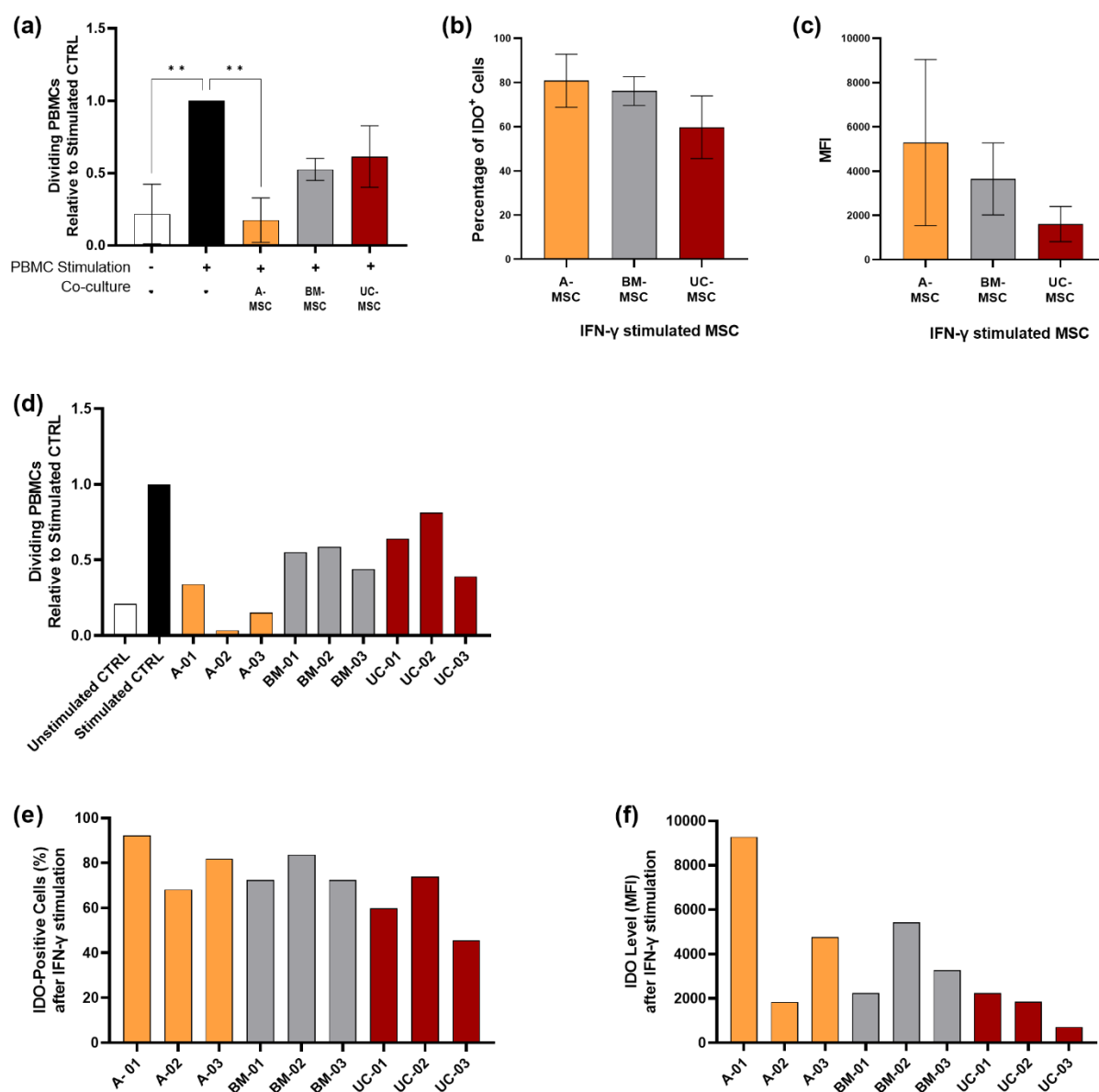


Figure 16. A-MSCs exhibited the highest immunomodulatory capacities than the other MSC types PBMC proliferation measured after five days co-culture with MSCs under PHA stimulation. All values were normalised to PHA-stimulated monoculture PBMCs (a). The percentage of cells positive for IDO intracellular staining (b). Mean fluorescence intensity of intracellular IDO of MSCs after being treated with IFN- γ for 24h (c). Donor-by-donor breakdown of PBMC proliferation (d), percentage of IDO-positive cells (e), and IDO levels (f). Two-Way ANOVA with Tukey's multiple comparison corrections. All graphs: MSC N=3, PBMC n = 3. ⁷⁸

Given that previous studies have shown the importance of IDO-kynurenine axis in MSC immunomodulation on T-cells ²², we next compared MSC ability to secrete IDO upon IFN- γ stimulation. **Figure 16b** shows that A-MSCs displayed the highest percentage of cells positive for intracellular IDO staining, followed by BM- and UC-MSCs ($88.77 \pm$

12.04%, $76.17 \pm 6.52\%$ and $59.77 \pm 14.15\%$ for A-, BM-, UC-MSCs, respectively), with relatively low donor-to-donor variation. In line with the percentage of positive cells, the level of intracellular IDO, as indicated by mean fluorescence intensity (MFI), also followed the same pattern (**Figure 16c**) with A-MSCs expressing the highest IDO level upon IFN- γ stimulation. In contrast to the generally accepted concept that MSC inhibitory effect on T-cell proliferation is mainly mediated by IDO, the A-MSC donor with the highest inhibitory effect (**Figure 16d**), A-02, surprisingly showed the lowest IDO level (**Figure 16e-f**). Meanwhile, donor A-01 which exhibited the highest IDO level upon exerted the most inert inhibitory effect amongst all A-MSC donors (**Figure 16d-f**).

4.2 Part 2: Inter-species Immuno-Compatibility Study

To evaluate the compatibility of MSC immunomodulation across species, MSCs and macrophages from human (h-Mac) and rat (r-Mac) were used in this part of thesis. For human MSCs, we interrogated A- and ABCB5+ MSCs since, based on the previous part, A-MSCs showed the strongest immunomodulation, meanwhile ABCB5+ MSCs are clinically manufactured MSCs undergoing multiple clinical trials.

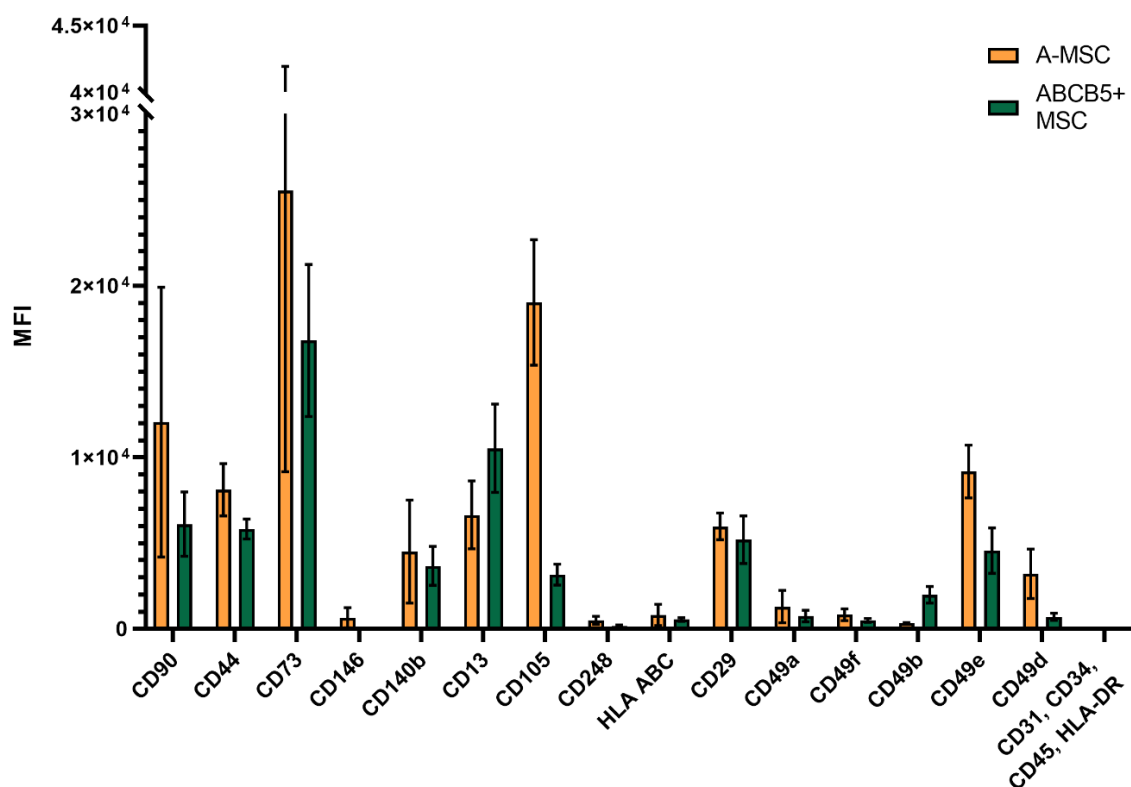


Figure 17. Extended analysis of immunophenotyping revealed the difference in surface marker expression between A- and ABCB5+ MSCs

Data displayed as mean \pm SD; N=3.

To investigate the difference between A- and ABCB5+ MSCs, we performed a more comprehensive evaluation of their surface marker expression (**Figure 17**). While both of the MSC types fulfil the minimum ISCT criteria for negative and positive markers, A-MSCs appeared to express MSC markers in higher intensity than ABCB5+ MSCs, especially CD105. The only surface markers that were found higher in ABCB5+ MSCs include CD13 and CD49b. Of note, donor-to-donor variability is more prominent in A- than that in ABCB5+ MSCs.

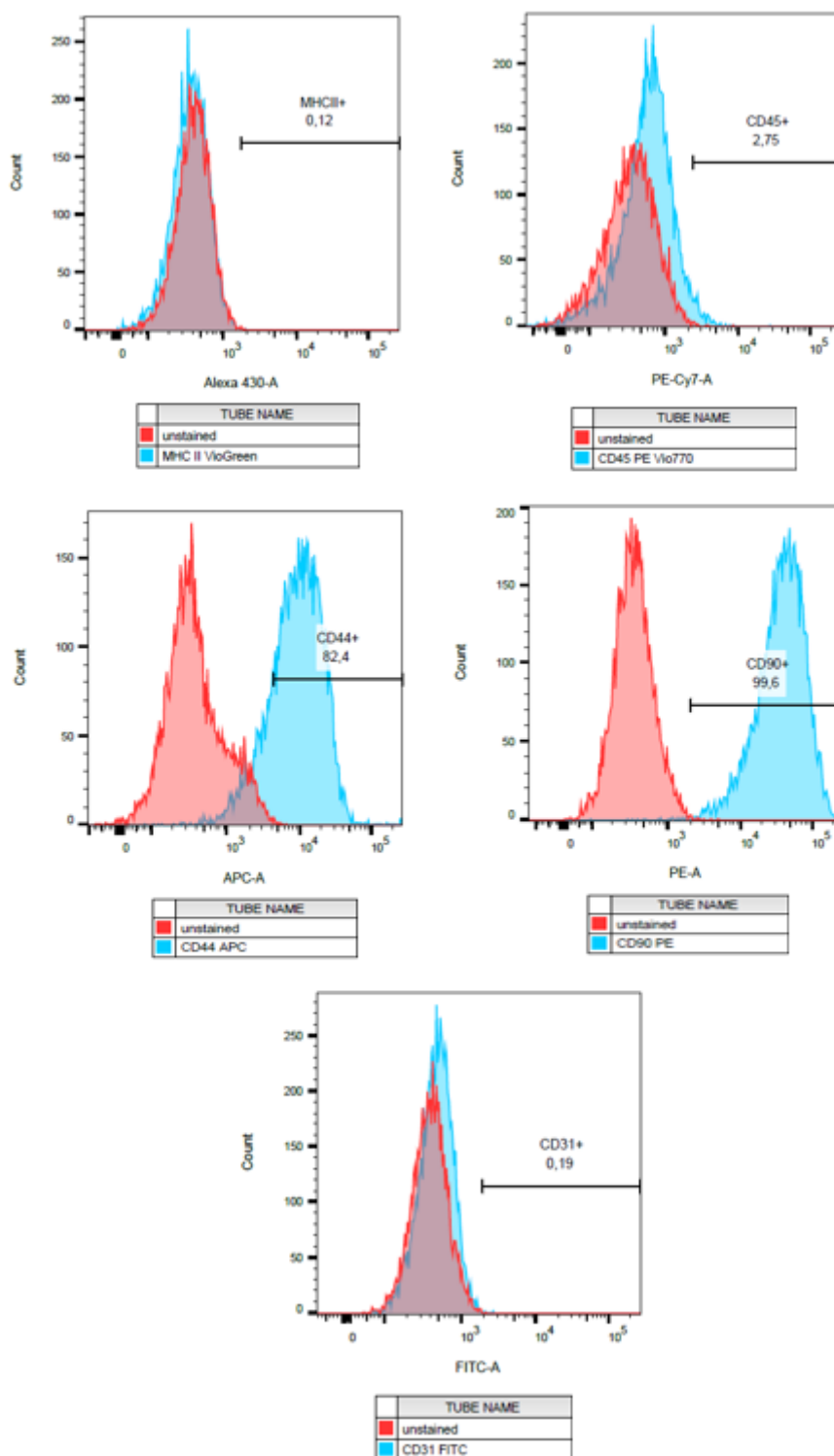


Figure 18. Representative r-MSCs characterization using FACS

In addition to human MSCs, MSCs isolated from rat bone marrow (r-MSCs) were included in the experiments. Before the production of CM, the surface marker of r-MSCs were measured with FACS as part of MSC characterization. As seen in **Figure 18**, r-MSCs were positive for typical MSC markers, such as CD90 and CD44, while negative for CD45, HLA-DR, and CD31.

Given that the MSC therapeutical effects were mostly mediated via paracrine factors⁹, we tested MSC secretome/their CM for this part of thesis.

The morphology of A-, ABCB5+, and r-MSCs after CM production are depicted in **Figure 19**. ABCB5+ MSCs appeared to be more fibroblast-like than the other cells and showed smaller size. On the other hand, r-MSCs exhibited a flatter morphology with extended cytoplasm.

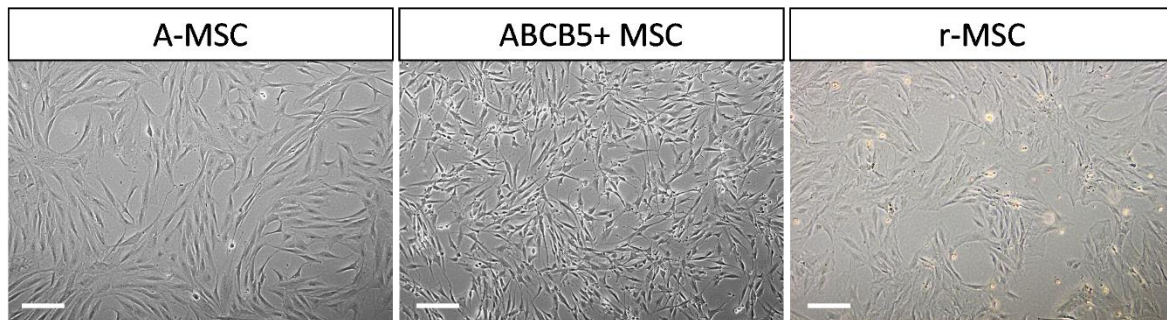


Figure 19. Representative images of A-, ABCB5+, and r-MSCs after CM production.

Scale bars indicate 200 μm .

4.2.1 h- and r-MSCs suppressed TNF- α production of LPS-stimulated macrophage despite xenogeneic setting

The immunomodulatory capacity of h- and r-MSCs in xenogeneic setting was first investigated by their ability to suppress TNF- α secretion by macrophages. CM treatment from all MSC types on h-Mac resulted in the decrease of TNF- α secretion, compared to the positive control (**Figure 20a**). h-Mac treated with CM from A-MSCs showed the lowest level of TNF- α (fold change of A-MSC: 0.38 ± 0.36), followed by those treated with r- and ABCB5+ MSC CM (fold change of rMSC: 0.4 ± 0.35 , ABCB5+: 0.56 ± 0.24). Inversely, in r-Mac, ABCB5+ CM-treated macrophages secreted the lowest level of TNF- α (fold change of ABCB5+: 0.30 ± 0.12), followed by r-MSC- and A-MSC CM-treated macrophages (fold change of rMSC: 0.53 ± 0.24 , A-MSC: 0.62 ± 0.30) (**Figure 20b**). Although at a glimpse all CM seemed to be able to suppress TNF- α secretion, it is important to note that the CM treatment itself affected the viability of h-Mac and r-Mac. h-Mac treated with r-MSC CM showed notably less viable cells as compared to the other groups, while r-Mac treated with both ABCB5+ and r-MSC CM showed more dead cells and debris, as compared to the rest (**Figure 20c**). To account for this, we always normalized values to the confluence. Only macrophages treated with A-MSC CM consistently showed high viability in both human and rat system.

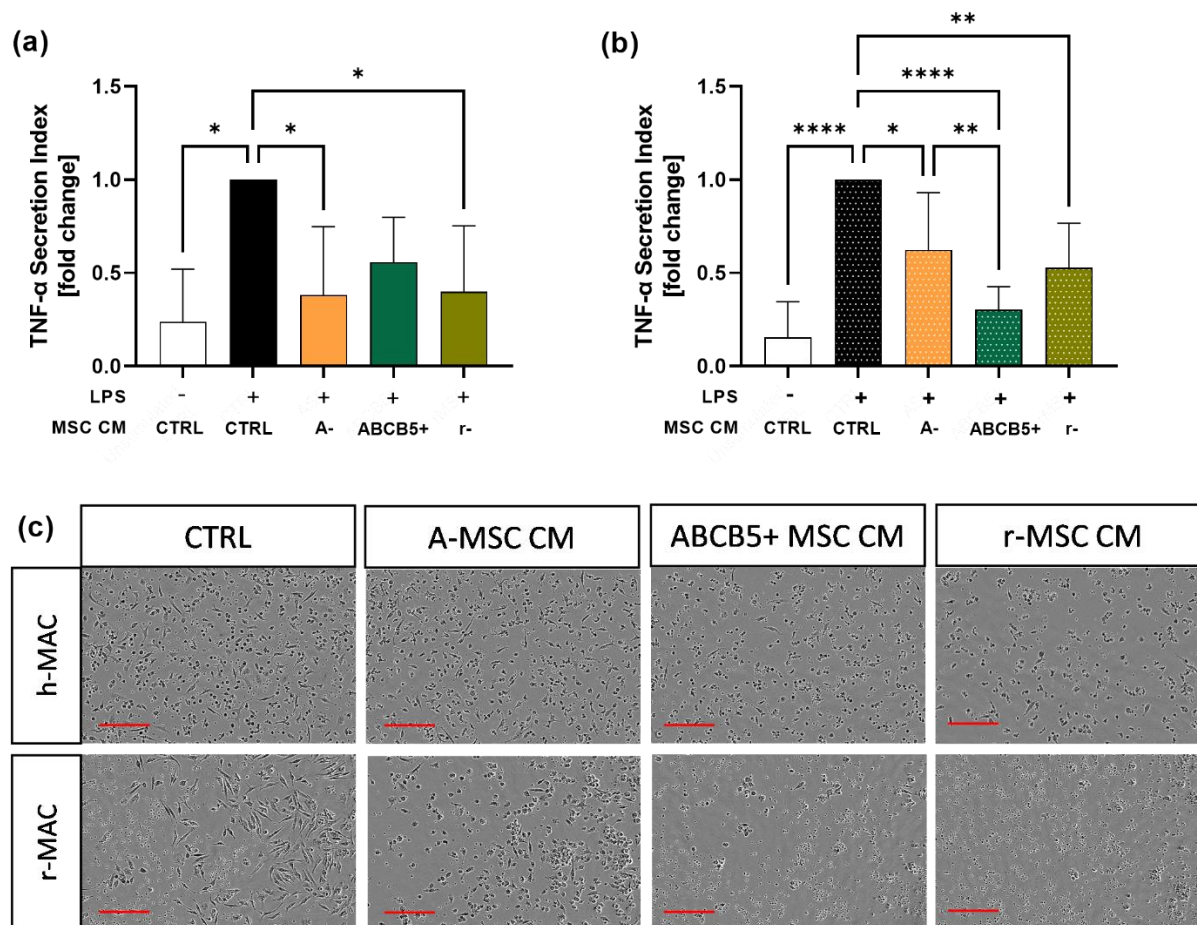


Figure 20. MSCs were able to inhibit LPS-stimulated TNF- α secretion by macrophages despite xenogenic setting

TNF- α secretion of hMac (a) and rMac (b) after 24h LPS stimulation (100ng/ml) in the presence and absence of CM. Two-Way ANOVA with Tukey's multiple comparison corrections. h-Mac N=4 and r-Mac N=4: CTRL N=1, ABCB5+, A-MSC and rMSC CM N=3. Representative image of h-Mac and r-Mac after being cultured with CM during the maturation period (6 days) (c). Scale bars indicate 200 μ m.

4.2.2 A-MSC promoted human and rat macrophages but the mediators differed

Next, we assessed the effect of CM derived from A-, ABCB5+, and r-MSCs on macrophage phagocytosis. As seen in **Figure 21a**, CM from A-MSCs elicited the highest phagocytosis of h-Mac (fold change: 1.6 ± 0.3), followed by r- (fold change: 1.2 ± 0.2) and ABCB5+ MSCs with the lowest phagocytosis (fold change: 0.5 ± 0.2). A similar pattern was also observed on r-Mac, where r-Mac treated with A-MSC CM exhibited the highest phagocytosis, followed by r- and ABCB5+ MSC CM (fold change: 1.8 ± 1.4 , 0.6 ± 0.5 and 0.5 ± 0.2 , respectively) (**Figure 21c**). The phagocytosis activity elicited by A-MSC CM in r-Mac showed notably higher standard deviation as compared to that in hMac (1.4 vs. 0.3 for r-Mac and h-Mac), which we attributed to the high variability of

A-MSD donors. In order to investigate the main factors responsible for MSD effect on macrophages, we attempted to inhibit factors described to be involved in macrophage polarization. IL-6R Ab, GW788, L161 and Bindarit were used concomitantly with CM treatment to inhibit IL-6, TGF- β 1, PGE-2 and MCP-1, respectively. In h-Mac, all the inhibitors seemed to have some effects on phagocytosis of CM-treated macrophages with PGE-2 inhibitor, L161, to be the most potent inhibitor, regardless of the CM source (**Figure 21b**). Yet, CTRL medium also showed the same inhibition pattern indicating that the inhibited factors were secreted by macrophages themselves in an autocrine fashion (**Figure 21b**). Meanwhile, in r-Mac the inhibitor of TGF- β 1, GW788, was able to significantly reduced r-Mac phagocytosis in the group treated with human MSD CM: A- and ABCB5+ MSD CM (**Figure 21d**). Phagocytosis reduction in GW788 treated r-MAC compared to corresponding group without inhibitor were 36%, 48%, 76%, and 76% for CTRL, A-, ABCB5+ and r-MSD CM, respectively (**Figure 21d**). All in all, MSD CM showed immune-compatibility in macrophages across species by skewing their polarization towards M2. Interestingly, we found out that the mediator of MSD in exerting this effect in h- and r-MSDs differed: while PGE-2 seemed to mediate MSD immunomodulation on h-Mac, TGF- β 1 appeared to play a more significant role on r-Mac.

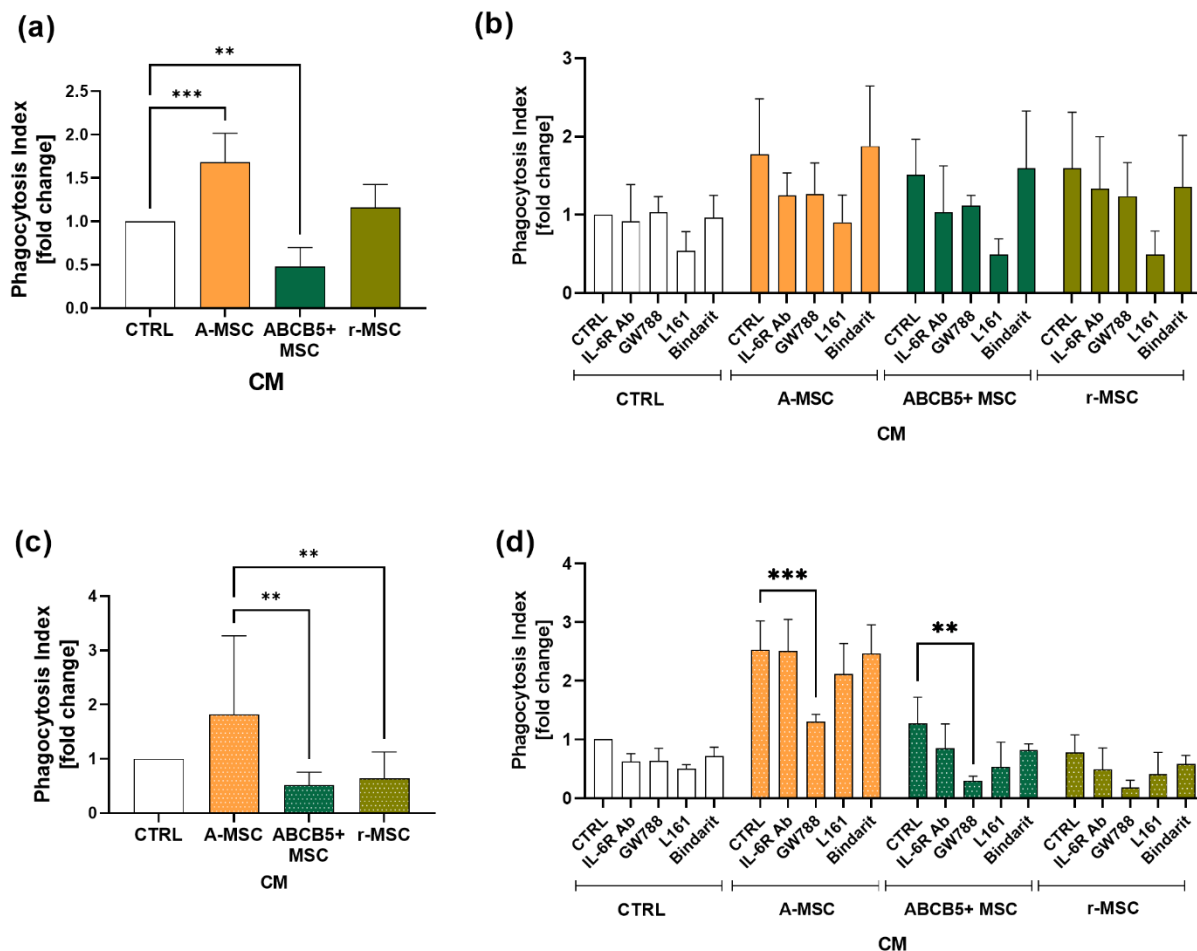


Figure 21. CM from A-MSCs showed the highest pro-phagocytosis effect in both species

Phagocytosis capacity of h-Mac (a) and r-Mac (c) after CM treatment. Phagocytosis of h-Mac (b) and r-Mac (d) after inhibition of MSC factors in the presence and absence of CM (pooled from N=3 MSC). One-Way ANOVA (a,c) and Two-Way ANOVA (b,d) with Tukey's multiple comparisons test. H-Mac N=4; r-Mac N=3.

4.3 Part 3: MSCs role in ciPTECs and macrophages crosstalk in *in vitro* cisplatin injury

Having established the importance of MSC manufacturing and immune-compatibility, we sought to define how MSCs deliver their therapeutic effect in a renal disease model *in vitro*. To investigate how the MSC secretome modulates ciPTECs and macrophages crosstalk, the pro-regenerative and immunomodulatory capacities of MSC CM were evaluated separately on ciPTECs and macrophages. The important mediator in the CM responsible to deliver its therapeutic effect on each cell type was also investigated.

4.3.1 Development of *in-vitro* cisplatin-induced AKI

We first developed an *in vitro* model for cisplatin AKI using ciPTECs. Matured ciPTECs were treated with cisplatin in SFM for 24h and their viability was assessed by measuring their mitochondrial metabolism with PrestoBlue. As expected, cisplatin decreased ciPTEC viability in a dose-dependent manner (**Figure 22a**). The intracellular ATP level of ciPTECs treated with the lowest cisplatin concentrations were also measured. An abrupt decrease of ATP levels was observed from ciPTECs treated with 15 μM and 31 μM of cisplatin (fold change: 0.83 and 0.4 for 15 μM and 31 μM of cisplatin, respectively) (**Figure 22b**). On the contrary, 62 μM of cisplatin did not significantly add to ATP reduction compared to that of 31 μM . Furthermore, to analyse the long-term effect of cisplatin toxicity, we did wound scratch assay and measured ciPTEC migratory capacity to close the wound. As depicted in **Figure 22c**, even the lowest cisplatin concentration, 15 μM , was able to decrease ciPTEC migration by 62%, compared to the CTRL. Meanwhile, 31 and 62 μM of cisplatin caused drastic drop of ciPTEC migration which accounted to 87 and 91% decrease that might be irreversible. Based on these results, we decided to proceed with 15 μM of cisplatin as it appeared to deliver enough toxicity on ciPTECs that was still reversible.

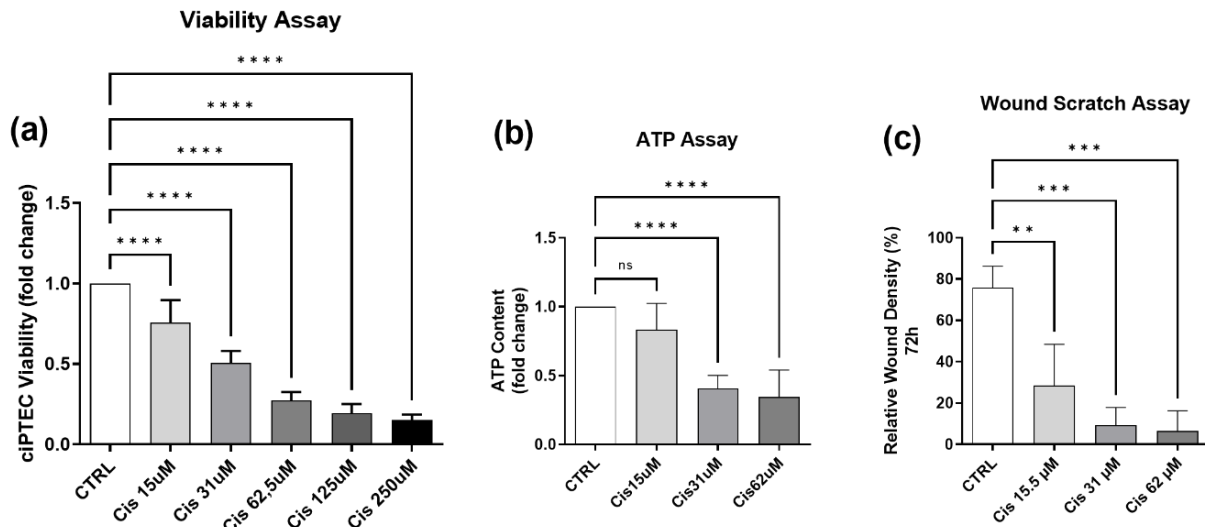


Figure 22. The development of *in vitro* model for cisplatin-induced AKI

Matured ciPTECs were treated with different concentrations of cisplatin for 24h, before their viability (a) and intracellular ATP were measured (b). To assess their migratory capacity, after 24h of cisplatin treatment ciPTEC monolayer was scratched and cisplatin-containing medium was replaced with SFM. The closing of the wound was monitored for monitored using live-cell imaging and quantified 3 days after cisplatin removal (c). One-Way ANOVA with Tukey's multiple comparisons test. All graphs: ciPTEC n=3.

4.3.2 Direct effect of MSC CM on cisplatin-treated ciPTECs

4.3.2.1 A-MSCs demonstrated higher protective effect on cisplatin-induced apoptosis of ciPTECs than ABCB5+ MSCs

Next, the anti-apoptotic capacity of A- and ABCB5+ MSC secretomes in CM was compared in cisplatin-injured ciPTECs. 24h treatment of cisplatin induced ciPTEC apoptosis which progressed overtime as marked by the increase of Apotracker-labeled cells - even after being removed (**Figure 23a**). Apoptosis quantification 3 days after cisplatin removal revealed that ciPTECs treated with ABCB5+ CM showed on average 37% less apoptosis as compared to cisplatin CTRL, however the apoptosis reduction was not statistically significant due to high variability between ABCB5+ donors (fold change: 0.63 ± 0.37 , **Figure 23b**). Meanwhile, A-MSC CM was able to significantly suppress ciPTEC apoptosis on average by 70% as compared to cisplatin control (fold change: 0.31 ± 0.23). It is also noteworthy that ciPTECs treated with A-MSC CM showed higher confluence than the control and ABCB5+ CM groups (**Figure 23a**). Our data suggests that A-MSC CM was superior to ABCB5+ MSC CM in attenuating ciPTEC apoptosis. Therefore, only CM from A-MSCs was used for the rest of this study.

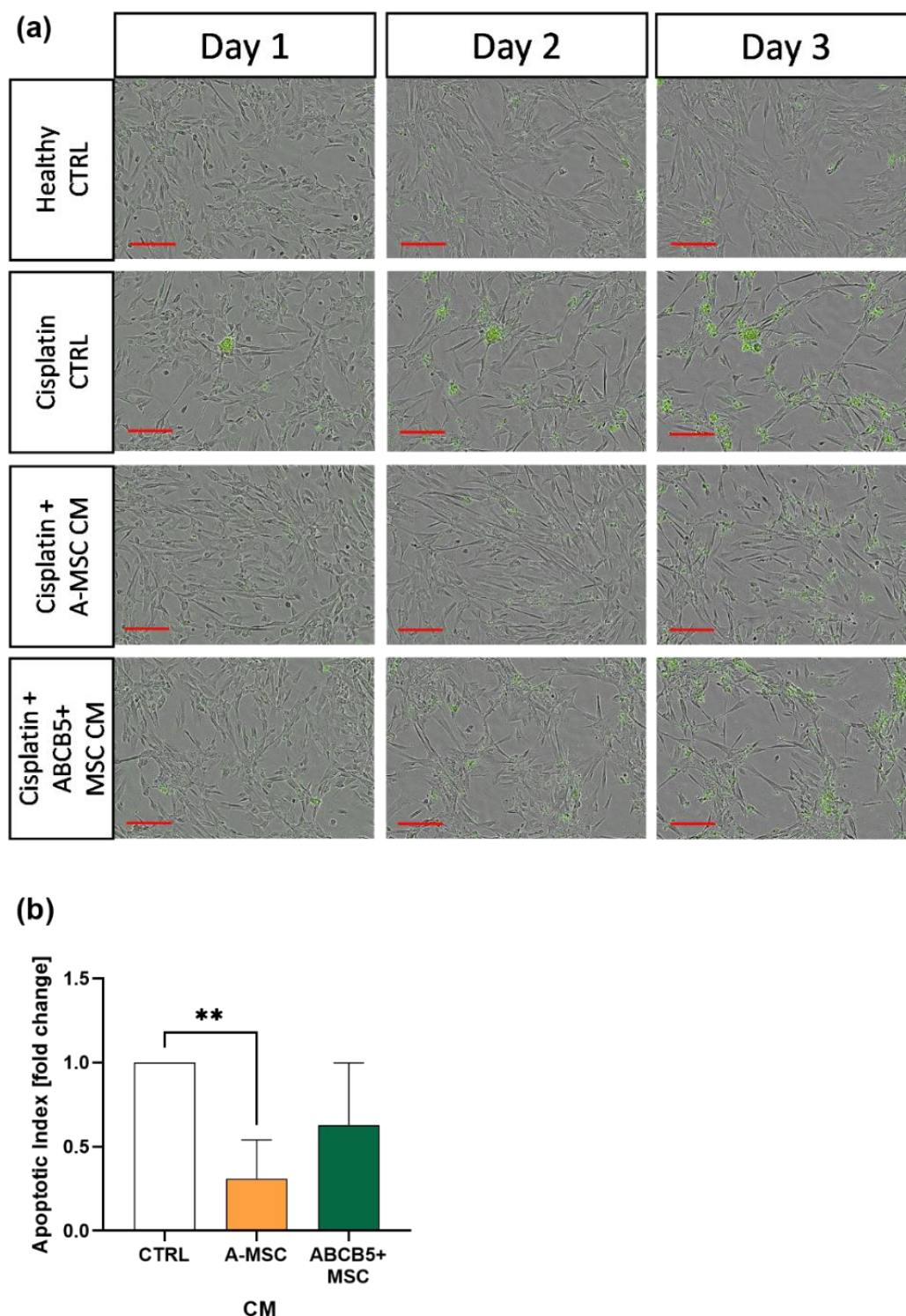


Figure 23. CM from A- and ABCB5+ MSCs decreased cisplatin-induced apoptosis of ciPTECs
ciPTECs were treated with cisplatin in the presence or absence of CM. After 24h cisplatin-containing medium was replaced with fresh CM or CTRL medium without cisplatin and in the presence of apotracker. Apoptosis of ciPTECs were monitored by live cell imaging for 3 days. **(a)** Representative images of ciPTEC day 1, 2 and 3 after cisplatin treatment started. Green: apoptotic cells. Scale bars: 200 μ m. **(b)** Quantification of ciPTEC apoptosis on day 3. One-Way ANOVA with Tukey's multiple comparisons test; cisplatin CTRL N=1, ABCB5+ CM N= 3, A-MS-CM CM N= 4, ciPTEC n=3.

4.3.2.2 A-MSC CM increased ciPTEC viability and migratory, while suppressing apoptosis

To further investigate the direct effect of A-MSC CM on ciPTECs treated with 15 μ M cisplatin, we measured ciPTEC viability, cytokine release, apoptosis, and migration. The scheme of cisplatin and CM treatment is illustrated on **Figure 24a**. After 24h of treatment, cisplatin decreased ciPTEC viability by 13%, meanwhile, CM significantly increased ciPTEC viability in both groups, cisplatin-untreated (UT-CM) and treated (Cis-CM) groups (**Figure 24b**). Cytokine release of ciPTECs was evaluated by measuring the IL-8 in cell culture SN. Interestingly, even though CM elevated IL-8 in untreated ciPTECs, it decreased IL-8 secretion in cisplatin-treated group (**Figure 24c**).

Furthermore, cisplatin was shown to exert lasting cytotoxicity. As depicted in **Figure 24d**, on day 4 after the treatment started, ciPTECs that were initially treated with cisplatin in the presence of CTRL media (Cis-CTRL) gradually exhibited increased apoptosis. This cisplatin-induced apoptosis was dampened by CM. The apoptosis quantification on d4 revealed that ciPTECs treated with cisplatin and CM (Cis-CM) demonstrated 55.68% reduction of apoptosis, compared to Cis-CTRL (**Figure 24e**). Not only rescuing from cell death, CM also promoted ciPTEC migratory capacity (**Figure 24f-g**) as shown by the increased Relative Wound Density (cell density in the initial wound area relative to the rest of the culture) in UT-CM and Cis-CM overtime after cisplatin removal, as compared to CTRL groups.

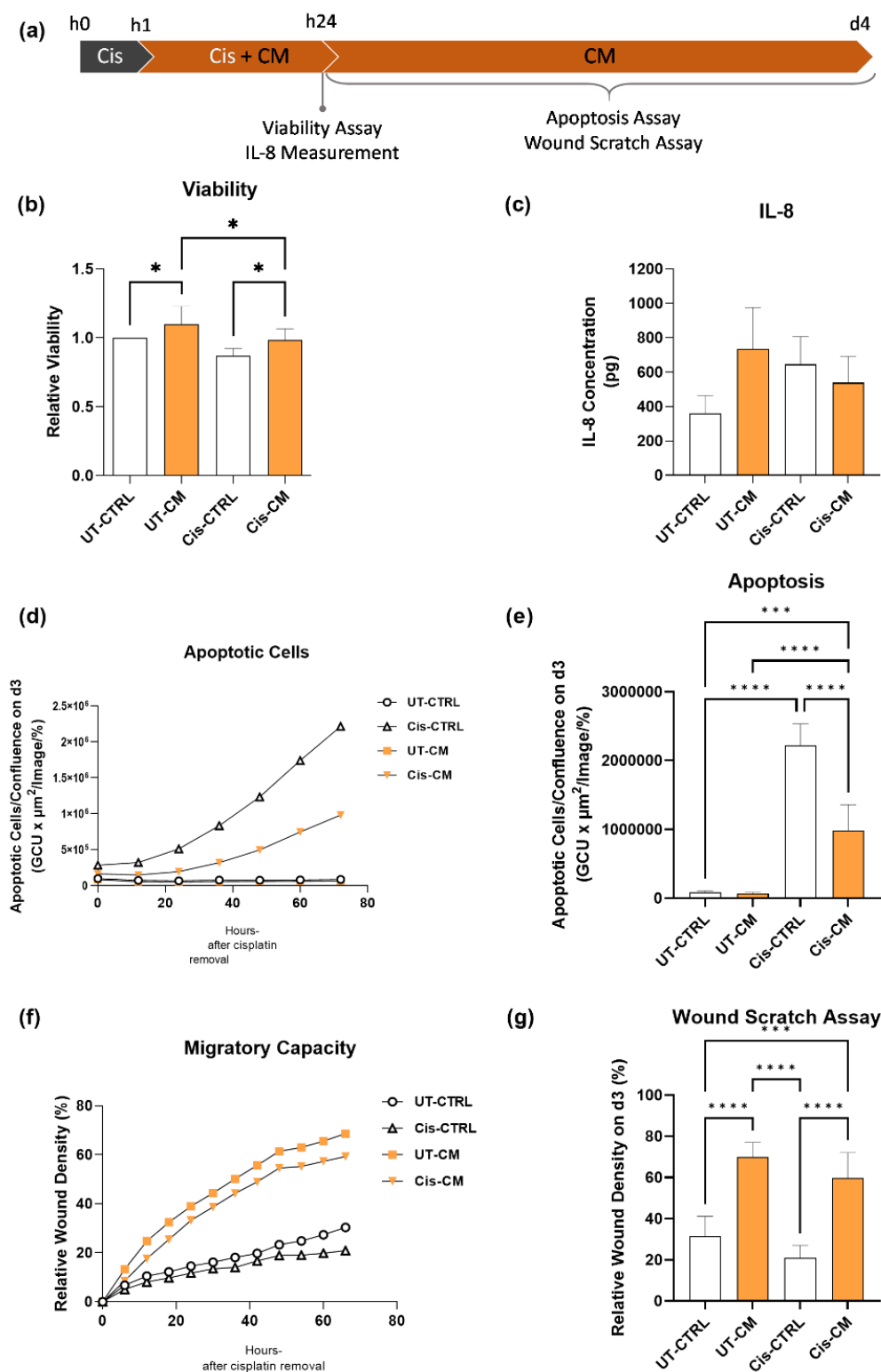


Figure 24. CM protected ciPTECs from cisplatin cytotoxicity

The scheme of cisplatin and CM treatment on ciPTECs **(a)**. ciPTECs were treated with cisplatin for a total of 24h in the absence and presence of CM and the viability **(b)** and IL-8 release **(c)** were measured using PrestoBlue and ELISA, respectively. The following day, the cisplatin-containing medium was replaced with either CM or CTRL medium and the apoptosis was monitored for additional 3 days **(d-e)**. To measure migratory capacity of ciPTECs, the monolayer was scratched to assess after cisplatin removal.

The closing of the wound also was monitored for another 3 days (**f-g**). Two-way ANOVA with Tukey's multiple comparisons test. For viability and wound scratch assay: UT-CTRL and Cis-CTRL n= 4, UT-CM and Cis-CM N= 4. For apoptosis assay: UT-CTRL and Cis-CTRL n= 3, UT-CM and Cis-CM N= 4.

4.3.2.3 CM attenuated cisplatin-induced modification of ciPTEC gene expression

To better understand the molecular pathway by which cisplatin and CM exert their effects, we performed a PCR array for nephrotoxicity and found out that cisplatin did indeed change the ciPTEC gene expression profile (**Figure 25a**). Meanwhile, CM was able to partly abrogate cisplatin-induced gene expression. Furthermore, to confirm our finding, we did qPCR for genes involved in DNA damage and apoptosis (CDKN1a and GADD45a), oxidative stress (HMOX-1), and cellular stress (ATF-3). As illustrated in **Figure 25b-e**, cisplatin elevated all of those markers, while CM repressed their expression.

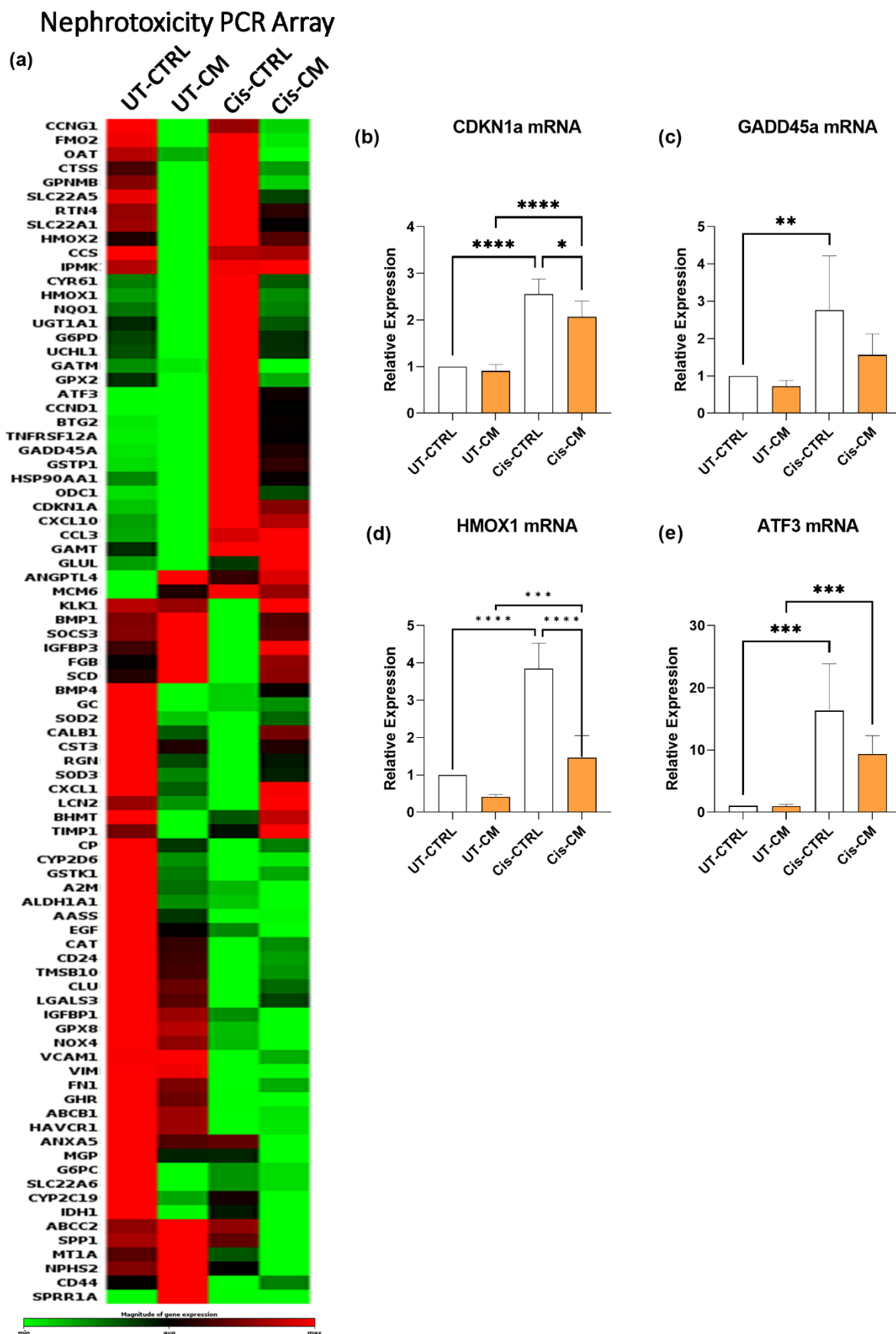


Figure 25. Gene expression analysis showed that CM dampened cisplatin effect on DNA damage and oxidative stress

ciPTEC mRNA was isolated and subjected PCR array for nephrotoxicity **(a)** and qPCR for GADD45a **(b)**, CKN1a **(c)**, ATF3 **(d)**, and HMOX-1 **(e)**. Two-way ANOVA with Tukey's multiple comparisons test. For qPCR: UT-CTRL and Cis-CTRL n= 3, UT-CM and Cis-CM N= 4. For PCR array: UT-CTRL and Cis-CTRL n= 2, UT-CM and Cis-CM N= 4.

4.3.2.4 Extracellular vesicular was dispensable for anti-apoptotic function of CM

As EVs have been reported to be the mediator responsible for MSC therapeutic effect⁸⁶, we then investigated the anti-apoptotic effect of CM after EV depletion. Ultra-filtration with a 100 kDa cut-off membrane was used to deplete EVs from the CM. The concentrations of EVs or the particles with a size larger than 100 kDa before and after the ultra-filtration are depicted in **Figure 26a**. CM from different donors contained a wide variant of EV concentration, which was effectively depleted by ultra-filtration as seen in CM-FT. EVs were not detected in the CTRL medium before and after ultra-filtration. Results of the apoptosis assay on cisplatin-treated ciPTECs were similar despite the depletion of EV, as there was no significant discrepancy in apoptosis between the ciPTECs treated with original CM and CM-FT (**Figure 26b**) relative to their corresponding cis-CTRL and cis-CTRL-FT, respectively. It has been shown that, ultra-filtration can also deplete other soluble factors from CM, not only EVs, through electrostatic interactions between the soluble factors and the membrane⁸⁰. To account for this, the apoptotic level of cis-CM and cis-CM-FT were normalized to their respective CTRL to compensate for the loss of media supplements due to the ultra-filtration process.

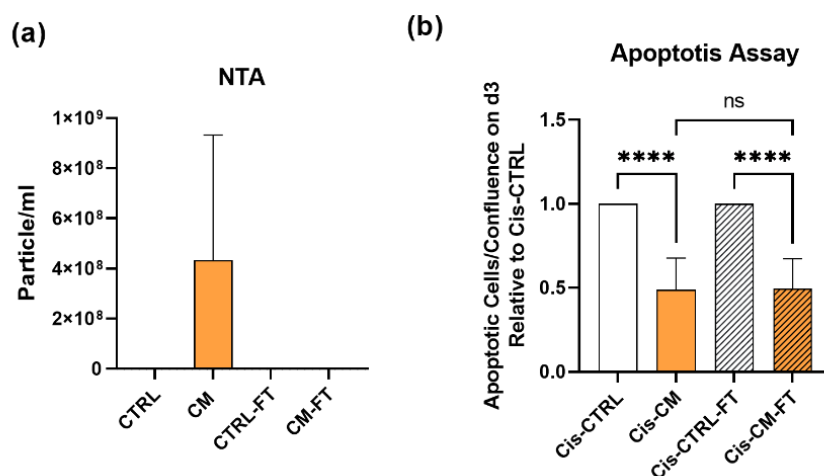


Figure 26. Anti-apoptotic of CM was not affected by EV depletion

The concentration of EVs in CTRL medium and CM with and without EV depletion by 100kDa ultra-filtration **(a)**. The apoptosis level of ciPTEC 3d after cisplatin removal as presented in relative value of the corresponding cis-CTRL **(b)**. Two-way ANOVA with Tukey's multiple comparisons test. For NTA: CTRL n= 3, CM N= 4. For Apoptosis Assay: cis-CTRL and cis-CTRL-FT n= 4; cis-CM and cis-CM-FT N= 4.

4.3.2.5 Despite high concentration of IL-6 in CM, it could not increase phosphorylation of STAT3 in ciPTECs

Not only EVs, CM also contained a high concentration of IL-6 (**Figure 27a**), known as a pleiotropic cytokine responsible for both pro- and anti-inflammatory responses of immune cells, and which has been postulated to play an important role in kidney injury^{87,88}. IL-6 produced by MSCs has also been shown to suppress the cytokine release of endothelial cells treated with TNF- α , which led to downregulation of leukocytes recruitment in endothelial cells and leukocytes co-culture⁸⁹. Given the possible regenerative effect of IL-6, we investigated whether IL-6 might be responsible for the protective effect of CM against cisplatin toxicity on ciPTECs. To do this, we measured the phosphorylation of signal transducer and activator of transcription 3 (STAT3) which takes place upon IL-6 binding to its receptor and is responsible for the activation of multiple cellular pathways⁹⁰. ciPTECs were first treated with cisplatin for 1 hour in ciPTEC SFM or the CTRL media for ciPTECs. Following cisplatin treatment, the medium was replaced with CM or CTRL medium with or without cisplatin. After 20 minutes, ciPTECs were quickly harvested and fixed for intracellular staining of pSTAT3. Considering that the culture supplements in ciPTEC SFM might affect pSTAT3, healthy ciPTECs cultured in the ciPTEC basal medium, DF12, were used as negative control. Indeed, the supplement in ciPTEC medium, even without serum, already provoked the phosphorylation of STAT3 by 25%, as compared to the ciPTECs cultured in DF12 alone (**Figure 27b**). Meanwhile the treatment of CM did not increase the level of pSTAT3 in ciPTECs, probably because pSTAT3 was already high due to the stimulation of ciPTEC culture supplements. Given that the downstream pSTAT3 was not upregulated by the presence of high levels of IL-6, we concluded that IL-6 was not essential for the protective effect of CM on cisplatin-treated ciPTECs.

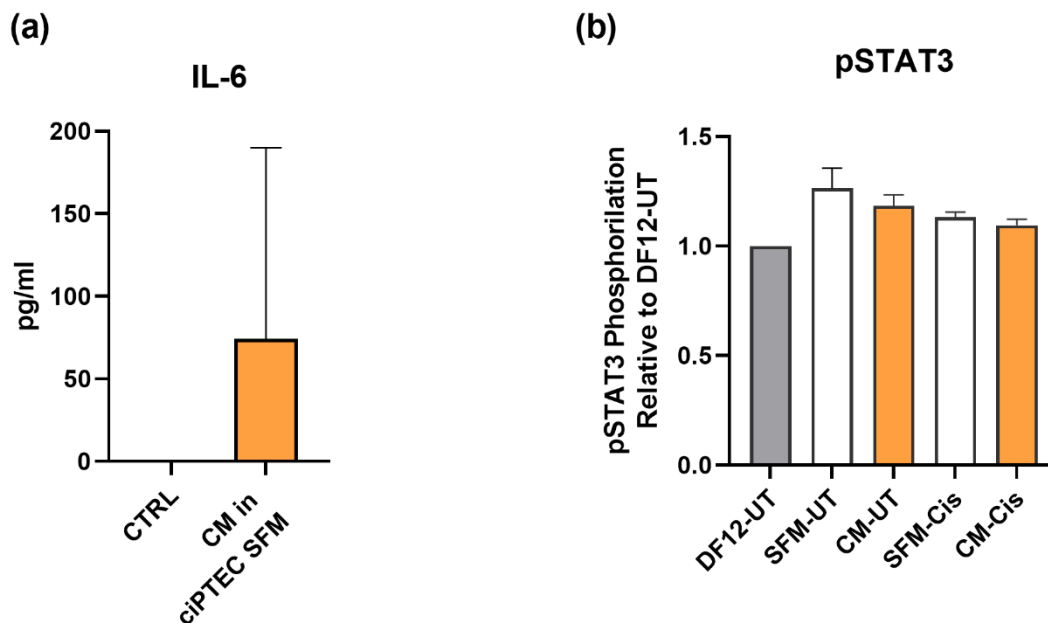


Figure 27. Despite its high concentration, IL-6 was not responsible for CM protective effect on ciPTECs

The concentration of IL-6 in CM from 4 donors, measured by ELISA **(a)**. The phosphorylation of STAT3 on ciPTECs after 1 hour cisplatin treatment followed by 20 minutes of CM treatment, measured by intracellular staining and FACS **(b)**. One-way ANOVA with Tukey's multiple comparisons test: no statistical significance. For IL-6 ELISA: N=4. For pSTAT3: n=2.

4.3.2.6 CM contained high free thiols which linked to decreased oxidative stress

We then shifted our focus to the anti-oxidant content of CM, as oxidative stress is a hallmark of cisplatin cytotoxicity^{46,47} and our gene expression results suggested that CM could intervene with this pathway. The level of anti-oxidant in the CM was assessed by measuring free thiols as they act as ROS scavenger⁸². As seen in **Figure 28a**, CM had higher free thiol content as compared to the empty media used to produce CM. The level of free thiols differed greatly as indicated by the high standard deviation due to the heterogeneity of MSC donors. ROS measurement of ciPTECs revealed that CM was able to decrease ROS level in both UT- and cis-treated ciPTECs by 43% and 79%, respectively (**Figure 28b**). It is also noteworthy that a Spearman test suggested that the free thiol content correlated with suppression of ROS (in UT- and cis- groups, **Figure 28c-d**) as well as apoptosis inhibition (**Figure 28e**). In aggregate, we attribute the anti-apoptotic effect of CM to its free thiol content, instead of EVs.

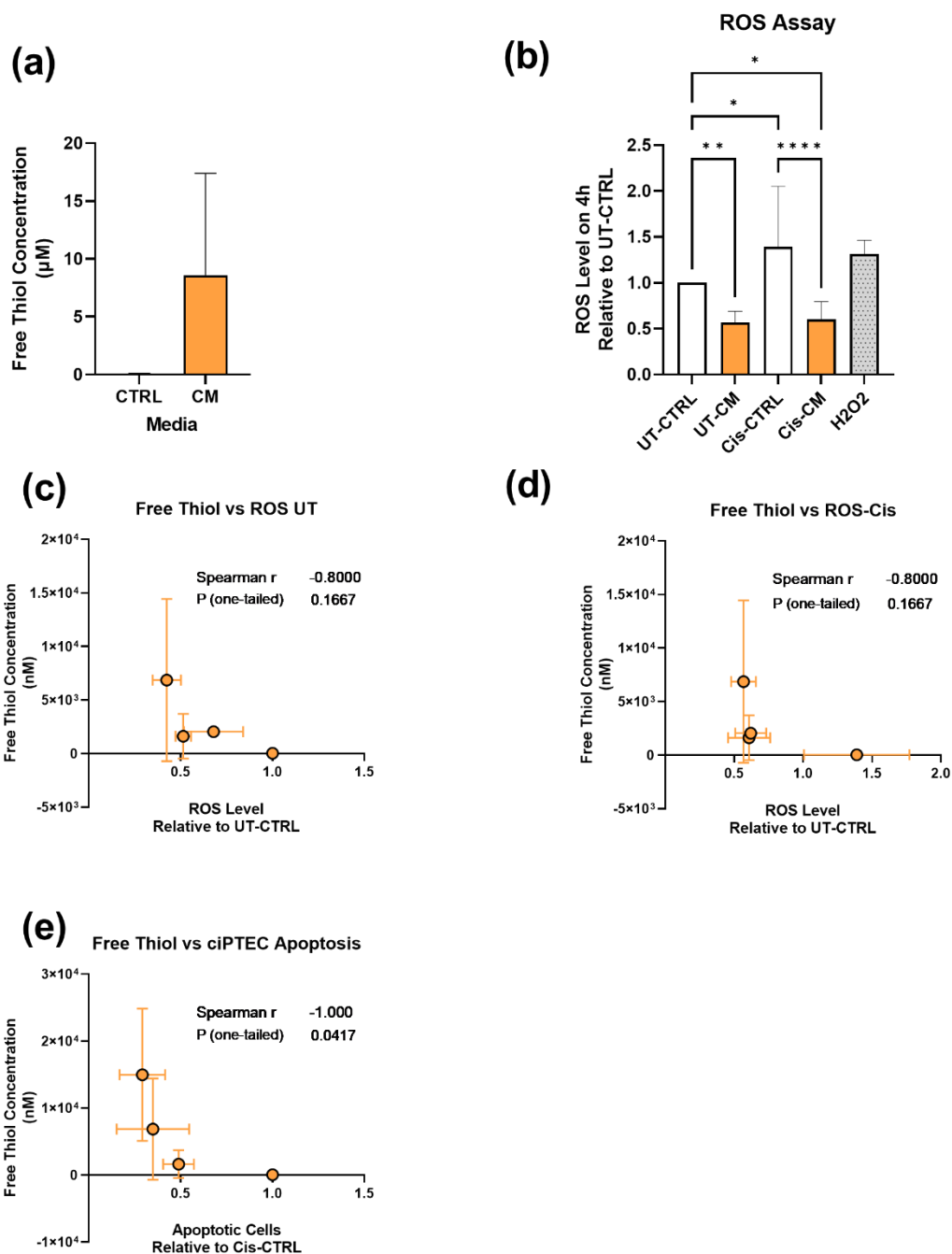


Figure 28. Free thiol content in CM might deliver anti-oxidative stress in ciPTECs

The concentration of free thiol in the CTRL medium and CM **(a)**. The intracellular ROS level of ciPTECs treated with cisplatin and CM **(b)**. Two-way ANOVA with Tukey's multiple comparisons test. For free thiol measurement: CTRL n= 3, CM N= 4. For ROS Assay: CT-CTRL, Cis-CTRL, and H₂O₂ n= 3; UT-CM and Cis-CM N= 4. Spearman test of free thiol content in CM with ROS level in UT-CM **(c)** and Cis-CM ciPTECs **(d)**. Spearman test of free thiol content with apoptosis level in Cis-CM group **(e)**. For all tests:CM N=3, ciPTECs n=3.

4.3.3 Immunomodulation of CM on cisplatin-treated macrophage

4.3.3.1 CM promoted M2 polarization of macrophage, while cisplatin compromised CM effects

Next, we elucidated how cisplatin and CM influence the macrophage phenotype. The cisplatin and CM treatments on macrophages were done according to the scheme depicted on **Figure 29a**. **Figure 29b-d** shows that unlike in ciPTECs, cisplatin barely affected macrophages. The M1 surface marker of macrophages remained stable, while CM significantly suppressed HLA-DR and CD86 levels in both cisplatin-treated and untreated groups, except for CD38 levels. Cisplatin also did not affect the decreasing effect exerted by CM on these M1 markers. Looking at the M2 markers CD206 and CD163, there was no direct effect of cisplatin on these markers, while CM increased the level of these two M2 surface markers (**Figure 29e-f**). However, cisplatin appeared to attenuate the CM effect on the CD206 level as marked by the loss of significant difference between cis-CTRL and cis-CM, and the gained statistical significance between UT-CM and cis-CM (**Figure 29e**).

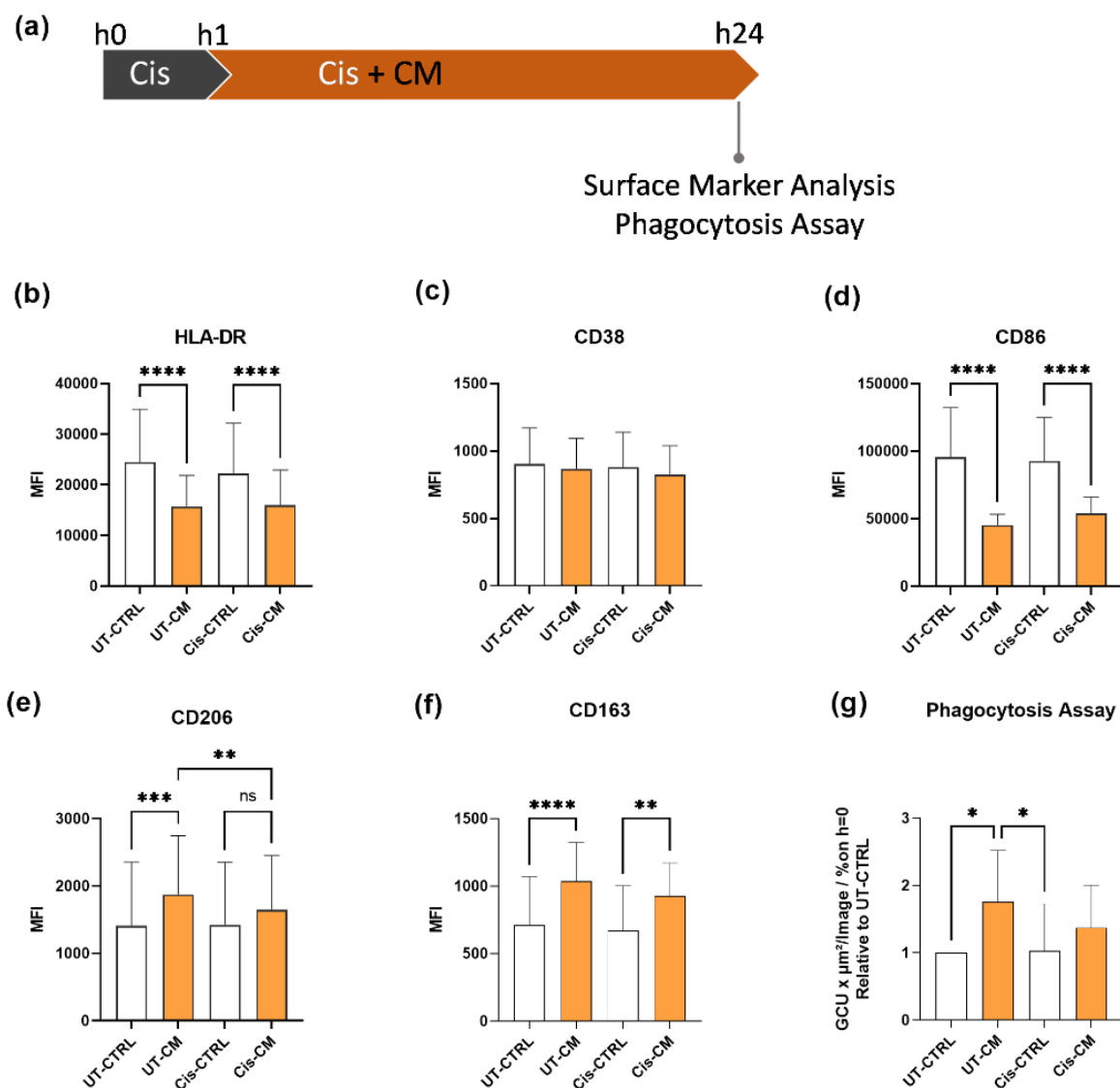


Figure 29. CM skewed macrophages phenotypes towards M2, while cisplatin slightly attenuated this effect

Scheme of cisplatin and CM treatment on macrophages (a). Macrophages were treated with cisplatin in the presence and absence of CM for a total of 24h, harvested, and their surface markers were measured using FACS. The mean fluorescence intensity (MFI) for HLA-DR (b), CD38 (c), CD86 (d), CD206 (e), CD163 (f) was shown. Meanwhile, the phagocytosis capacity of macrophages after the treatment was assessed using *E. coli* Green bioparticles and monitored for 6h by live-cell imaging. The phagocytosis on 6h was presented as relative value to that of UT-CTRL macrophages (g). Two-way ANOVA with Tukey's multiple comparisons test. For surface marker measurements: UT-CTRL and cis-CTRL N= 5; UT-CM and Cis-CM

To see whether the effect of cisplatin and CM on macrophage surface markers has any functional implication, their phagocytosis capacity was assessed. As expected, CM enhanced the phagocytosis activity of macrophages significantly (Figure 29g). Meanwhile, cisplatin, which did not alter the phagocytosis of macrophages in the CTRL

groups (1.00 ± 0.00 vs. 1.02 ± 0.70 - fold change for UT-CTRL and Cis-CTRL, respectively), tended to attenuate phagocytosis in groups treated with CM, albeit not significant (1.77 ± 0.76 vs. 1.38 ± 0.63 - fold change for UT-CM and Cis-CM, respectively). It is also noteworthy that we can calculate a positive correlation between CM free thiols and phagocytosis activity elicited by CM (**Figure 30a-b**).

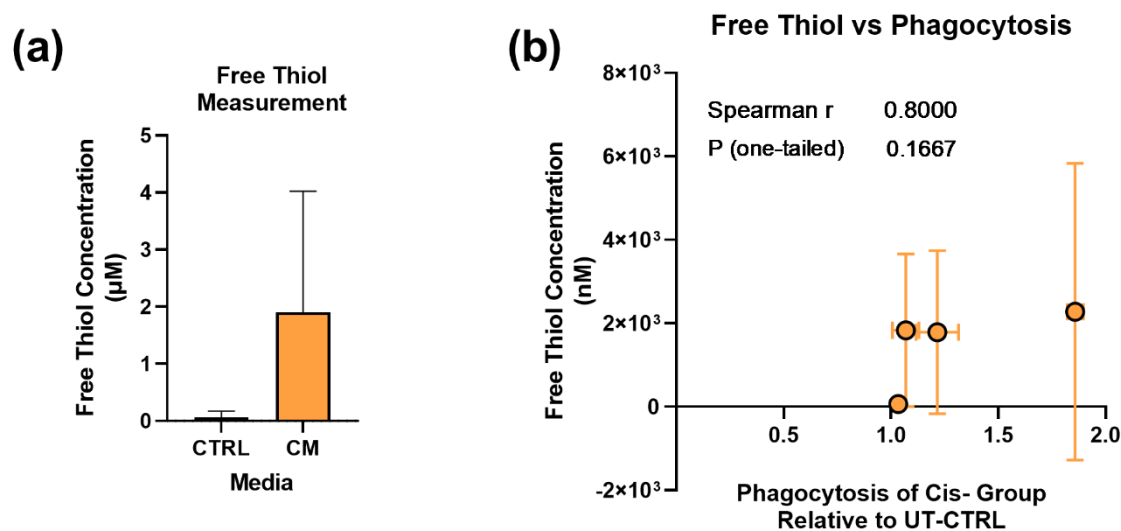


Figure 30. CM free thiols correlate to the promotion of phagocytosis.

Free thiols content measured in CM that was generated in X-Vivo 10 (used for producing CM for macrophages experiments) **(a)**. Spearman test between free thiol content and phagocytosis level of Cis-CM macrophages **(b)**. For thiol measurement: CTRL n=3; CM N=3. For Spearman test: CM N=3, macrophages N=4.

4.3.4 Modification of ciPTEC-macrophage interaction by CM

Once the effect of CM on each cell type was established, we attempted to investigate how CM influences the interaction of those cell types using an indirect co-culture system. Of note, the concentration of cisplatin used within the co-culture system was doubled to $30 \mu\text{M}$ as it seemed that the membrane coating increased ciPTEC tolerance to cisplatin (data not shown) and, therefore, $15 \mu\text{M}$ was no longer toxic. Following the maturation of ciPTECs and macrophages, both cell types were treated with cisplatin separately for 1h. Subsequently, the ciPTECs and macrophages culture were combined and media were refreshed with CM containing cisplatin in both compartments, the apical and basolateral side with the respective CM. The co-cultures were then incubated for another 23h before subjected for further analysis.

4.3.4.1 Cocultured macrophages did not boost CM protective effect on ciPTECs

Upon treatment of ciPTECs-macrophages co-culture with cisplatin and CM, the markers of cell stress and death were measured in ciPTECs. The images of ciPTECs stained for CX-43, an apoptotic marker, and nuclei are shown in **Figure 31a**.

The level of CX-43, a gap junction protein whose expression has been implicated in various nephropathologies⁹¹, was elevated by the cisplatin treatment up to 4 ± 3.46 - and 3.2 ± 1.32 -fold in ciPTEC mono-culture and ciPTEC-Mac co-culture, respectively (**Figure 31b**). There was a small decrease in CX-43 level when ciPTECs were co-cultured with macrophages, but this reduction was overruled by CM that further inhibited CX-43 levels to 1.9 ± 0.65 - and 1.97 ± 0.83 -fold in ciPTEC mono-culture and ciPTEC-Mac co-culture, respectively. A similar pattern was observed using Apotracker staining of ciPTECs which showed the translocation of phosphatidylserine to the cell surface in apoptotic cells (**Figure 31c**). The anti-apoptotic properties of CM completely surpassed the co-culture effect (apoptotic levels were 2.42 ± 1.08 - and 2.44 ± 1.49 -fold for cis-CM in ciPTEC alone and ciPTEC-Mac co-culture, respectively). When assessing the nuclei fragmentation of ciPTECs, CM also exerted a greater effect in suppressing the number of fragmented nuclei and nuclei fragments than the co-culture (**Figure 31d-e**).

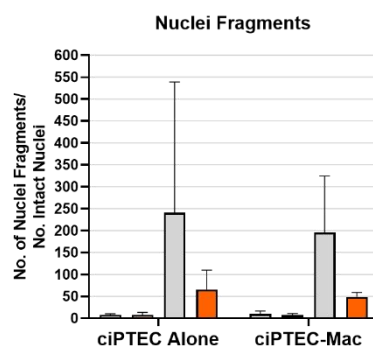
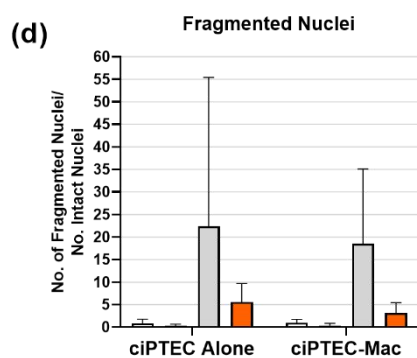
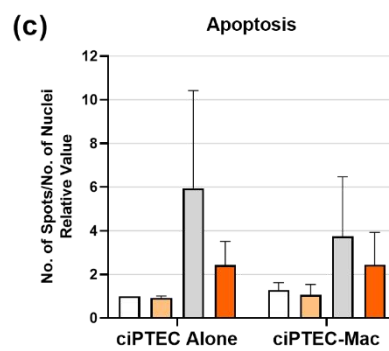
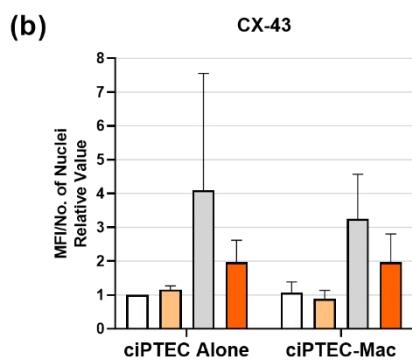
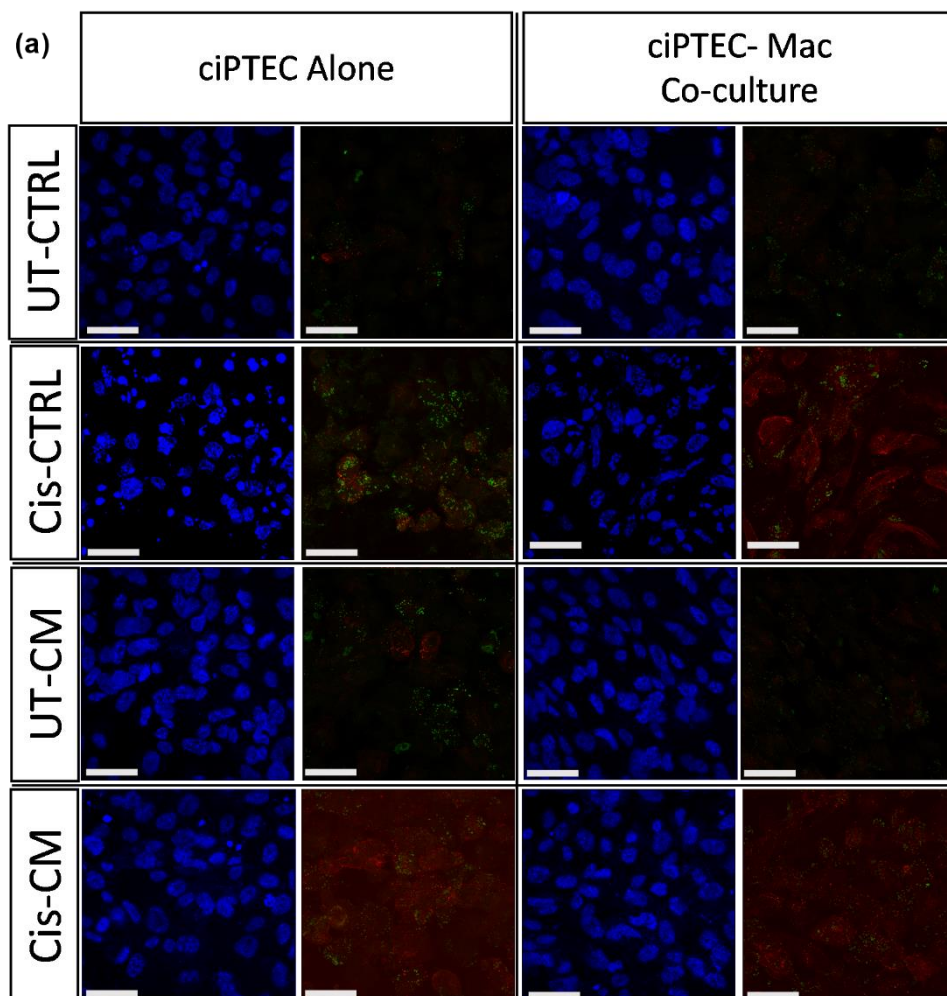


Figure 31. The expression of CX-43, apoptosis and nuclei fragmentation of ciPTECs after co-culture with macrophages

Representative images of ciPTECs on the transwell membrane after being cultured alone or co-cultured with macrophages in the presence or absence of cisplatin with or without CM (a). Following cisplatin treatment for 24h, the cells were stained for CX-43 (in Red), apoptosis marker (in Green) and DAPI (Blue) and imaged using confocal microscopy. Scale bars represent 40 μ m. The quantification of the fluorescence intensity of CX-43 (b), the number of Apotracker spots (c), the fragmented nuclei (e) and nuclei fragments (e), normalized by the number of intact nuclei, were presented as relative value to UT-CTRL ciPTEC cultured alone. Using three-way ANOVA with Tukey's multiple comparisons test, no significance difference was found. For surface CX-43, fragmented nuclei and nuclei fragments staining: all groups N=4. For apoptosis staining: all groups N=3.

Furthermore, given the importance of TNF- α in cisplatin-induced AKI^{92,93}, the SN from the apical side of the co-culture (ciPTEC) was subjected to TNF- α measurement by ELISA. The increase of TNF- α level caused by cisplatin treatment in a co-culture setting was lower in SN of the ciPTEC-Mac co-culture than that of the ciPTEC monoculture (12.76 ± 12.34 - and 10.59 ± 10.59 - fold, for Cis-CTRL in ciPTEC alone vs ciPTEC-Mac co-culture, respectively, **Figure 32**). TNF- α levels in both culture settings were further suppressed by CM treatment to 5.99 ± 5.02 - and 4.76 ± 4.33 - fold in ciPTEC alone and ciPTEC-Mac co-culture, respectively.

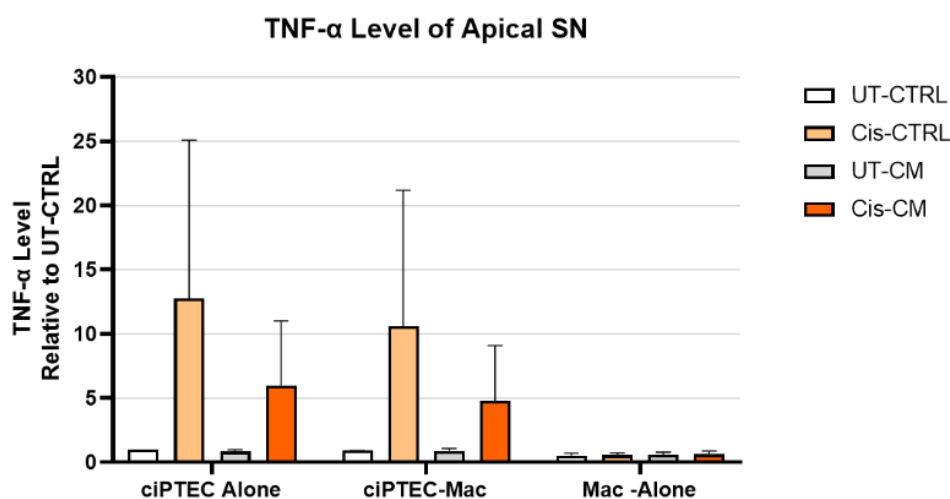


Figure 32. Macrophages' influence on TNF- α production was overcome by CM

The level of TNF- α on the supernatant of the apical side of the co-culture after 24h of cisplatin treatment in the presence or absence of CM, measured by ELISA and presented as relative value to the UT-CTRL of ciPTEC cultured alone. Three-way ANOVA with Tukey's multiple comparisons test, no significance difference was found. For TNF- α ELISA: all groups N=3.

4.3.4.2 ciPTECs enhanced macrophage phagocytosis but the effect was overruled by CM

With respect to the co-culture effect on macrophages, untreated macrophages (UT-CTRL) co-cultured with ciPTECs showed 47 % higher phagocytosis activity than macrophages cultured alone (**Figure 33**). CM stimulated the phagocytosis even more in both culture systems (4.37 ± 3.09 - and 4.32 ± 2.59 -fold for UT-CM of macrophage alone and ciPTEC-Mac co-culture, respectively). In contrast to the lower concentration of cisplatin, 15 μM , which did not affect macrophage phagocytosis directly (Figure 3F), 30 μM cisplatin was able to reduce phagocytosis (0.72 ± 0.24 - and 0.9 ± 0.39 -fold for Cis-CTRL of macrophage alone and ciPTEC-Mac co-culture, respectively). Interestingly, this cisplatin-mediated inhibition of phagocytosis also persisted in presence of CM (2.80 ± 1.13 - and 2.62 ± 0.65 -fold for Cis-CM of macrophage alone and ciPTEC-macrophage co-culture, respectively).

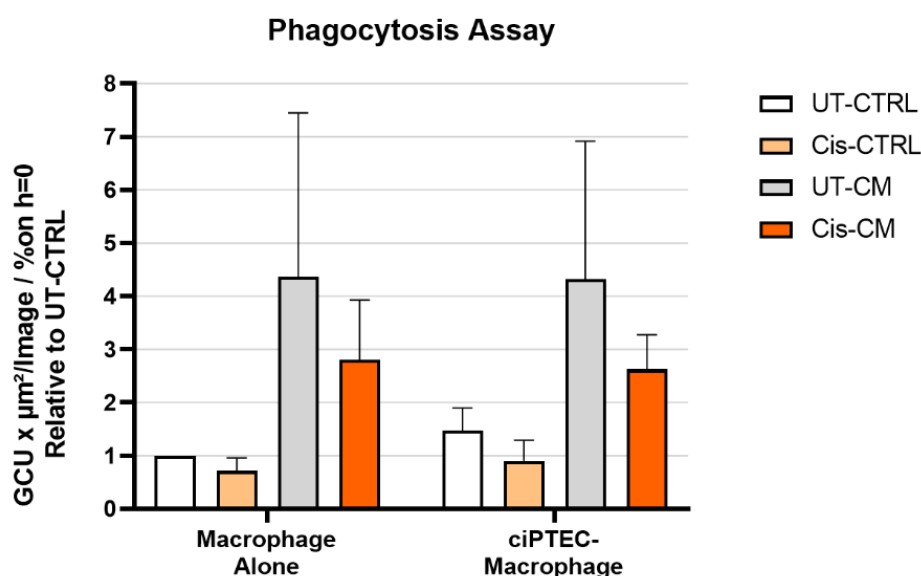


Figure 33. While the co-culture tended to increase macrophage phagocytosis, it did not add up to CM pro-phagocytotic effect

Phagocytosis after 24h of cisplatin treatment as presented as relative value to UT-CTRL of macrophage cultured alone. Three-way ANOVA with Tukey's multiple comparisons test, no significant difference was found. For phagocytosis: all groups N=3.

4.3.4.3 CM attenuated ciPTEC-induced secretion of cytokines and DAMP by macrophage

To unravel the interaction between ciPTECs and macrophages, the SN from the basolateral side of the co-culture (macrophages) was probed for the factors listed in **Figure 29**. Of note, all the values were normalized by the UT-CTRL of macrophages cultured alone. As expected, it seemed that the majority of analytes detected in the basolateral SN were secreted by macrophages as the values in ciPTEC mono-culture were lower than in macrophage monoculture and co-culture.

Within the group without CM, ciPTECs generally stimulated the secretion of certain factors by macrophages, including IL-8, arginase-1, fractalkine, and IL-1 β with 71%, 61%, 44%, and 30% increase in UT-CTRL of ciPTEC-Mac co-culture, respectively, as compared to UT-CTRL of macrophages cultured alone. Some analytes that remained unchanged included S100A8/9, IP-10, HGF, and HSP60. Cisplatin, on the other hand, decreased the secretion of all those factors, except IL-8 and MMP-9, which were elevated in Cis-CTRL of macrophage monoculture when compared to the UT-CTRL counterparts (74% and 19% increase for IL-8 and MMP-9, respectively). However, these cisplatin-induced increases of IL-8 and MMP-9 were not found in the co-culture groups. Even though in lower proportion than macrophages, ciPTECs in monoculture also released some factors into the basolateral compartment, which appeared to be stimulated by cisplatin, such as arginase-1, fractalkine, and IL-33.

Furthermore, it is important to note that CM attenuated the secretion of factors, induced by co-culture of ciPTECs and macrophages. In general, the secretion of the factors probed in this study was downregulated by CM in all groups, except for HGF and PDGF-BB. The high levels of HGF and PDGF-BB were clearly from the CM itself, especially the CM used to treat macrophages (**Figure 34, Table 1**), which appeared to contain noticeably higher levels of cytokines and growth factors than the CM for ciPTECs. Meanwhile, the steady level of IL-33 across all groups in both culture systems were found within the original basal medium of both ciPTECs and macrophages. Yet, it is rather unlikely that IL-33 was added to both basal media, we thus assume its detection to be an artefact.

We cannot rule out that factors were exchanged between the ciPTEC and macrophage medium from the apical to basolateral side and vice versa, this could not be precisely determined.

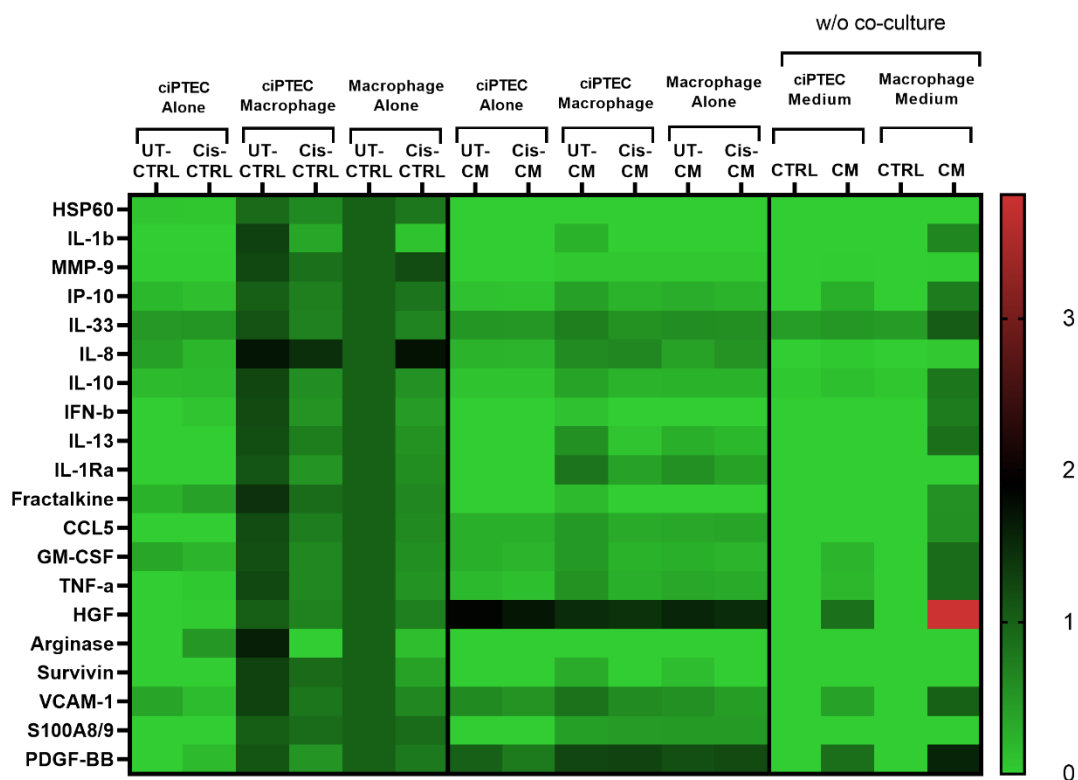


Figure 34. CM down-regulated macrophage secretion in co-culture system

The heatmap showing the level of analytes measured using LUMINEX in the SN of basolateral side relative to the value of UT-CTRL macrophages cultured alone. All values were normalized to the value of UT-CTRL of macrophage mono-culture. For LUMINEX: all groups N=3.

Table 1. The concentrations of analytes in the co-culture SN measured using LUMINEX 200b

			Analytes (pg/ml)																					
			HSP60	IL-1b	MMP-9	IP-10 (CXCL10)	IL-33	TIMP-1	IL-8 (CXCL8)	IL-10	IFN-b	IL-13	IL-1RA	Fractalkine (CX3CL1)	Rantes (CCL5)	GM-CSF	TNF-a	HGF	Arginase-1	M-CSF	Survivin (BIRC5)	VCAM-1	S100A8/A9	PDGF-BB
ciPTEC Monoculture	UT-CTRL	Mean	197	BDL*	1	4	10	ADL#	815	1	BDL*	BDL*	BDL*	2	BDL*	33	BDL*	BDL*	BDL*	15	BDL*	12	BDL*	BDL*
		SD	12	0	0	0	0	0	906	0	0	0	0	0	0	10	0	0	0	0	0	3	0	0
		N	3	3	3	3	3	3	3	3	3	3	3	3	3	3	3	3	3	3	3	3	3	3
	Cis-CTRL	Mean	156	BDL*	4	4	11	65532	266	1	6	0	BDL*	2	BDL*	21	6	13	8	14	BDL*	8	BDL*	24
		SD	23	0	4	1	1	0	90	0	0	0	0	1	0	4	0	0	0	2	0	0	0	0
		N	3	3	3	3	3	3	3	3	3	3	3	3	3	3	3	3	3	3	3	3	3	3
ciPTEC-Macro- phage Co-culture	UT-CTRL	Mean	2237	5	1577	22	25	ADL#	2178	10	27	17	5633	8	5	115	55	146	21	ADL#	307	31	13846	50
		SD	451	2	147	8	7	0	242	5	10	4	4894	3	1	39	22	80	9	0	70	10	2783	13
		N	3	3	3	3	3	3	3	3	3	3	3	3	3	3	3	3	3	3	3	3	3	3
	Cis-CTRL	Mean	1515	3	1212	15	15	ADL#	2845	4	11	10	2654	5	3	61	27	97	BDL*	ADL#	216	19	11868	39
		SD	241	1	498	4	3	0	2163	1	5	4	2412	1	1	18	9	48	0	0	56	5	1644	14
		N	3	3	3	3	3	3	3	3	3	3	3	3	3	3	3	3	3	3	3	3	3	3
Macrophage Monoculture	UT-CTRL	Mean	2608	4	1425	21	22	28393	1813	8	22	14	6435	6	4	97	44	140	17	ADL#	237	24	13483	45
		SD	1131	2	510	5	6	17227	1152	3	8	4	7546	2	1	28	14	71	6	0	43	6	2998	7
		N	3	3	3	3	3	3	3	3	3	3	3	3	3	3	3	3	3	3	3	3	3	3
	Cis-CTRL	Mean	1915	2	1587	17	14	70966	3358	4	9	8	2964	3	3	54	22	100	BDL*	22	155	15	11947	35
		SD	418	0	256	4	1	52589	2321	1	3	2	2685	1	1	7	2	51	0	0	2	1	1196	4
		N	3	3	3	3	3	3	3	3	3	3	3	3	3	3	3	3	3	3	3	3	3	3
ciPTEC Monoculture	UT-CM	Mean	BDL*	BDL*	BDL*	2	10	ADL#	312	1	BDL*	BDL*	BDL*	BDL*	1	26	7	217	BDL*	ADL#	BDL*	15	BDL	44
		SD	0	0	0	0	0	0	102	0	0	0	0	0	0	6	0	20	0	0	0	3	0	6
		N	3	3	3	3	3	3	3	3	3	3	3	3	3	3	3	3	3	3	3	3	3	3
	Cis-CM	Mean	BDL*	BDL*	BDL*	3	10	ADL#	312	1	BDL*	BDL*	BDL*	BDL*	1	20	7	193	BDL*	ADL#	BDL*	12	BDL	48
		SD	0	0	0	0	0	0	107	0	0	0	0	0	0	5	0	22	0	0	0	2	0	0
		N	3	3	3	3	3	3	3	3	3	3	3	3	3	3	3	3	3	3	3	3	3	3

		N	3	3	3	3	3	3	3	3	3	3	3	3	3	3	3	3	3	3	3	3	3	3
ciPTEC-Macrophage Co-culture	UT-CM	Mean	BDL*	4	65	9	16	ADL#	912	3	8	9	3719	3	2	47	24	197	BDL*	ADL#	245	20	5705	56
		SD	0	0	24	6	6	0	474	2	0	7	2834	0	1	24	17	81	0	0	0	6	1496	7
		N	3	3	3	3	3	3	3	3	3	3	3	3	3	3	3	3	3	3	3	3	3	3
	Cis-CM	Mean	BDL*	BDL*	68	5	11	ADL#	975	2	BDL*	4	2082	BDL*	1	23	11	177	BDL*	ADL#	BDL*	14	6259	56
		SD	0	0	18	1	0	0	318	1	0	0	1880	0	0	6	2	48	0	0	0	2	2200	10
		N	3	3	3	3	3	3	3	3	3	3	3	3	3	3	3	3	3	3	3	3	3	3
Macrophage Monoculture	UT-CM	Mean	95	BDL*	63	6	12	ADL#	635	2	BDL*	7	3158	BDL*	2	27	15	196	BDL*	ADL#	109	14	6333	52
		SD	0	0	20	2	1	0	315	1	0	0	3193	0	1	10	6	61	0	0	0	2	1100	5
		N	3	3	3	3	3	3	3	3	3	3	3	3	3	3	3	3	3	3	3	3	3	3
	Cis-CM	Mean	BDL*	BDL*	62	5	12	ADL#	833	2	BDL*	5	1839	BDL*	2	21	13	182	BDL*	ADL#	BDL*	10	6203	53
		SD	0	0	17	1	1	0	318	1	0	0	1437	0	0	3	2	39	0	0	0	1	542	7
		N	3	3	3	3	3	3	3	3	3	3	3	3	3	3	3	3	3	3	3	3	3	3
ciPTEC Medium	CTRL		BDL*	BDL*	BDL*	BDL*	9	BDL*	BDL*	0	BDL*	BDL*	BDL*	BDL*	N/A	BDL*	BDL*	BDL*	N/A	ADL#	BDL*	BDL*	BDL*	BDL*
	CM	Mean	BDL*	BDL*	2	6	10	ADL#	48	1	BDL*	BDL*	BDL*	BDL*	1	20	8	96	BDL*	ADL#	N/A	10	BDL*	38
		N (pooled)	3	3	3	3	3	3	3	3	3	3	3	3	3	3	3	3	3	3	3	3	3	3
Macrophage Medium	CTRL		BDL*	BDL*	BDL*	BDL*	9	N/A	BDL*	0	BDL*	BDL*	BDL*	BDL*	BDL*	BDL*	BDL*	BDL*	N/A	ADL#	BDL*	BDL*	BDL*	N/A
	CM	Mean	BDL*	2	2	15	22	ADL#	47	6	15	11	BDL*	3	2	83	37	431	BDL*	ADL#	BDL*	23	BDL*	69
		N (pooled)	3	3	3	3	3	3	3	3	3	3	3	3	3	3	3	3	3	3	3	3	3	3

*BDL: below detection limit; #ADL: above detection limit; N/A: unquantifiable due to beads gating/doublets.

Lastly, long-term cisplatin treatment reduced macrophage viability as shown in **Figure 35a**, cisplatin-treated macrophages showed more cell debris and less viable cells than their untreated counterparts. The constant presence of cisplatin in both the Cis-CTRL and Cis-CM groups reduced macrophage confluence which started even from day 2 (**Figure 35b-c**) indicating that despite the CM effect in enhancing phagocytosis, CM could not attenuate macrophage death induced by cisplatin.

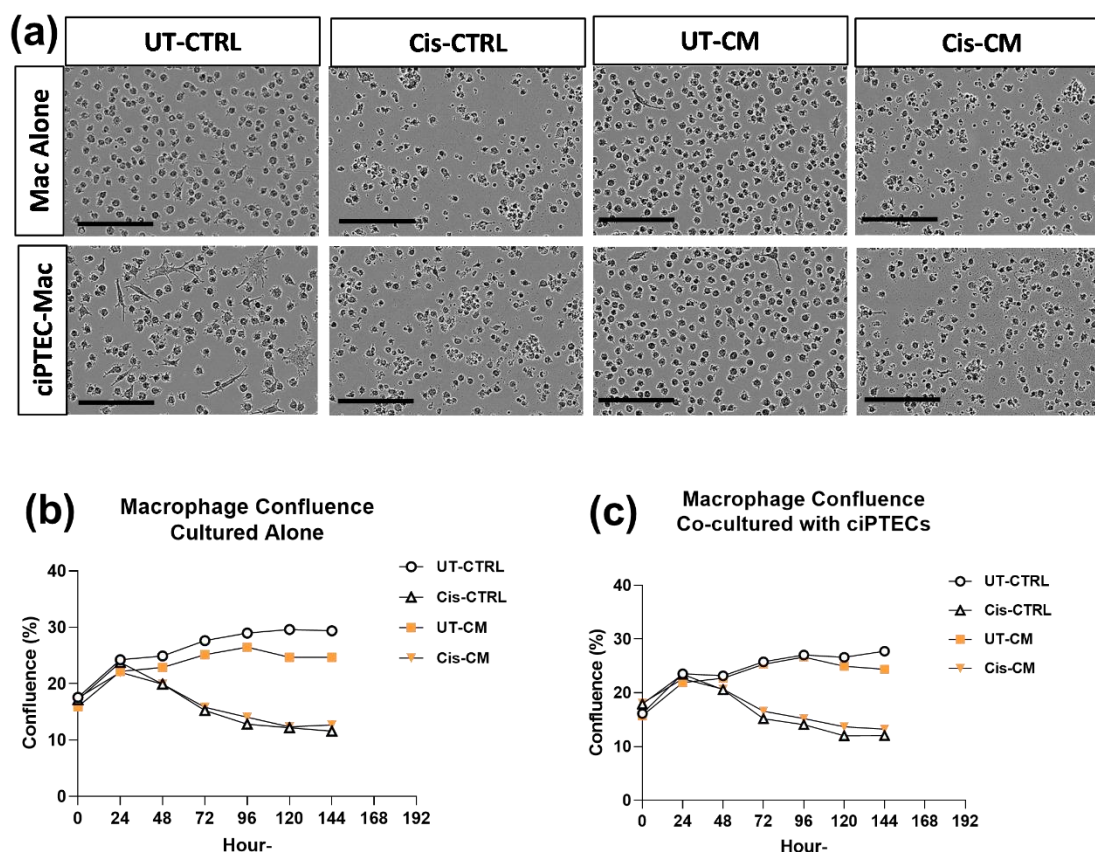


Figure 35. Cisplatin negatively influenced macrophage viability in a long-term treatment

Following 24h of co-culture, the transwell containing ciPTECs were removed and the macrophages were monitored using live-cell imaging in the same medium used for co-culture treatment. The morphology of macrophages 6 days after co-culture (**a**). The confluence of macrophages that were cultured alone (**b**) or with ciPTECs (**c**) throughout 6 days of monitoring. Scale bars represent 100 μ m. For macrophage confluence: all groups N=2.

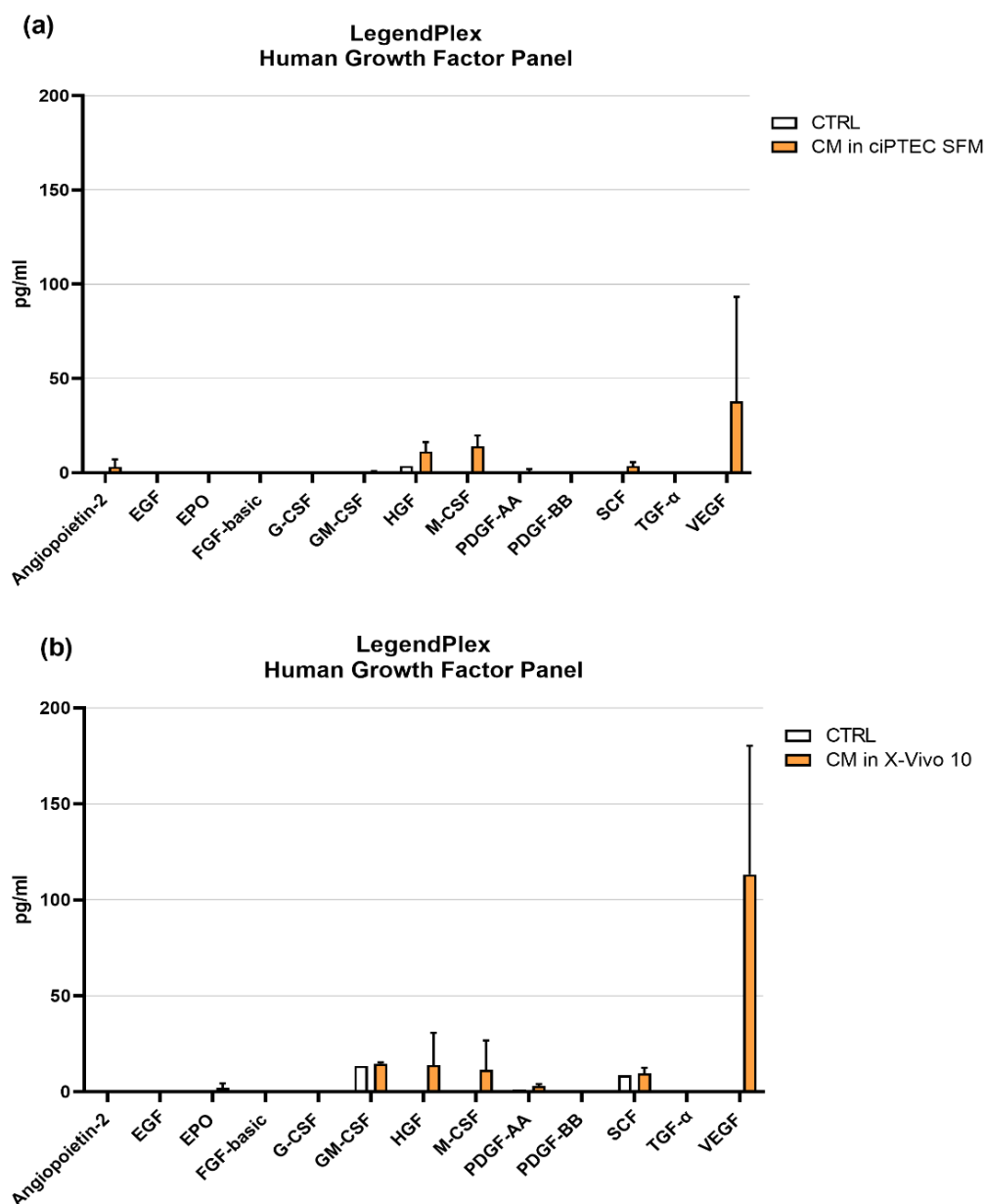


Figure 36. The concentration of growth factors in CM, measured by LegendPlex Human Growth Factor Panel.

The level of growth factors in CM produced in ciPTEC SFM **(a)** and X-Vivo 10 **(b)**. All: N=4.

Given the strong association of free thiol content with the anti-apoptotic capacity of CM, we then compared the thiol concentration in CM intended for ciPTECs and macrophages (**Figure 28a** and **Figure 30a**). Interestingly, while CM for macrophages contained a higher concentration of cytokines and growth factors than that for ciPTECs (**Figure 36a-b**), its free thiol concentration was 4.5X lower than the CM for ciPTECs ($1.9 \pm 2.12 \mu\text{M}$ vs $8.59 \pm 8.8 \mu\text{M}$, for CM intended for macrophages and ciPTECs, respectively (**Figure 28a** and **Figure 30a**). Even though in our study most readouts were obtained in a 1-3 days treatment period, this observation might be important and should be taken into consideration for future *in vivo* studies.

5 DISCUSSION

5.1 Part 1: Inter-laboratory and tissue source comparison of MSC culture

Despite the growing amount of data, it is still difficult to value the clinical benefit of MSC therapy. One of the major challenges of this is the high variability of MSCs used in each of the trials. Those cells were not only manufactured by different laboratories using a variety of culture protocols, but also sourced from different types of tissues. In order to tackle these issues, we dedicated Part 1 of this project to standardize MSC culture protocols.

Within the Innovative Training Network RenalToolBox funded by the EU's Marie Skłodowska-Curie actions, we collaborated with other laboratories in NUIG Galway and UOL Liverpool to attest whether protocol standardization can, at least, reduce the inter-laboratories variability on their biological characteristics. Then, we also compared how the difference in tissue of origin affects MSC function, particularly their immunomodulatory capacity.

Interestingly, the discrepancy of MSC characteristics could already be observed during the harmonization of culture seeding density. Unlike BM- and UC-MSCs, A-MSCs showed better morphology and growth when cultured on lower density. This is in line with a previous study⁹⁴ reporting that A-MSCs cultured at lower density exhibited thinner, spindle shaped morphology, while the cells cultured at higher seeding density showed extensive cell-to-cell contacts and an expanded volume. Not only the morphology, proliferation-associated genes, including CDC45L, CDC20A, and KIF20A, were expressed more in the cells cultured at lower density, as compared to the higher density counterpart. In addition to this, the density when harvesting A-MSCs also profoundly affected their stemness. A-MSCs that were seeded and harvested at lower density showed higher levels of Nanog and c-Myc expression, than those at higher density⁹⁵. Therefore, for the inter-laboratory comparison, we decided to culture A-MSCs at lower density, while BM- and UC-MSCs were cultured at higher densities.

When comparing the proliferation and doubling time across the centres, we, indeed, improved data comparability⁷⁸: the trend of growth curves across the centres between the three MSC types was relatively consistent. BM-MSCs exhibit the longest doubling time as well as the highest inter-donor variability, meanwhile A-MSCs consistently

showed the least donor-to-donor variation regardless where they were cultured. Our study showed for the first time that the protocol harmonisation does, to some extent, reduced site-to-site variation that the intrinsic influence of the tissue source on cell growth can still be observed.

Yet, the harmonization of the culture protocol was not able to entirely eliminate the differences between the centres which is consistent with previous reports ^{26,96}. In fact, despite the culture harmonization, there were still some variables that were not standardized, such as the human handling of the cells and the methods in counting the cells, amongst others.

Assessment of the adipogenic and osteogenic differentiation showed a high inter-donor variability in all of the centres. Not only between the donors, the differentiation potential of MSCs also differed greatly between the centres, although the cells were cultured using harmonised and standardized protocol. Of note, the harmonisation also included the differentiation protocols and kits and the methods of quantitative analysis, underlining how much cell handling apparently influences the characteristics of the cells. Indeed, the variations amongst the centres were particularly noticeable in the magnitude of the differentiation value, which eventually hindered the inter-laboratories comparison to interrogate the effect of tissue source on the differentiation capacity. Nonetheless, some effect of tissue source can still be seen, particularly due to the absence of adipogenic and osteogenic differentiation of UC-MSCs in all the centres. While the lack of adipogenic differentiation has been observed in perinatal MSCs before ^{97,98}, the complete lack of osteogenic differentiation in UC-MSCs was not anticipated ⁹⁹. As the MSC field develops, it has been postulated in the recent years that the therapeutic properties of MSCs are mainly attributed to their paracrine effect that mediates pro-regenerative and immunomodulatory abilities. Therefore, the notion of MSC homing and differentiation into the damaged tissue upon in vivo administration has been slowly relinquished. With the field evolving towards cell-free products ¹⁰, the heterogeneous and conflictive results we have detailed here match with those reported previously ¹⁷ and adds to the discussion of including differentiation abilities as a selection criteria when defining the best source of MSC for therapeutic applications ^{17,25}.

Next, immunophenotypes were compared, comparing tissue sources and centres. The presence of surface markers (including CD73, CD90 and CD105) and absence of hematopoietic (including CD11b, CD19, CD34 and CD45) and major histocompatibility

complex (MHC) class II (like HLA-DR) are defining cells as MSCs ⁶. Even though all the three centres demonstrated the positivity of at least 98% of the cells positive for the MSC expression markers, some variability persisted for the non-expressed markers. A-MSCs, in particular, exhibited elevated levels of CD34 (> 2% in UHEI and UOL) and CD45 expression (in UOL). CD34 positivity has been previously seen in A-MSC preparations, at least in the early passage of culture. Comparably, 2 of the 3 BM-MSCs showed a low variability in the level of HLA-DR in UHEI and UOL. This finding is in line with previous report by Marta Gru-Vorster who analysed 130 batches of BM-MSCs produced for clinical applications and revealed variability among all those samples, concluding that the absence or presence of HLA-DR does not have an impact on the overall properties ¹⁰⁰. It is worthy to note that the CD34 and HLA-DR expression observed in the two separate sites is consistent to the same donors, implying clear donor-related variability as a main cause. Differences in detection can be attributed to the sensitivity of the used flow cytometers, (different antibody clones and fluorochromes used, antibody titration) and manual gating.

It is important to emphasize that in this study each MSC type was isolated in one specific centre, cryopreserved, and internationally shipped on dry ice to the other centres before being expanded and compared there. Although cryopreservation has been reported not to affect the proliferation of the cells, it has been proven to impact the differentiation potential ¹⁰¹ and the immunosuppressive properties ¹⁰². However, the effect of cryopreservation has been reported to be only temporary, which stems from the heat-shock stress that takes place during the thawing process. This stress eventually dissipates and the cell functionality can be restored following a certain period of culture ¹⁰³. Furthermore, the effect of international shipping has not been elucidated yet and should be taken into consideration in the interpretation of the variability presented in this study.

In addition to the basic characterization, we also sought to investigate how the tissue of origin might affect their immunomodulatory abilities. Our results indicated that A-MSCs have the highest ability to inhibit mitogen-induced PBMC proliferation which can be attributed to the high level of intracellular IDO upon IFN- γ stimulation. In fact, A-MSCs exhibit the highest level of IDO as compared to the other MSC sources. However, amongst A-MSC donors, the donor which shows the highest inhibition unexpectedly exhibits the least intracellular IDO and vice versa. Even though previous study in

our lab showed that IDO is the responsible mediator in inhibiting PHA- stimulated PBMCs²², our current data suggests that it might not be the only factor by which MSCs exert this effect. A study by Chinnadurai elegantly showed that MSCs also inhibit T-cell proliferation via the PD1/PD-L1 axis¹⁰⁴.

All in all, we have shown in this part that, indeed, MSC characteristics varied between the centres, specifically in the magnitude of results. Yet the harmonisation was able, at least to some extent, to minimise centre-to-centre variability that the difference amongst the tissue of origin was still conserved as indicated by similar trends shown in all centres. While centre-to-centre variability can be minimised by culture harmonisation, we were still unable to entirely eliminate it. Perhaps, further and highly detailed standardisation of operational procedures, including SOPs and operator training is required to decrease this variability as much as possible. Lastly, functional assays on MSC immunomodulatory capacity also revealed the difference attributed to the tissue of origin. Such a functional assay could prove to be beneficial to select the most suitable type of MSCs to target certain illnesses.

5.2 Part 2: Inter-species Immuno-Compatibility Study

In the pre-clinical setting where mostly xenogeneic transplantation is done, it is pivotal to understand the immune response in a cross-species setting, especially in light of findings that interspecies incompatibilities exist that question whether animal models are able to fully model the therapeutic potential of MSC therapies³⁸. Since from the previous part, we found that A-MSCs were the type of MSCs with the highest immunomodulatory capacities, we decided to proceed only with A-MSCs for this part of the study. We also included ABCB5+ MSCs since these MSCs have been undergoing multiple pre-clinical and clinical studies, therefore we deemed it important to compare these two human-derived MSCs.

Before assessing their immunomodulatory capacity in the xenogeneic setting, we first elucidated their surface markers using an extended FACS panel and analyzed differences in expression intensities (MFI). We found that analyzing MFI is better for interrogating subtler differences of surface marker expression, compared to positive cell percentage. A-MSCs showed higher MFI of surface markers related to the cell-to-cell or cell-to-matrix interaction (CD90, CD49d, and CD49e)^{105,106}, which help for cell adherence to the culture flask. Higher expression of these surface markers can be attributed

to the fact that A-MSCs were longer in culture than ABCB5+ MSCs, because ABCB5+ MSCs cannot be cultured for longer period without losing their ABCB5 expression. Other surface markers that were found higher in A-MSCs than in ABCB5+ MSCs include CD105 and CD73, that contribute to angiogenesis¹⁰⁷ and adenosine metabolism¹⁰⁸, respectively. Meanwhile, ABCB5+ MSCs expressed higher CD13, compared to A-MSCs, which plays role in digestion of peptide¹⁰⁹. Our data suggest that there is a distinct expression of surface marker between A- and ABCB5+ MSCs, however whether this discrepancy may affect their therapeutic capacity needs to further investigated.

Macrophages are part of innate immune system that play an important role in maintaining tissue homeostasis^{110,111}, thus it is imperative to understand whether inter-species compatibility might affect MSC modulation on these cells. Having observed that human A-MSCs fail to inhibit murine PBMC proliferation²², we expected that a similar pattern would be observed in macrophages. On the contrary, our data suggest that MSCs can modulate macrophage phenotypes, despite the cross-species barrier. All the MSC CM showed modified TNF- α production upon LPS stimulation in both species. However, ABCB5+ CM showed inferior effect on macrophage phagocytosis both in human and rat, as compared to A-MSCs. Phagocytosis is particularly important as it is one of the first immune responses by which dead cells are cleaned up to maintain tissue homeostasis¹¹² and can prime macrophages to promote tissue repair¹¹³. A-MSCs appeared to be the strongest MSCs in inducing phagocytosis in both species, human and rats. However, it is important to note that the key mediator of the A-MSC CM differed between human and rat. While pro-phagocytosis effect of A-MSC CM in rats was mediated by TGF- β 1, PGE-2 might play a more important role in human macrophages. In conclusion, MSCs are able to modulate the macrophage phenotype regardless of the species, however the factor and thus the mechanism employed to exert this effect might differ depending on the species. This observation warrants further investigations.

5.3 Part 3: Part 3: MSCs role in ciPTECs and macrophages crosstalk in *in vitro* cisplatin injury

In the third part of this thesis, we explored the therapeutic benefit of MSCs for cisplatin-induced AKI. In this part, both the pro-regenerative and immunomodulatory capacity of

MSCs was investigated in the context of renal and immune cells crosstalk. We hypothesized that MSC CM will have an additive effect in PTEC and macrophages cocultures by modulating both cells and perpetuating a vicious cycle of cisplatin-induced inflammatory responses.

Consistent to our observation in the previous part, our results revealed that A-MSCs-derived CM was superior in suppressing cisplatin-induced apoptosis, compared to that of ABCB5+ MSCs. Therefore, we then proceeded to use only CM from A-MSCs for the rest of the study.

5.3.1 How CM affect cisplatin-induced toxicity on ciPTECs?

Our findings demonstrated the protective effect of A-MSC secretome, which was harnessed through their CM, against cisplatin-induced injury in both ciPTECs and macrophages. The protective effect on ciPTECs involved suppression of apoptosis and enhanced migratory capacity. Based on our PCR array and qPCR data, CM partially reversed the modification of gene expression caused by cisplatin. The expression of CDKN1a, also known as p21, and GADDH45a are both induced by various cellular stresses, including DNA damage and oxidative stress and contribute to inhibition of cell cycle arrest¹¹⁴⁻¹¹⁶. Activation of these genes has been linked to a defense mechanism in response to cellular stress that halts the cell cycle while the DNA repair takes place. HMOX1, the gene encoding the heme oxygenase-1, which degrades heme to biliverdin, iron, and carbon monoxide, is also sensitive to oxidative stress stimulation as it plays role in anti-oxidative defense mechanism¹¹⁷. Meanwhile, ATF-3 expression, a transcription factor that is can be triggered by ER stress, chemokines, and cytokines stimulation¹¹⁸. ER stress and immune response (TNF- α and FasL) triggered by cisplatin have also been demonstrated to be associated with oxidative stress. The attenuation of cisplatin-induced upregulation of these genes shows that CM rescued ciPTECs by alleviating cellular stress, especially oxidative stress (**Figure 37**).

5.3.2 What is the mediator of CM anti-apoptotic effect on ciPTECs?

Within the composition of CM, EVs have been reported as the mediator by which MSCs exert their therapeutic effect⁸⁶. However, we showed that EVs were not the key mediator for the anti-apoptotic effects of CM, suggesting that soluble factors or smaller EVs (< 100 kDa) are the ones responsible. Our finding is in agreement with a previous study showing that EVs are dispensable for angiogenesis of endothelial cells, implying this the main mediator is the soluble factors⁸⁰. This, of course, does not imply that EVs do

not play any role at all in MSC pro-angiogenesis benefit, they rather boost the pro-angiogenesis of the soluble factors⁸⁰. The ability of EVs in boosting the effect of soluble factors might be the result of their ability in acquiring the soluble factors on their surface which later can modulate their function and docking on the surface of target cells¹¹⁹. Therefore, depletion of EV might compromise, but not eliminate the efficacy of CM, especially if the concentration of the key soluble factors is very high.

Next, given the high concentration of IL-6, we then sought to elucidate IL-6 involvement in the MSC anti-apoptotic effect. Indeed, IL-6 is a pleiotropic cytokine that can be pro-inflammatory, but it has also been reported to contribute to apoptosis suppression and anti-oxidative defense¹²⁰. Not only IL-6, MSCs were also shown to shed soluble IL-6 receptor as part of their secretome which played an important role in their anti-inflammatory effect^{89,121}. Upon the binding of IL-6 to its receptor, phosphorylation of STAT3 takes place which then commence a myriad of cellular responses. Therefore, we assessed the level of pSTAT3 upon CM treatment. However, our data implies that IL-6 role in pSTAT3 was inferior, as the ciPTEC culture supplements themselves, were already sufficient to invoke pSTAT3. This also suggests that the presence of IL-6 in the CM might not play a major role in the anti-apoptotic effect on ciPTECs.

Given the pivotal role of oxidative stress in ciPTEC apoptosis, we then investigated the anti-oxidative capacity of CM. Free thiols or sulfhydryl groups (R-SH) are very easily reduced by ROS and therefore reflect the fluctuation of the redox state of their environments and can be found in various serum proteins as well as some antioxidant enzymes, such as glutathione^{81,82}. Due to their sensitivity to ROS, not only do free thiols serve as a good indicator of the progression of various degenerative diseases (e.g. digestive, respiratory, cardiovascular, metabolic, and cancer diseases), but also play an important role in dampening oxidative stress by scavenging ROS^{81,82,122,123}. The anti-oxidant properties of free thiols are important to maintain the homeostasis of various cellular processes including enzymatic reactions, signal transduction, detoxification, transcription, and apoptosis activation¹²⁴. Accordingly, the treatment of ciPTECs with CM led to a remarkable decrease in intracellular ROS levels and, subsequently, reduced apoptosis. It is also noteworthy, that a high variance of free thiol content across MSC donors was present. We attribute the ability of MSCs to produce a high level of free thiols to the cell vitality, including the doubling time, cell size, and morphology (data not shown), however this hypothesis should be tested in a larger

study with a higher number of MSC donors. Furthermore, given the importance of free thiols in cellular redox homeostasis, measuring free thiols presents an easy, robust, and reliable option of potency assay to select or predict the anti-oxidative properties of MSCs.

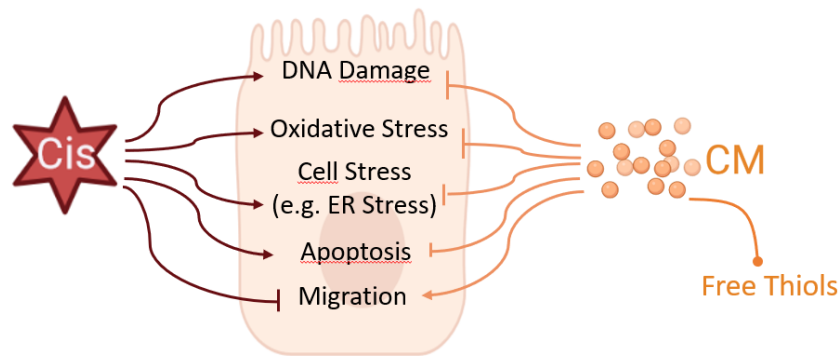


Figure 37. CM counteracts cisplatin-induced toxicity by delivering anti-oxidative activity through free thiols

This image was created using BioRender.

5.3.3 How do CM and cisplatin affect macrophage phenotype and function?

When evaluating the effect of cisplatin and CM on macrophages with lower cisplatin concentration (15 μM as used in mono-culture experiments), no detrimental effects were observed. However, when cisplatin concentration was doubled to 30 μM (as used in coculture experiments), not only it downregulated macrophage phagocytosis but also compromised their viability. It has been reported that alveolar macrophages express the transporters capable of uptaking cisplatin, such as MATE, OCTN1, and OCTN2¹²⁵. Recent findings also showed that cisplatin uptake was significantly higher in THP1 cells, a human monocyte cell line, that were polarized into M2 macrophages, as compared to M1 and M0 counterparts, and the monocytic cells¹²⁶. This might explain why cisplatin, even in lower concentration and shorter period of treatment, could partly compromise the effect of CM in skewing macrophage polarization towards M2 macrophages. Considering that M2 macrophages are fueled by oxidative phosphorylation in mitochondria^{127,128} and that MSCs promote this metabolic shift¹²⁹, cisplatin's ability to affect mitochondrial function¹³⁰ can eventually hinder the M2 polarization promoted by CM.

Furthermore, it is clear that CM supported macrophage polarization towards M2 as seen in decreased M1 surface markers such as HLA-DR and CD86, increased M2 markers, including CD163 and CD206, and higher phagocytosis capacity. In regards to the key mediator of CM that is responsible for the M2 polarization of macrophages, we have found in the second part of this thesis that inhibition of IL-6¹³¹, prostaglandin-2 (PGE-2) and transforming growth factor beta 1 (TGF- β 1) can partly but not entirely reduce CM effect in enhancing phagocytosis. This is in line with previous findings showing those factors, amongst others promote M2 polarization of macrophage¹³². Other possible mediators important for M2 polarization in our CM include HGF¹³³ and vascular endothelial growth factor (VEGF)¹³⁴.

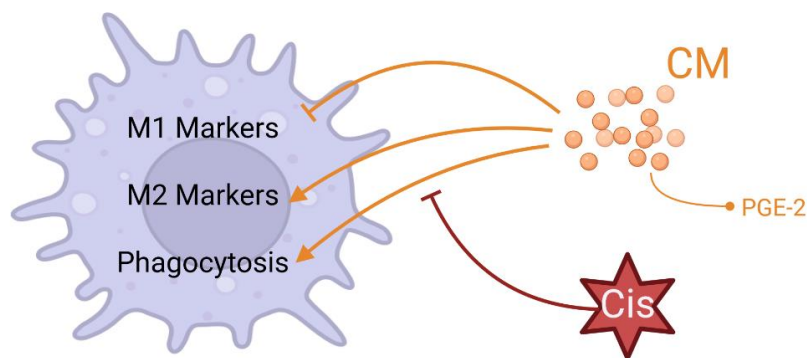


Figure 38. CM promotes M2 polarization on macrophages through PGE-2, while cisplatin compromises this effect

This image was created using BioRender.

CM could not ameliorate cisplatin-induced cell death for a longer period, despite the ability in improving the phagocytosis of macrophages and its rich content of cytokines and growth factors. The measurement of free thiols revealed that CM produced using X-Vivo 10 for macrophage culture contained 4.5X lower free thiols than CM produced in ciPTEC SFM. Of note, X-Vivo 10 is a chemically defined medium for blood-derived cells and therefore, might contain certain cytokines, while ciPTECs SFM is supplemented with multiple growth factors for ciPTEC (see Material and Method section). Of course, the discrepancy in the secretome composition between CM produced in X-Vivo 10 and ciPTECs is to be expected as MSC secretome is highly influenced by microenvironmental cues^{8,135}. Whether or not the lower free thiol level of CM in X-Vivo is the reason why it could not attenuate macrophage death by cisplatin is not evaluated

in this study. Nonetheless, it is noteworthy that the level of growth factors and cytokines does not always positively correlate with the anti-oxidative property of CM.

5.3.4 How does CM and cisplatin modulate ciPTEC and macrophage crosstalk?

Our study demonstrated that ciPTECs and macrophages could sense and respond to each other's stimuli. In co-culture without cisplatin, macrophages were activated by ciPTECs as indicated by elevated phagocytosis and increased production of various factors comprising cytokines (IL-33, IL-8), chemokines (Fractalkine), growth factors (HGF), lipoxin (survivin) and matrix metalloproteinase (MMP-9). This is in line with a previous study that showed that both direct and indirect co-culture of PTEC and monocytes resulted in the inhibition of monocyte maturation into dendritic cells, marked by lower levels of HLA-DR and CD86, and elevated level of phagocytosis¹³⁶. In contrast to healthy PTECs, in injury model for using albumin, hypoxia, and Adriamycin, PTECs drove macrophage polarization into M1 by releasing EV containing miR-199a-5p, miRNA-23a, and miR-19b-3p, respectively¹³⁷⁻¹³⁹, and switched macrophage metabolism towards glycolysis¹⁴⁰. In our co-culture system, cisplatin induced pro-inflammatory TNF- α secretion on ciPTECs which most likely also affected macrophage polarization and, to some degree, contributed to the downregulation of macrophage phagocytosis in co-culture treated with cisplatin. Surprisingly, unlike another study suggesting that macrophages augmented the albumin-induced cytokine release by PTECs¹⁴¹, in our system, co-culturing ciPTEC with macrophage tended to decrease TNF- α secretion of ciPTECs. It is also noteworthy that the cisplatin-induced ciPTEC death markers were slightly reduced in the co-culture setting, compared to monoculture, implying macrophage's regulatory effect, this albeit warrants further investigations.

CM downregulated overall macrophage secretion, affecting e.g. IL-1 β , IL-33, IL-13, IL-8, TNF- α , and IP-10. A similar effect has been previously shown: the MSC secretome suppressed secretion of pro-inflammatory cytokines on macrophages stimulated by LPS¹⁴². Yet, in our study not only pro-, but also anti-inflammatory cytokines and enzymes decreased upon CM treatment, such as IL-10, IL-1RA, and arginase-1. This is in contrast to another study that showed that MSC treatment increased the production of IL-10 and arginase-1¹⁴³. This discrepancy might be caused¹⁴³ by the fact that in most of the previous studies, macrophages were also stimulated with LPS^{33,143}, or M1 polarizing medium¹⁴⁴, which might be stronger stimuli than the mere co-culture with (in-

jured) ciPTECs. In addition, the upregulation of those anti-inflammatory and pro-regenerative in macrophages was also mostly observed in *in vivo* models with higher cell interaction, thus more macrophage stimulation ¹³².

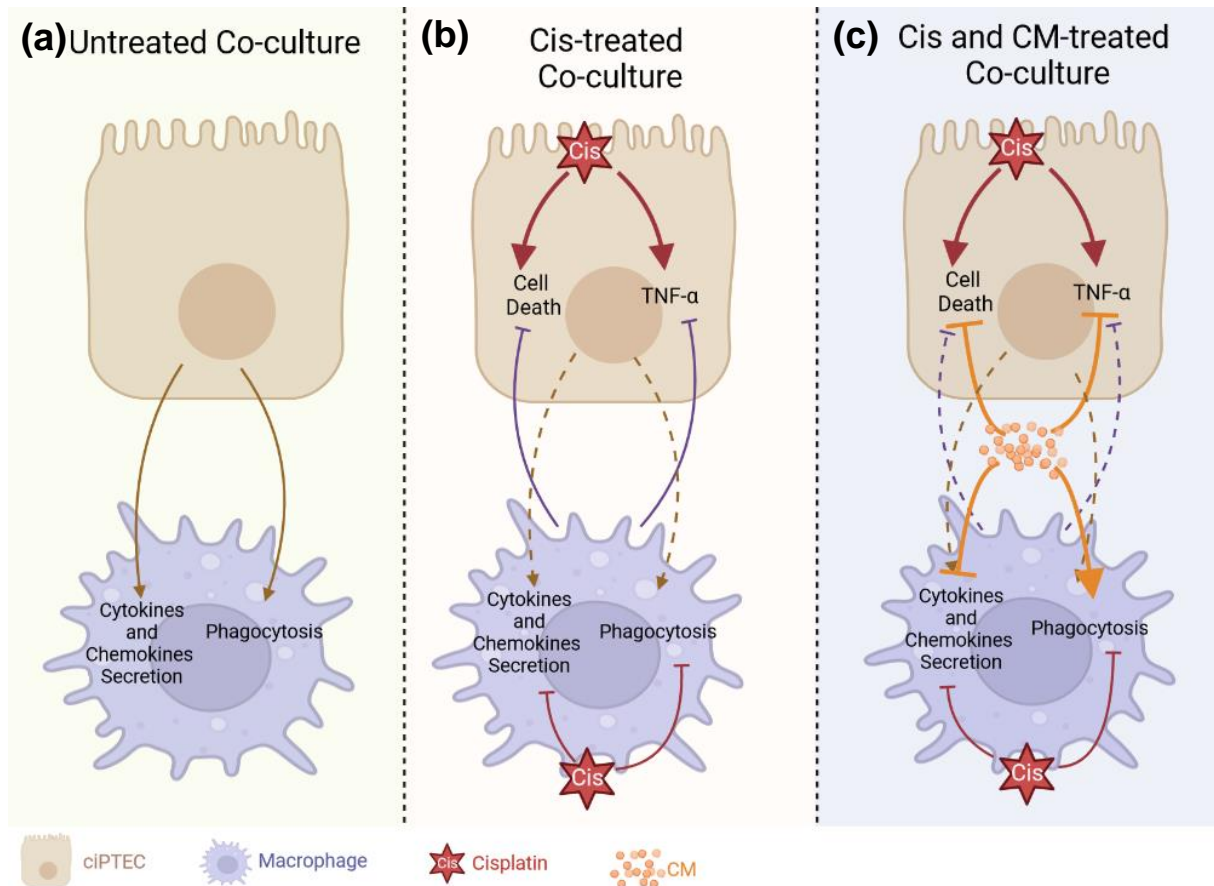


Figure 39. The dynamic of ciPTEC and macrophage interaction is modified by cisplatin and CM treatment

In untreated co-culture, ciPTECs induced cytokines and chemokines secretion and phagocytosis by macrophages (a). ciPTECs influence on macrophages was diminished (dashed lines) by cisplatin which reduced both macrophage secretion and phagocytosis. Cisplatin also induced ciPTEC death and TNF- α release, which was slightly attenuated by macrophages (b). Addition of CM further decreased cisplatin-induced ciPTEC death and TNF- α release, overruling the regulatory effect of macrophages on the renal cells. Interestingly, although CM also suppressed macrophage secretion of cytokines and chemokines, it strongly boosted phagocytosis (c). This image was created using BioRender.

Under CM treatment, co-culturing ciPTECs with macrophage did not add up to the protective effect exerted by CM. Indeed, ciPTEC and macrophage co-culture in the absence of CM showed a slight trend of injury attenuation, however this co-culture benefit was overruled by the protective effect of CM. This might be caused by the fact

that CM's protective effect on ciPTECs was already very strong that macrophage regulatory effect could not be any more advantageous in our system (Figure 39). Nonetheless, given the dramatic increase of phagocytosis elicited by CM, the role of macrophage upon CM treatment might be more significant in an *in vivo* model, as phagocytosis of dead cells is an important step to prevent prolonged inflammation^{145,146}. In fact, in a mouse unilateral ureteral obstruction (UUO) model that develops renal fibrosis, the population of highly phagocytotic macrophages decreased, while the ones with low phagocytosis ability increased¹⁴⁵. Interestingly, the infusion of highly phagocytic macrophages attenuated renal fibrosis in this animal model. Indeed, M2 macrophages have been proven to contribute to the development of renal fibrosis. However, given the oversimplification of M1 and M2 macrophage polarization, it is noteworthy that macrophage polarization is far more nuanced, and M2 depletion also leads to worsening renal fibrosis⁴². It has been postulated that the M2 macrophage responsible for renal fibrosis express CD206, CD204, and HLA-DR^{high}, meanwhile the ones responsible for tissue homeostasis express CD206, CD163, and HLA-DR^{low}¹⁴⁷. Given that our CM boosted macrophage phagocytosis, and increased the expression of CD206, CD163, while decreasing the level of HLA-DR, the CM treatment for cisplatin-induced AKI might be beneficial to prevent the progression of renal fibrosis *in vivo*. Moreover, the phagocytosis of dead cells can also stimulate macrophages further to promote tubular recovery¹⁴⁵. These open questions remain to be answered, most likely in well-planned and focussed *in vivo* studies as the mere *in vitro* nature of the experiments performed within this study cannot fully represent the complexity of interactions occurring *in vivo*.

The strength of our study is that it provides more insight into the interaction between PTEC and macrophages under cisplatin treatment with and without CM. We also shed light on the importance of free thiols in CM as a metric to assess the anti-oxidative properties of CM, as well as the profound effect of cisplatin on macrophage viability and phagocytosis that is often overlooked in cisplatin-induced AKI. The *in vitro* nature of this study also allows to limit the variables that might affect the interaction of PTEC and macrophage which consequently enables us to gain detailed and focused insight of the crosstalk. Of course, this also means that the *in vitro* setting does not allow to investigate the complex interplay between other cell types in its entirety. To tackle this, future *in vivo* study, or microphysiological organ-on-chip systems, are required.

Another important strength of this thesis is that we provide some mechanistic insights of CM effects on both ciPTEC and macrophages, by using inhibitors. We also demonstrate that EVs are not essential for the anti-apoptotic effect of MSC, documenting that certain mechanisms rather rely on secreted soluble factors. Other noteworthy findings are that MSC effect on different cell types seem to be caused by different mediators. These add up to our knowledge on the mechanisms of action of MSC and or MSC secretome. The overall increasing knowledge may help to fine-tune MSC therapies, eventually engineering MSCs fit for purpose- over-expressing certain key features for certain disease entities. For instance, priming MSCs with anti-oxidants or certain cytokines might further boost the free-thiol production or their PGE-2 secretion, respectively.

Indeed, treating cancer patients with MSC therapy comes with the risk of compromising the anti-cancer effect of cisplatin, which has to be addressed before implementing MSC pro-regenerative benefit in a clinical setting. Thus, further engineering of MSC CM is imperative to locally restrict the delivery of CM in order to overcome this risk. Recent study demonstrated that the specificity of MSC-EVs delivery in the kidney can be improved by using a matrix metalloproteinase-2 (MMP-2) sensitive self-assembling peptide hydrogel. Given the fact that MMP-2 is normally upregulated following kidney injury, the administration of MSC-EV in this hydrogel led to higher local retention in the kidney ¹⁴⁸. Even though the feasibility of such strategy to reduce off-target of MSC therapy still has to be further evaluated, this study offers a breakthrough by which MSC secretome can be harnessed to prevent or treat AKI.

6 SUMMARY

In this study, we aimed at improving our knowledge on MSC therapy in acute kidney injury. Overall this work, being part of the International Research Training Group Renal Tool Box, addressed three different projects: 1. An inter-laboratory study on harmonising MSC culture and analysis procedures, 2. Evaluating whether human MSC therapeutic options can be fully understood in using xenogenic mouse models, given that the immune systems differ largely and MSCs function relies to a large extent on modulating immune responses and 3. Hypothesizing that adding MSC CM to a co-culture setting of PTEC and macrophages could have additive effects upon cisplatin injury.

In Part 1, we established standard tissue culture conditions for the expansion of adipose, bone marrow and umbilical cord MSCs among three independent centres across Europe to investigate the reproducibility of harmonised manufacturing procedures and its impact on their immunomodulatory capacity on PBMC proliferation. We show that harmonised protocols improve reproducibility across different centres emphasizing the need for worldwide standards to manufacture MSCs for clinical use. Further, tissue-specific differences in cell characteristics suggest selecting the optimal cell type for the intended clinical indication based on autologous or allogeneic use, source availability and functional characteristics. These results show the heterogeneous behaviour and regenerative properties of MSCs as a reflection of intrinsic tissue-origin while providing evidence that the use of standardized culture procedures can reduce, but not eliminate inter-lab and operator differences.

In Part 2, we demonstrated that MSCs/their secretome can modulate macrophage phenotypes even in xenogeneic setting. Despite the identical effect of MSC CM on macrophages from human and rat, the mediator contributing to it seemed to differ. We found out that in rat macrophage, TGF- β 1 seemed to be the key mediator for pro-phagocytosis effect of MSC while in human PGE-2 plays a more important role.

In Part 3, we showed that CM was protective against cisplatin-induced injury of ciPTECs, which seems to be associated with its anti-oxidative properties. In contrast, CM could not rescue macrophages from cisplatin-induced cell death, but it rather promoted M2 polarization which is, however, compromised by cisplatin. Furthermore, the CM treatment in ciPTECs and macrophages co-culture abrogated ciPTEC death and

dampened macrophage activation by attenuating macrophage cytokines and chemokines release. Surprisingly, this suppressing effect on macrophage secretion did not influence the CM effect on improving phagocytosis. Nonetheless, we did not observe the added benefit of macrophages in the CM renoprotective on ciPTECs. This might be caused by the fact that the CM already exerted very strong protective effect that it overruled the macrophage contribution in this system. Since our system did not allow direct phagocytosis of dead ciPTECs by macrophages, the macrophage role in CM-induced proximal tubule recovery could not be highlighted and should not be overlooked for clinical implementation of MSC secretome in the future.

7 REFERENCES

1. Galipeau, J., and Sensebe, L. (2018). Mesenchymal Stromal Cells: Clinical Challenges and Therapeutic Opportunities. *Cell Stem Cell* 22, 824-833. <https://doi.org/10.1016/j.stem.2018.05.004>.
2. Hoogduijn, M.J., and Lombardo, E. (2019). Mesenchymal Stromal Cells Anno 2019: Dawn of the Therapeutic Era? Concise Review. *Stem Cells Translational Medicine* 8, 1126-1134. <https://doi.org/10.1002/sctm.19-0073>.
3. Pittenger, M.F., Discher, D.E., Peault, B.M., Phinney, D.G., Hare, J.M., and Caplan, A.I. (2019). Mesenchymal stem cell perspective: cell biology to clinical progress. *NPJ Regen Med* 4, 22. <https://doi.org/10.1038/s41536-019-0083-6>.
4. Rodriguez-Fuentes, D.E., Fernandez-Garza, L.E., Samia-Meza, J.A., Barrera-Barrera, S.A., Caplan, A.I., and Barrera-Saldana, H.A. (2021). Mesenchymal Stem Cells Current Clinical Applications: A Systematic Review. *Arch Med Res* 52, 93-101. <https://doi.org/10.1016/j.arcmed.2020.08.006>.
5. Krampera, M., and Le Blanc, K. (2021). Mesenchymal stromal cells: Putative microenvironmental modulators become cell therapy. *Cell Stem Cell* 28, 1708-1725. <https://doi.org/10.1016/j.stem.2021.09.006>
6. Dominici, M., Le Blanc, K., Mueller, I., Slaper-Cortenbach, I., Marini, F., Krause, D., Deans, R., Keating, A., Prockop, D., and Horwitz, E. (2006). Minimal criteria for defining multipotent mesenchymal stromal cells. The International Society for Cellular Therapy position statement. *Cytotherapy* 8, 315-317. <https://doi.org/10.1080/14653240600855905>.
7. Torres Crigna, A., Daniele, C., Gamez, C., Medina Balbuena, S., Pastene, D.O., Nardozi, D., Brenna, C., Yard, B., Gretz, N., and Bieback, K. (2018). Stem/Stromal Cells for Treatment of Kidney Injuries With Focus on Preclinical Models. *Frontiers in Medicine* 5. <https://doi.org/10.3389/fmed.2018.00179>.
8. Daneshmandi, L., Shah, S., Jafari, T., Bhattacharjee, M., Momah, D., Saveh-Shemshaki, N., Lo, K.W., and Laurencin, C.T. (2020). Emergence of the Stem Cell Secretome in Regenerative Engineering. *Trends Biotechnol* 38(12), 1373-1384. <https://doi.org/10.1016/j.tibtech.2020.04.013>
9. Caplan, A.I., and Correa, D. (2011). The MSC: an injury drugstore. *Cell Stem Cell* 9(1), 11-15. <https://doi.org/10.1016/j.stem.2011.06.008>.
10. Vizoso, F.J., Eiro, N., Cid, S., Schneider, J., and Perez-Fernandez, R. (2017). Mesenchymal Stem Cell Secretome: Toward Cell-Free Therapeutic Strategies in Regenerative Medicine. *Int J Mol Sci* 18(9), 1852. <https://doi.org/10.3390/ijms18091852>
11. Lukomska, B.A.-O., Stanaszek, L.A.-O., Zuba-Surma, E.A.-O., Legosz, P.A.-O., Sarzynska, S.A.-O., and Drela, K.A.-O. (2019). Challenges and Controversies in Human Mesenchymal Stem Cell Therapy. *Stem cells international* 9628536. <https://doi.org/10.1155/2019/9628536>.
12. Turinetto, V., Vitale, E., and Giachino, C. (2016). Senescence in Human Mesenchymal Stem Cells: Functional Changes and Implications in Stem Cell-Based Therapy. *International Journal of Molecular Sciences* 17, 1164. <https://doi.org/10.3390/ijms17071164>.
13. Maguire, G. (2013). Stem cell therapy without the cells. *Commun Integr Biol* 6, e26631. <https://doi.org/10.4161/cib.26631>.
14. Han, Y., Yang, J., Fang, J., Zhou, Y., Candi, E., Wang, J., Hua, D., Shao, C., and Shi, Y. (2022). The secretion profile of mesenchymal stem cells and

- potential applications in treating human diseases. *Signal Transduction and Targeted Therapy* 7, 92. <https://doi.org/10.1038/s41392-022-00932-0>.
15. Le Blanc, K., and Davies, L.C. (2018). MSCs—cells with many sides. *Cytotherapy* 20, 273-278. <https://doi.org/10.1016/j.jcyt.2018.01.009>.
 16. Bieback, K., Kuci, S., and Schafer, R. (2019). Production and quality testing of multipotent mesenchymal stromal cell therapeutics for clinical use. *Transfusion* 59, 2164-2173. <https://doi.org/10.1111/trf.15252>.
 17. Calcat, I.C.S., Sanz-Nogues, C., and O'Brien, T. (2021). When Origin Matters: Properties of Mesenchymal Stromal Cells From Different Sources for Clinical Translation in Kidney Disease. *Front Med (Lausanne)* 8, 728496. <https://doi.org/10.3389/fmed.2021.728496>.
 18. Petrenko, Y., Vackova, I., Kekulova, K., Chudickova, M., Koci, Z., Turnovcova, K., Kupcova Skalnikova, H., Vodicka, P., and Kubinova, S. (2020). A Comparative Analysis of Multipotent Mesenchymal Stromal Cells derived from Different Sources, with a Focus on Neuroregenerative Potential. *Sci Rep* 10, 4290. <https://doi.org/10.1038/s41598-020-61167-z>.
 19. Medrano-Trochez, C., Chatterjee, P., Pradhan, P., Stevens, H.Y., Ogle, M.E., Botchwey, E.A., Kurtzberg, J., Yeago, C., Gibson, G., and Roy, K.A.-O. (2021). Single-cell RNA-seq of out-of-thaw mesenchymal stromal cells shows tissue-of-origin differences and inter-donor cell-cycle variations. *Stem Cell Res Ther* 12. <https://doi.org/10.1186/s13287-021-02627-9>.
 20. Hsiao, S.T.-F., Asgari, A., Lokmic, Z., Sinclair, R., Dusting, G.J., Lim, S.Y., and Dilley, R.J. (2011). Comparative Analysis of Paracrine Factor Expression in Human Adult Mesenchymal Stem Cells Derived from Bone Marrow, Adipose, and Dermal Tissue. *Stem Cells and Development* 21, 2189-2203. <https://doi.org/10.1089/scd.2011.0674>.
 21. Kehl, D., Generali, M., Mallone, A., Heller, M., Uldry, A.-C., Cheng, P., Gantenbein, B., Hoerstrup, S.P., and Weber, B. (2019). Proteomic analysis of human mesenchymal stromal cell secretomes: a systematic comparison of the angiogenic potential. *npj Regenerative Medicine* 4, 8. <https://doi.org/10.1038/s41536-019-0070-y>.
 22. Torres Crigna, A., Uhlig, S., Elvers-Hornung, S., Kluter, H., and Bieback, K. (2020). Human Adipose Tissue-Derived Stromal Cells Suppress Human, but Not Murine Lymphocyte Proliferation, via Indoleamine 2,3-Dioxygenase Activity. *Cells* 9. <https://doi.org/10.3390/cells9112419>.
 23. Ma, Y., Wang, L., Yang, S., Liu, D., Zeng, Y., Lin, L., Qiu, L., Lu, J., Chang, J., and Li, Z. (2021). The tissue origin of human mesenchymal stem cells dictates their therapeutic efficacy on glucose and lipid metabolic disorders in type II diabetic mice. *Stem Cell Research & Therapy* 12, 385. <https://doi.org/10.1186/s13287-021-02463-x>.
 24. Netsch, P., Elvers-Hornung, S., Uhlig, S., Klüter, H., Huck, V., Kirschhöfer, F., Brenner-Weiß, G., Janetzko, K., Solz, H., Wuchter, P., et al. (2018). Human mesenchymal stromal cells inhibit platelet activation and aggregation involving CD73-converted adenosine. *Stem Cell Research & Therapy* 9, 184. <https://doi.org/10.1186/s13287-018-0936-8>.
 25. Wilson, A.J., Rand, E., Webster, A.J., and Genever, P.G. (2021). Characterisation of mesenchymal stromal cells in clinical trial reports: analysis of published descriptors. *Stem Cell Res Ther* 12, 360. <https://doi.org/10.1186/s13287-021-02435-1>.
 26. Stroncek, D.F., Jin, P., McKenna, D.H., Takanashi, M., Fontaine, M.J., Pati, S., Schafer, R., Peterson, E., Benedetti, E., and Reems, J.A. (2020). Human

- Mesenchymal Stromal Cell (MSC) Characteristics Vary Among Laboratories When Manufactured From the Same Source Material: A Report by the Cellular Therapy Team of the Biomedical Excellence for Safer Transfusion (BEST) Collaborative. *Front Cell Dev Biol* 8, 458. <https://doi.org/10.3389/fcell.2020.00458>.
27. Ballikaya, S., Sadeghi, S., Niebergall-Roth, E., Nimtz, L., Frindert, J., Norrick, A., Stemler, N., Bauer, N., Rosche, Y., Kratzenberg, V., et al. (2020). Process data of allogeneic ex vivo-expanded ABCB5+ mesenchymal stromal cells for human use: off-the-shelf GMP-manufactured donor-independent ATMP. *Stem Cell Research & Therapy* 11, 482. <https://doi.org/10.1186/s13287-020-01987-y>.
 28. Vander Beken, S., Vries, J.C., Meier-Schiesser, B., Meyer, P., Jiang, D., Sindrilaru, A., Ferreira, F.F., Hainzl, A., Schatz, S., Muschhammer, J., et al. (2019). Newly Defined ATP-Binding Cassette Subfamily B Member 5 Positive Dermal Mesenchymal Stem Cells Promote Healing of Chronic Iron-Overload Wounds via Secretion of Interleukin-1 Receptor Antagonist. *Stem Cells* 37, 1057-1074. <https://doi.org/10.1002/stem.3022>.
 29. Niebergall-Roth, E., Frank, N.Y., Ganss, C., Frank, M.H., and Kluth, M.A. (2023). Skin-Derived ABCB5+ Mesenchymal Stem Cells for High-Medical-Need Inflammatory Diseases: From Discovery to Entering Clinical Routine. *International Journal of Molecular Sciences* 24. <https://doi.org/10.3390/ijms24010066>.
 30. Riedl, J., Pickett-Leonard, M., Eide, C., Kluth, M.A., Ganss, C., Frank, N.Y., Frank, M.H., Ebens, C.L., and Tolar, J. (2021). ABCB5+ Dermal Mesenchymal Stromal Cells with Favorable Skin Homing and Local Immunomodulation for Recessive Dystrophic Epidermolysis Bullosa Treatment. *Stem Cells* 39, 897-903. <https://doi.org/10.1002/stem.3356>.
 31. Németh, K., Leelahavanichkul, A., Yuen, P.S.T., Mayer, B., Parmelee, A., Doi, K., Robey, P.G., Leelahavanichkul, K., Koller, B.H., Brown, J.M., et al. (2009). Bone marrow stromal cells attenuate sepsis via prostaglandin E2-dependent reprogramming of host macrophages to increase their interleukin-10 production. *Nature Medicine* 15, 42-49. <https://doi.org/10.1038/nm.1905>.
 32. Giri, J., Das, R., Nysten, E., Chinnadurai, R., and Galipeau, J. (2020). CCL2 and CXCL12 Derived from Mesenchymal Stromal Cells Cooperatively Polarize IL-10+ Tissue Macrophages to Mitigate Gut Injury. *Cell Reports* 30, 1923-1934.e1924. <https://doi.org/10.1016/j.celrep.2020.01.047>.
 33. Ko, J.H., Kim, H.J., Jeong, H.J., Lee, H.J., and Oh, J.Y. (2020). Mesenchymal Stem and Stromal Cells Harness Macrophage-Derived Amphiregulin to Maintain Tissue Homeostasis. *Cell Reports* 30, 3806-3820.e3806. <https://doi.org/10.1016/j.celrep.2020.02.062>.
 34. Le Blanc, K., Frasson, F., Ball, L., Locatelli, F., Roelofs, H., Roelofs, H., Lewis, I., Lanino, E., Sundberg, B., Bernardo, M.E., Remberger, M., Dini, G., et al. (2008). Mesenchymal stem cells for treatment of steroid-resistant, severe, acute graft-versus-host disease: a phase II study. *Lancet* 371, 1579–1586. [https://doi.org/10.1016/S0140-6736\(08\)60690-X](https://doi.org/10.1016/S0140-6736(08)60690-X).
 35. Reinders, M.E.J., de Fijter, J.W., Roelofs, H., Bajema, I.M., de Vries, D.K., Schaapherder, A.F., Claas, F.H.J., van Miert, P.P.M.C., Roelen, D.L., van Kooten, C., et al. (2013). Autologous Bone Marrow-Derived Mesenchymal Stromal Cells for the Treatment of Allograft Rejection After Renal

- Transplantation: Results of a Phase I Study. *STEM CELLS Translational Medicine* 2, 107-111. <https://doi.org/10.5966/sctm.2012-0114>.
36. Forbes, G.M., Sturm, M.J., Leong, R.W., Sparrow, M.P., Segarajasingam, D., Cummins, A.G., Phillips, M., and Herrmann, R.P. (2014). A phase 2 study of allogeneic mesenchymal stromal cells for luminal Crohn's disease refractory to biologic therapy. *Clin Gastroenterol Hepatol* 12, 64–71. <https://doi.org/10.1016/j.cgh.2013.06.021>.
 37. Zhou, T., Yuan, Z., Weng, J., Pei, D., Du, X., He, C., and Lai, P. (2021). Challenges and advances in clinical applications of mesenchymal stromal cells. *Journal of Hematology & Oncology* 14, 24. <https://doi.org/10.1186/s13045-021-01037-x>.
 38. Lohan, P., Treacy, O., Morcos, M., Donohoe, E., O'Donoghue, Y., Ryan, A.E., Elliman, S.J., Ritter, T., and Griffin, M.D. (2018). Interspecies Incompatibilities Limit the Immunomodulatory Effect of Human Mesenchymal Stromal Cells in the Rat. *Stem Cells* 36, 1210-1215. <https://doi.org/10.1002/stem.2840>.
 39. Su, J., Chen, X., Huang, Y., Li, W., Li, J., Cao, K., Cao, G., Zhang, L., Li, F., Roberts, A.I., et al. (2014). Phylogenetic distinction of iNOS and IDO function in mesenchymal stem cell-mediated immunosuppression in mammalian species. *Cell Death & Differentiation* 21, 388-396. <https://doi.org/10.1038/cdd.2013.149>.
 40. Peshkova, M., Korneev, A., Suleimanov, S., Vlasova, I.I., Svistunov, A., Kosheleva, N., and Timashev, P. (2023). MSCs' conditioned media cytokine and growth factor profiles and their impact on macrophage polarization. *Stem Cell Research & Therapy* 14, 142. <https://doi.org/10.1186/s13287-023-03381-w>.
 41. Ross, E.A., Devitt, A., and Johnson, J.R. (2021). Macrophages: The Good, the Bad, and the Gluttony. *Frontiers in Immunology* 12. <https://doi.org/10.3389/fimmu.2021.708186>.
 42. Baek, J.-H. (2019). The Impact of Versatile Macrophage Functions on Acute Kidney Injury and Its Outcomes. *Frontiers in Physiology* 10. <https://doi.org/10.3389/fphys.2019.01016>
 43. Huen, S.C., and Cantley, L.G. (2015). Macrophage-mediated injury and repair after ischemic kidney injury. *Pediatric nephrology* 30, 199–209. <https://doi.org/10.1007/s00467-013-2726-y>.
 44. Schulz, D., Severin, Y., Zanotelli, V.R.T., and Bodenmiller, B. (2019). In-Depth Characterization of Monocyte-Derived Macrophages using a Mass Cytometry-Based Phagocytosis Assay. *Scientific Reports* 9, 1925. <https://doi.org/10.1038/s41598-018-38127-9>.
 45. Lu, D., Xu, Y., Liu, Q., and Zhang, Q. (2021). Mesenchymal Stem Cell-Macrophage Crosstalk and Maintenance of Inflammatory Microenvironment Homeostasis. *Frontiers in Cell and Developmental Biology* 9. <https://doi.org/10.3389/fcell.2021.681171>
 46. McSweeney, K.A.-O., Gadanec, L.A.-O., Qaradakh, T., Ali, B.A.-O., Zulli, A., and Apostolopoulos, V.A.-O. (2021). Mechanisms of Cisplatin-Induced Acute Kidney Injury: Pathological Mechanisms, Pharmacological Interventions, and Genetic Mitigations. *Cancers* 13, 1572. <https://doi.org/10.3390/cancers13071572>.
 47. Miller, R.P., Tadagavadi, R.K., Ramesh, G., and Reeves, W.B. (2010). Mechanisms of Cisplatin Nephrotoxicity. *Toxins* 2, 2490-2518. <https://doi.org/10.3390/toxins2112490>.

48. Motohashi, H., and Inui, K. (2013). Organic cation transporter OCTs (SLC22) and MATEs (SLC47) in the human kidney. *The AAPS journal* 15, 581–588. <https://doi.org/10.1208/s12248-013-9465-7>.
49. Nonnekens, J., and Hoeijmakers, J.H. (2017). After surviving cancer, what about late life effects of the cure? *EMBO molecular medicine* 9, 4–6. <https://doi.org/0.15252/emmm.201607062>.
50. Oh, G.S., Kim, H.J., Shen, A., Lee, S.B., Khadka, D., Pandit, A., and So, H.S. (2014). Cisplatin-induced Kidney Dysfunction and Perspectives on Improving Treatment Strategies. *Electrolyte Blood Press* 12, 55-65. <https://doi.org/10.5049/EBP.2014.12.2.55>.
51. Safirstein, R., Miller, P., and Guttenplan, J.B. (1984). Uptake and metabolism of cisplatin by rat kidney. *Kidney International* 25, 753-758. <https://doi.org/10.1038/ki.1984.86>.
52. Lieberthal, W., Triaca, V., and Levine, J. (1996). Mechanisms of death induced by cisplatin in proximal tubular epithelial cells: apoptosis vs. necrosis. *American Journal of Physiology-Renal Physiology* 270, F700-F708. <https://doi.org/10.1152/ajprenal.1996.270.4.F700>.
53. Volarevic, V., Djokovic, B., Jankovic, M.G., Harrell, C.R., Fellabaum, C., Djonov, V., and Arsenijevic, N. (2019). Molecular mechanisms of cisplatin-induced nephrotoxicity: a balance on the knife edge between renoprotection and tumor toxicity. *Journal of Biomedical Science* 26, 25. <https://doi.org/10.1186/s12929-019-0518-9>.
54. Zhu, S., Pabla, N., Tang, C., He, L., and Dong, Z. (2015). DNA damage response in cisplatin-induced nephrotoxicity. *Arch Toxicol* 89, 2197–2205. <https://doi.org/10.1007/s00204-015-1633-3>.
55. Manohar, S., and Leung, N.A.-O. (2018). Cisplatin nephrotoxicity: a review of the literature. *Journal of Nephrology* 31, 15-25. <https://doi.org/0.1007/s40620-017-0392-z>.
56. Yan, M., Shu, S., Guo, C., Tang, C., and Dong, Z. (2018). Endoplasmic reticulum stress in ischemic and nephrotoxic acute kidney injury. *Annals of medicine* 50, 381–390. <https://doi.org/10.1080/07853890.2018.1489142>.
57. Chirino, Y.I., and Pedraza-Chaverri, J. (2009). Role of oxidative and nitrosative stress in cisplatin-induced nephrotoxicity. *Experimental and Toxicologic Pathology* 61, 223-242. <https://doi.org/10.1016/j.etp.2008.09.003>.
58. Ramesh, G., and Reeves, W.B. (2005). p38 MAP kinase inhibition ameliorates cisplatin nephrotoxicity in mice. *American Journal of Physiology-Renal Physiology* 289, F166-F174. <https://doi.org/10.1152/ajprenal.00401.2004>.
59. Soni, H., Kaminski, D., Gangaraju, R., and Adebisi, A. (2018). Cisplatin-induced oxidative stress stimulates renal Fas ligand shedding. *Renal Failure* 40, 314-322. <https://doi.org/10.1080/0886022X.2018.1456938>.
60. Sancho-Martínez, S.M., Piedrafita, F.J., Cannata-Andía, J.B., López-Novoa, J.M., and López-Hernández, F.J. (2011). Necrotic Concentrations of Cisplatin Activate the Apoptotic Machinery but Inhibit Effector Caspases and Interfere with the Execution of Apoptosis. *Toxicological Sciences* 122, 73-85. <https://doi.org/10.1093/toxsci/kfr098>.
61. Xu, Y., Ma, H., Shao, J., Wu, J., Zhou, L., Zhang, Z., Wang, Y., Huang, Z., Ren, J., Liu, S., et al. (2015). A Role for Tubular Necroptosis in Cisplatin-Induced AKI. *J Am Soc Nephrol* 26, 2647-2658. <https://doi.org/10.1681/ASN.2014080741>.

62. Zhang, J., Ye, Z.W., Tew, K.D., and Townsend, D.M. (2021). Cisplatin chemotherapy and renal function. *Adv Cancer Res* 152, 305–327. <https://doi.org/10.1016/bs.acr.2021.03.008>.
63. Zhang, B., Ramesh G Fau - Uematsu, S., Uematsu S Fau - Akira, S., Akira S Fau - Reeves, W.B., and Reeves, W.B. (2008). TLR4 signaling mediates inflammation and tissue injury in nephrotoxicity. *J Am Soc Nephrol* 19, 923-932. <https://doi.org/10.1681/ASN.2007090982>.
64. Ozkok, A., and Edelstein, C.L. (2014). Pathophysiology of Cisplatin-Induced Acute Kidney Injury. *BioMed Research International* 2014, 967826. <https://doi.org/10.1155/2014/967826>.
65. Ramesh, G., and Reeves, W.B. (2002). TNF-alpha mediates chemokine and cytokine expression and renal injury in cisplatin nephrotoxicity. *J Clin Invest* 110, 835-842. <https://doi.org/10.1172/JCI15606>.
66. Cantero-Navarro, E., Rayego-Mateos, S., Orejudo, M., Tejedor-Santamaria, L., Tejera-Muñoz, A., Sanz, A.B., Marquez-Exposito, L., Marchant, V., Santos-Sanchez, L., Egido, J., et al. (2021). Role of Macrophages and Related Cytokines in Kidney Disease. *Front Med (Lausanne)* 8, 688060. . <https://doi.org/10.3389/fmed.2021.688060>.
67. Wen, Y., Yan, H.-R., Wang, B., and Liu, B.-C. (2021). Macrophage Heterogeneity in Kidney Injury and Fibrosis. *Frontiers in Immunology* 12. <https://doi.org/10.3389/fimmu.2021.681748>
68. Liu, F., Dai, S., Feng, D., Qin, Z., Peng, X., Sakamuri, S.S.V.P., Ren, M., Huang, L., Cheng, M., Mohammad, K.E., et al. (2020). Distinct fate, dynamics and niches of renal macrophages of bone marrow or embryonic origins. *Nature Communications* 11, 2280. <https://doi.org/10.1038/s41467-020-16158-z>.
69. Nakagawa, M., Karim, M.A.-O., Izawa, T.A.-O., Kuwamura, M., and Yamate, J. (2021). Immunophenotypical Characterization of M1/M2 Macrophages and Lymphocytes in Cisplatin-Induced Rat Progressive Renal Fibrosis. *Cells* 10, 257. <https://doi.org/10.3390/cells10020257>.
70. Engel, J.E., and Chade, A.R. (2019). Macrophage polarization in chronic kidney disease: a balancing act between renal recovery and decline? *American Journal of Physiology-Renal Physiology* 317, F1409-F1413. <https://doi.org/10.1152/ajprenal.00380.2019>.
71. Cao, Q., Wang Y Fau - Harris, D.C.H., and Harris, D.C. (2013). Pathogenic and protective role of macrophages in kidney disease. *American journal of physiology. Renal physiology* 305, F3–F11. <https://doi.org/10.1152/ajprenal.00122.2013>.
72. Cao, Q., Wang, Y., and Harris, D.C. (2014). Macrophage heterogeneity, phenotypes, and roles in renal fibrosis. *Kidney international supplements* 4, 16–19. <https://doi.org/10.1038/kisup.2014.4>.
73. Furuichi, K., Wada T Fau - Iwata, Y., Iwata Y Fau - Kitagawa, K., Kitagawa K Fau - Kobayashi, K.-I., Kobayashi K Fau - Hashimoto, H., Hashimoto H Fau - Ishiwata, Y., Ishiwata Y Fau - Asano, M., Asano M Fau - Wang, H., Wang H Fau - Matsushima, K., Matsushima K Fau - Takeya, M., et al. (2003). CCR2 signaling contributes to ischemia-reperfusion injury in kidney. *Journal of the American Society of Nephrology* 14, 2503-2515. <https://doi.org/10.1097/01.ASN.0000089563.63641.A8>.
74. Li, L., Huang L Fau - Sung, S.-S.J., Sung Ss Fau - Vergis, A.L., Vergis Al Fau - Rosin, D.L., Rosin DI Fau - Rose, C.E., Jr., Rose Ce Jr Fau - Lobo, P.I., Lobo Pi Fau - Okusa, M.D., and Okusa, M.D. (2008). The chemokine receptors CCR2 and CX3CR1 mediate monocyte/macrophage trafficking in kidney ischemia-

- reperfusion injury. *Kidney International* 74, 1526-1537. <https://doi.org/10.1038/ki.2008.500>.
75. Han, H.I., Skvarca, L.B., Espiritu, E.B., Davidson, A.J., and Hukriede, N.A.-O. (2019). The role of macrophages during acute kidney injury: destruction and repair. *Pediatric nephrology* 34, 561–569. <https://doi.org/10.1007/s00467-017-3883-1>.
76. Lee, S., Huen S Fau - Nishio, H., Nishio H Fau - Nishio, S., Nishio S Fau - Lee, H.K., Lee Hk Fau - Choi, B.-S., Choi Bs Fau - Ruhrberg, C., Ruhrberg C Fau - Cantley, L.G., and Cantley, L.G. (2011). Distinct macrophage phenotypes contribute to kidney injury and repair. *Journal of the American Society of Nephrology* 22, 317–326. <https://doi.org/10.1681/ASN.2009060615>.
77. Cao, Q., Harris, D.C., and Wang, Y. (2015). Macrophages in kidney injury, inflammation, and fibrosis. *Physiology* 30, 183-194. <https://doi.org/10.1152/physiol.00046.2014>.
78. Calcat, I.C.S.A.-O., Rendra, E., Scaccia, E., Amadeo, F.A.-O., Hanson, V., Wilm, B.A.-O.X., Murray, P.A.-O.X., O'Brien, T., Taylor, A.A.-O., and Bieback, K.A.-O. (2023). Harmonised culture procedures minimise but do not eliminate mesenchymal stromal cell donor and tissue variability in a decentralised multicentre manufacturing approach. *Stem Cell Res Ther* 14. <https://doi.org/10.1186/s13287-023-03352-1>.
79. Wilmer, M.J., Saleem, M.A., Masereeuw, R., Ni, L., van der Velden, T.J., Russel, F.G., Mathieson, P.W., Monnens, L.A., van den Heuvel, L.P., and Levtchenko, E.N. (2010). Novel conditionally immortalized human proximal tubule cell line expressing functional influx and efflux transporters. *Cell and Tissue Research* 339, 449-457. <https://doi.org/10.1007/s00441-009-0882-y>.
80. Whittaker, T.E., Nagelkerke, A., Nele, V., Kauscher, U., and Stevens, M.M. (2020). Experimental artefacts can lead to misattribution of bioactivity from soluble mesenchymal stem cell paracrine factors to extracellular vesicles. *Journal of Extracellular Vesicles* 9, 1807674. <https://doi.org/10.1080/20013078.2020.1807674>.
81. Baba, S.P., and Bhatnagar, A. (2018). ROLE OF THIOLS IN OXIDATIVE STRESS. *Current opinion in toxicology* 7, 133–139. <https://doi.org/10.1016/j.cotox.2018.03.005>.
82. Ulrich, K., and Jakob, U. (2019). The role of thiols in antioxidant systems. *Free Radical Biology and Medicine* 140, 14-27. <https://doi.org/10.1016/j.freeradbiomed.2019.05.035>.
83. Ershov, D., Phan, M.-S., Pylvänäinen, J.W., Rigaud, S.U., Le Blanc, L., Charles-Orszag, A., Conway, J.R.W., Laine, R.F., Roy, N.H., Bonazzi, D., et al. (2022). TrackMate 7: integrating state-of-the-art segmentation algorithms into tracking pipelines. *Nature Methods* 19, 829-832. <https://doi.org/10.1038/s41592-022-01507-1>.
84. Zheng, X., Baker, H., Hancock, W.S., Fawaz, F., McCaman, M., and Pungor, E., Jr. (2006). Proteomic analysis for the assessment of different lots of fetal bovine serum as a raw material for cell culture. Part IV. Application of proteomics to the manufacture of biological drugs. *Biotechnol Prog* 22, 1294-1300. <https://doi.org/10.1021/bp060121o>.
85. Higuera, G., Schop, D., Janssen, F., van Dijkhuizen-Radersma, R., van Boxtel, T., and van Blitterswijk, C.A. (2009). Quantifying in vitro growth and metabolism kinetics of human mesenchymal stem cells using a mathematical model. *Tissue Eng Part A* 15, 2653-2663. <https://doi.org/10.1089/ten.TEA.2008.0328>.

86. Gowen, A., Shahjin, F., Chand, S., Odegaard, K.E., and Yelamanchili, S.V. (2020). Mesenchymal Stem Cell-Derived Extracellular Vesicles: Challenges in Clinical Applications. *Frontiers in Cell and Developmental Biology* 8. <https://doi.org/10.3389/fcell.2020.00149>.
87. Su, H., Lei, C.-T., and Zhang, C. (2017). Interleukin-6 Signaling Pathway and Its Role in Kidney Disease: An Update. *Frontiers in Immunology* 8. <https://doi.org/10.3389/fimmu.2017.00405>
88. Nechemia-Arbely, Y., Barkan D Fau - Pizov, G., Pizov G Fau - Shriki, A., Shriki A Fau - Rose-John, S., Rose-John S Fau - Galun, E., Galun E Fau - Axelrod, J.H., and Axelrod, J.H. (2008). IL-6/IL-6R axis plays a critical role in acute kidney injury. *Journal of the American Society of Nephrology* 19, 1106–1115. <https://doi.org/10.1681/ASN.2007070744>.
89. Thin Luu, N., McGettrick, H.M., Buckley, C.D., Newsome, P.N., Ed Rainger, G., Frampton, J., and Nash, G.B. (2013). Crosstalk Between Mesenchymal Stem Cells and Endothelial Cells Leads to Downregulation of Cytokine-Induced Leukocyte Recruitment. *STEM CELLS* 31, 2690-2702. <https://doi.org/10.1002/stem.1511>.
90. Taub, R. (2003). Hepatoprotection via the IL-6/Stat3 pathway. *The Journal of Clinical Investigation* 112, 978-980. <https://doi.org/10.1172/JCI19974>.
91. Roger, E., Boutin, L., and Chadjichristos, C.E. (2022). The Role of Connexin 43 in Renal Disease: Insights from In Vivo Models of Experimental Nephropathy. *International Journal of Molecular Sciences* 23. <https://doi.org/10.3390/ijms232113090>.
92. Zhang, B., Ramesh G Fau - Norbury, C.C., Norbury Cc Fau - Reeves, W.B., and Reeves, W.B. (2007). Cisplatin-induced nephrotoxicity is mediated by tumor necrosis factor-alpha produced by renal parenchymal cells. *Kidney International* 72, 37-44. <https://doi.org/10.1038/sj.ki.5002242>.
93. Dong, Z., and Atherton, S.S. (2007). Tumor necrosis factor- α in cisplatin nephrotoxicity: A homebred foe? *Kidney International* 72, 5-7. <https://doi.org/10.1038/sj.ki.5002320>.
94. Kim, D.S., Lee, M.W., Ko, Y.J., Chun, Y.H., Kim, H.J., Sung, K.W., Koo, H.H., and Yoo, K.H. (2016). Cell culture density affects the proliferation activity of human adipose tissue stem cells. *Cell Biochemistry and Function* 34, 16-24. <https://doi.org/10.1002/cbf.3158>.
95. Kim, D.S., Lee, M.W., Lee, T.H., Sung, K.W., Koo, H.H., and Yoo, K.H. (2017). Cell culture density affects the stemness gene expression of adipose tissue-derived mesenchymal stem cells. *Biomed Rep* 6, 300-306. <https://doi.org/10.3892/br.2017.845>.
96. Liu, S., de Castro, L.F., Jin, P., Civini, S., Ren, J., Reems, J.-A., Cancelas, J., Nayak, R., Shaw, G., O'Brien, T., et al. (2017). Manufacturing Differences Affect Human Bone Marrow Stromal Cell Characteristics and Function: Comparison of Production Methods and Products from Multiple Centers. *Scientific Reports* 7, 46731. <https://doi.org/10.1038/srep46731>.
97. Karagianni, M., Brinkmann, I., Kinzebach, S., Grassl, M., Weiss, C., Bugert, P., and Bieback, K. (2013). A comparative analysis of the adipogenic potential in human mesenchymal stromal cells from cord blood and other sources. *Cytotherapy* 15, 76-88. <https://doi.org/10.1016/j.jcyt.2012.11.001>.
98. Rebelatto, C.K., Aguiar, A.M., Moretao, M.P., Senegaglia, A.C., Hansen, P., Barchiki, F., Oliveira, J., Martins, J., Kuligovski, C., Mansur, F., et al. (2008). Dissimilar differentiation of mesenchymal stem cells from bone marrow,

- umbilical cord blood, and adipose tissue. *Exp Biol Med (Maywood)* 233, 901-913. <https://doi.org/10.3181/0712-RM-356>.
99. Majore, I., Moretti, P., Stahl, F., Hass, R., and Kasper, C. (2011). Growth and differentiation properties of mesenchymal stromal cell populations derived from whole human umbilical cord. *Stem Cell Rev Rep* 7, 17-31. <https://doi.org/10.1007/s12015-010-9165-y>.
 100. Grau-Vorster, M., Laitinen, A., Nystedt, J., and Vives, J. (2019). HLA-DR expression in clinical-grade bone marrow-derived multipotent mesenchymal stromal cells: a two-site study. *Stem Cell Research & Therapy* 10, 164. <https://doi.org/10.1186/s13287-019-1279-9>.
 101. Bahsoun, S., Coopman, K., and Akam, E.C. (2020). Quantitative assessment of the impact of cryopreservation on human bone marrow-derived mesenchymal stem cells: up to 24 h post-thaw and beyond. *Stem Cell Res Ther* 11, 540. <https://doi.org/10.1186/s13287-020-02054-2>.
 102. François, M., Copland, I.B., Yuan, S., Romieu-Mourez, R., Waller, E.K., and Galipeau, J. (2012). Cryopreserved mesenchymal stromal cells display impaired immunosuppressive properties as a result of heat-shock response and impaired interferon- γ licensing. *Cytherapy* 14, 147-152. <https://doi.org/10.3109/14653249.2011.623691>.
 103. Marquez-Curtis, L.A., Janowska-Wieczorek, A., McGann, L.E., and Elliott, J.A. (2015). Mesenchymal stromal cells derived from various tissues: Biological, clinical and cryopreservation aspects. *Cryobiology* 71, 181-197. <https://doi.org/10.1016/j.cryobiol.2015.07.003>.
 104. Chinnadurai, R., Copland, I.B., Patel, S.R., and Galipeau, J. (2014). IDO-independent suppression of T cell effector function by IFN- γ -licensed human mesenchymal stromal cells. *J Immunol* 192, 1491-1501. <https://doi.org/10.4049/jimmunol.1301828>.
 105. Kisselbach, L., Merges, M., Bossie, A., and Boyd, A. (2009). CD90 Expression on human primary cells and elimination of contaminating fibroblasts from cell cultures. *Cytotechnology* 59, 31-44. <https://doi.org/10.1007/s10616-009-9190-3>.
 106. Hynes, R.O. (1992). Integrins: Versatility, modulation, and signaling in cell adhesion. *Cell* 69, 11-25. [https://doi.org/10.1016/0092-8674\(92\)90115-S](https://doi.org/10.1016/0092-8674(92)90115-S).
 107. Cleary, M.A., Narcisi, R., Focke, K., van der Linden, R., Brama, P.A.J., and van Osch, G.J.V.M. (2016). Expression of CD105 on expanded mesenchymal stem cells does not predict their chondrogenic potential. *Osteoarthritis and Cartilage* 24, 868-872. <https://doi.org/10.1016/j.joca.2015.11.018>.
 108. Chen, S., Wainwright, D.A., Wu, J.D., Wan, Y., Matei, D.E., Zhang, Y., and Zhang, B. (2019). CD73: an emerging checkpoint for cancer immunotherapy. *Immunotherapy* 11, 983-997. <https://doi.org/10.2217/imt-2018-0200>.
 109. Turner, A.J. (2004). 69 - Membrane alanyl aminopeptidase. In *Handbook of Proteolytic Enzymes (Second Edition)*, A.J. Barrett, N.D. Rawlings, and J.F. Woessner, eds. (Academic Press), pp. 289-294. <https://doi.org/10.1016/B978-0-12-079611-3.50077-X>.
 110. Wynn, T.A., Chawla, A., and Pollard, J.W. (2013). Macrophage biology in development, homeostasis and disease. *Nature* 496, 445-455. <https://doi.org/10.1038/nature12034>.
 111. Mosser, D.M., Hamidzadeh, K., and Goncalves, R. (2021). Macrophages and the maintenance of homeostasis. *Cellular & Molecular Immunology* 18, 579-587. <https://doi.org/10.1038/s41423-020-00541-3>.

112. Arandjelovic, S., and Ravichandran, K.S. (2015). Phagocytosis of apoptotic cells in homeostasis. *Nature Immunology* 16, 907-917. <https://doi.org/10.1038/ni.3253>.
113. Kourtzelis, I., Hajishengallis, G., and Chavakis, T. (2020). Phagocytosis of Apoptotic Cells in Resolution of Inflammation. *Frontiers in Immunology* 11. <https://doi.org/10.3389/fimmu.2020.00553>.
114. Miyaji, T., Kato, A., Yasuda, H., Fujigaki, Y., and Hishida, A. (2001). Role of the increase in p21 in cisplatin-induced acute renal failure in rats. *Journal of the American Society of Nephrology* 12, 900–908. <https://doi.org/10.1681/ASN.V125900>.
115. Abbas, T., and Dutta, A. (2009). p21 in cancer: intricate networks and multiple activities. *Nature Reviews Cancer* 9, 400-414. <https://doi.org/10.1038/nrc2657>.
116. Liebermann, D.A., and Hoffman, B. (2008). Gadd45 in stress signaling. *Journal of molecular signaling* 3. <https://doi.org/10.1186/1750-2187-3-15>.
117. Chiang, S.-K., Chen, S.-E., and Chang, L.-C. (2021). The Role of HO-1 and Its Crosstalk with Oxidative Stress in Cancer Cell Survival. *Cells* 10. <https://doi.org/10.3390/cells10092401>.
118. Ku, H.-C., and Cheng, C.-F. (2020). Master Regulator Activating Transcription Factor 3 (ATF3) in Metabolic Homeostasis and Cancer. *Frontiers in Endocrinology* 11. <https://doi.org/10.3389/fendo.2020.00556>
119. Ramos, A.P., Sebinelli, H.G., Ciancaglini, P., Rosato, N., Mebarek, S., Buchet, R., Millán, J.L., and Bottini, M. (2022). The functional role of soluble proteins acquired by extracellular vesicles. *Journal of Extracellular Biology* 1, e34. <https://doi.org/10.1002/jex2.34>.
120. Mitazaki, S., Honma, S., Suto, M., Kato, N., Hiraiwa, K., Yoshida, M., and Abe, S. (2011). Interleukin-6 plays a protective role in development of cisplatin-induced acute renal failure through upregulation of anti-oxidative stress factors. *Life Sciences* 88, 1142-1148. <https://doi.org/10.1016/j.lfs.2011.04.016>.
121. Dorransoro, A., Lang, V., Ferrin, I., Fernández-Rueda, J., Zabaleta, L., Pérez-Ruiz, E., Sepúlveda, P., and Trigueros, C. (2020). Intracellular role of IL-6 in mesenchymal stromal cell immunosuppression and proliferation. *Scientific Reports* 10, 21853. <https://doi.org/10.1038/s41598-020-78864-4>.
122. Visser, K., van der Horn, H.J., Bourgonje, A.R., Jacobs, B., de Borst, M.H., Vos, P.E., Bulthuis, M.L.C., van Goor, H., and van der Naalt, J. (2022). Acute serum free thiols: a potentially modifiable biomarker of oxidative stress following traumatic brain injury. *Journal of Neurology* 269, 5883-5892. <https://doi.org/10.1007/s00415-022-11240-6>.
123. Abdulle, A.E., Bourgonje, A.R., Kieneker, L.M., Koning, A.M., la Bastide-van Gemert, S., Bulthuis, M.L.C., Dijkstra, G., Faber, K.N., Dullaart, R.P.F., Bakker, S.J.L., et al. (2020). Serum free thiols predict cardiovascular events and all-cause mortality in the general population: a prospective cohort study. *BMC Medicine* 18, 130. <https://doi.org/10.1186/s12916-020-01587-w>.
124. Abdulsamed, K., Volkan, G., Ömer Faruk, B., Haci Ahmet, D., and Mahmut, K. (2021). Thiols: Role in Oxidative Stress-Related Disorders. In *Accenting Lipid Peroxidation*, A. Pinar, ed. (IntechOpen), pp. Ch. 3. <https://doi.org/10.5772/intechopen.96682>.
125. Berg, T., Hegelund-Myrbäck, T., Öckinger, J., Zhou, X.-H., Brännström, M., Hagemann-Jensen, M., Werkström, V., Seidegård, J., Grunewald, J., Nord, M., and Gustavsson, L. (2018). Expression of MATE1, P-gp, OCTN1 and OCTN2, in epithelial and immune cells in the lung of COPD and healthy individuals. *Respiratory Research* 19, 68. <https://doi.org/10.1186/s12931-018-0760-9>.

126. Schoeberl, A., Gutmann, M., Theiner, S., Schaier, M., Schweikert, A., Berger, W., and Koellensperger, G. (2021). Cisplatin Uptake in Macrophage Subtypes at the Single-Cell Level by LA-ICP-TOFMS Imaging. *Analytical Chemistry* 93, 16456-16465. <https://doi.org/10.1021/acs.analchem.1c03442>.
127. Kelly, B., and O'Neill, L.A.J. (2015). Metabolic reprogramming in macrophages and dendritic cells in innate immunity. *Cell Research* 25, 771-784. <https://doi.org/10.1038/cr.2015.68>.
128. Viola, A., Munari, F., Sánchez-Rodríguez, R., Scolaro, T., and Castegna, A. (2019). The Metabolic Signature of Macrophage Responses. *Frontiers in Immunology* 10. <https://doi.org/10.3389/fimmu.2019.01462>.
129. Luque-Campos, N., Bustamante-Barrientos, F.A., Pradenas, C., García, C., Araya, M.J., Bohaud, C., Contreras-López, R., Elizondo-Vega, R., Djouad, F., Luz-Crawford, P., and Vega-Letter, A.M. (2021). The Macrophage Response Is Driven by Mesenchymal Stem Cell-Mediated Metabolic Reprogramming. *Frontiers in Immunology* 12. <https://doi.org/10.3389/fimmu.2021.624746>.
130. Kleih, M., Böpple, K., Dong, M., Gaißler, A., Heine, S., Olayioye, M.A., Aulitzky, W.E., and Essmann, F. (2019). Direct impact of cisplatin on mitochondria induces ROS production that dictates cell fate of ovarian cancer cells. *Cell Death & Disease* 10, 851. <https://doi.org/10.1038/s41419-019-2081-4>.
131. Liu, C., Xu, Y., Lu, Y., Du, P., Li, X., Wang, C., Guo, P., Diao, L., and Lu, G. (2022). Mesenchymal stromal cells pretreated with proinflammatory cytokines enhance skin wound healing via IL-6-dependent M2 polarization. *Stem Cell Research & Therapy* 13, 414. <https://doi.org/10.1186/s13287-022-02934-9>.
132. Stevens, H.Y., Bowles, A.C., Yeago, C., and Roy, K. (2020). Molecular Crosstalk Between Macrophages and Mesenchymal Stromal Cells. *Frontiers in Cell and Developmental Biology* 8. <https://doi.org/10.3389/fcell.2020.600160>.
133. Deng, Y., Zhang, Y., Ye, L., Zhang, T., Cheng, J., Chen, G., Zhang, Q., and Yang, Y. (2016). Umbilical Cord-derived Mesenchymal Stem Cells Instruct Monocytes Towards an IL10-producing Phenotype by Secreting IL6 and HGF. *Scientific Reports* 6, 37566. <https://doi.org/10.1038/srep37566>.
134. Wheeler, K.C., Jena, M.K., Pradhan, B.S., Nayak, N., Das, S., Hsu, C.-D., Wheeler, D.S., Chen, K., and Nayak, N.R. (2018). VEGF may contribute to macrophage recruitment and M2 polarization in the decidua. *PLOS ONE* 13, e0191040. <https://doi.org/10.1371/journal.pone.0191040>.
135. Leuning, D.G., Beijer, N.R.M., du Fossé, N.A., Vermeulen, S., Lievers, E., van Kooten, C., Rabelink, T.J., and Boer, J.d. (2018). The cytokine secretion profile of mesenchymal stromal cells is determined by surface structure of the microenvironment. *Scientific Reports* 8, 7716. <https://doi.org/10.1038/s41598-018-25700-5>.
136. Sampangi, S., Kassianos, A.J., Wang, X., Beagley, K.W., Klein, T., Afrin, S., Healy, H., and Wilkinson, R. (2015). The Mechanisms of Human Renal Epithelial Cell Modulation of Autologous Dendritic Cell Phenotype and Function. *PLOS ONE* 10. <https://doi.org/10.1371/journal.pone.0134688>.
137. Li, M., Xie, H., Liu, Y., Xia, C., Cun, X., Long, Y., Chen, X., Deng, M., Guo, R., Zhang, Z., and He, Q. (2019). Knockdown of hypoxia-inducible factor-1 alpha by tumor targeted delivery of CRISPR/Cas9 system suppressed the metastasis of pancreatic cancer. *Journal of Controlled Release* 304, 204-215. <https://doi.org/10.1016/j.jconrel.2019.05.019>.
138. Li, Z.-L., Lv, L.-L., Tang, T.-T., Wang, B., Feng, Y., Zhou, L.-T., Cao, J.-Y., Tang, R.-N., Wu, M., Liu, H., et al. (2019). HIF-1 α inducing exosomal microRNA-23a expression mediates the cross-talk between tubular epithelial cells and

- macrophages in tubulointerstitial inflammation. *Kidney International* 95, 388-404. <https://doi.org/10.1016/j.kint.2018.09.013>.
139. Lv, L.-L., Feng, Y., Wu, M., Wang, B., Li, Z.-L., Zhong, X., Wu, W.-J., Chen, J., Ni, H.-F., Tang, T.-T., et al. (2020). Exosomal miRNA-19b-3p of tubular epithelial cells promotes M1 macrophage activation in kidney injury. *Cell Death & Differentiation* 27, 210-226. <https://doi.org/10.1038/s41418-019-0349-y>.
140. Jia, Y., Chen, J., Zheng, Z., Tao, Y., Zhang, S., Zou, M., Yang, Y., Xue, M., Hu, F., Li, Y., et al. (2022). Tubular epithelial cell-derived extracellular vesicles induce macrophage glycolysis by stabilizing HIF-1 α in diabetic kidney disease. *Molecular Medicine* 28, 95. <https://doi.org/10.1186/s10020-022-00525-1>.
141. Lai, K.N., Leung Jc Fau - Chan, L.Y.Y., Chan Ly Fau - Guo, H., Guo H Fau - Tang, S.C.W., and Tang, S.C. (2007). Interaction between proximal tubular epithelial cells and infiltrating monocytes/T cells in the proteinuric state. *Kidney international* 71, 526–538. <https://doi.org/10.1038/sj.ki.5002091>.
142. Jin, Q.-H., Kim, H.-K., Na, J.-Y., Jin, C., and Seon, J.-K. (2022). Anti-inflammatory effects of mesenchymal stem cell-conditioned media inhibited macrophages activation in vitro. *Scientific Reports* 12, 4754. <https://doi.org/10.1038/s41598-022-08398-4>.
143. Liu, F., Qiu, H., Xue, M., Zhang, S., Zhang, X., Xu, J., Chen, J., Yang, Y., and Xie, J. (2019). MSC-secreted TGF- β regulates lipopolysaccharide-stimulated macrophage M2-like polarization via the Akt/FoxO1 pathway. *Stem Cell Research & Therapy* 10, 345. <https://doi.org/10.1186/s13287-019-1447-y>.
144. Vasandan, A.B., Jahnavi, S., Shashank, C., Prasad, P., Kumar, A., and Prasanna, S.J. (2016). Human Mesenchymal stem cells program macrophage plasticity by altering their metabolic status via a PGE2-dependent mechanism. *Scientific Reports* 6, 38308. <https://doi.org/10.1038/srep38308>.
145. Calle, P., Játiva, S., Torrico, S., Muñoz, A., García, M., Sola, A., Serra, D., Mera, P., Herrero, L., and Hotter, G. (2021). Infusion of Phagocytic Macrophages Overexpressing CPT1a Ameliorates Kidney Fibrosis in the UUO Model. *Cells* 10. <https://doi.org/10.3390/cells10071650>.
146. Nelson, P.J., Rees Aj Fau - Griffin, M.D., Griffin Md Fau - Hughes, J., Hughes J Fau - Kurts, C., Kurts C Fau - Duffield, J., and Duffield, J. (2012). The renal mononuclear phagocytic system. *Journal of the American Society of Nephrology* 23, 194–203. <https://doi.org/10.1681/ASN.2011070680>.
147. Anders, H.J., and Ryu, M. (2011). Renal microenvironments and macrophage phenotypes determine progression or resolution of renal inflammation and fibrosis. *Kidney international* 80, 915–925. <https://doi.org/10.1038/ki.2011.217>
148. Zhou, Y., Liu, S., Zhao, M., Wang, C., Li, L., Yuan, Y., Li, L., Liao, G., Bresette, W., Zhang, J., et al. (2019). Injectable extracellular vesicle-released self-assembling peptide nanofiber hydrogel as an enhanced cell-free therapy for tissue regeneration. *Journal of Controlled Release* 316, 93-104. <https://doi.org/10.1016/j.jconrel.2019.11.003>.

8 CURRICULUM VITAE

PERSONALIEN

Name und Vorname : Erika Erika

Geburtsdatum : 22nd October 1990

Geburtsort : Pati, Indonesia

Familienstand : Ledig

SCHULISCHER WERDEGANG

(2005) – (2008) **High School Certificate**
Sedes Sapientiae High School

UNIVERSITÄRER WERDEGANG

08/2008 - 10/2012	Bachelor´s Degree in Biology Bandung Institute of Technology, Indonesia
08/2015 – 10/2017	Master´s Degree in Medical, Pharmaceutical, and Drug Innovation University of Groningen, The Netherlands
02/2016 – 06/2016	Research Internship, Master´s Degree Pathology and Medical Biology Department, University Medical Center Groningen, The Netherlands Project Title: Diabetes-induced dysregulation of redox status in adipose stromal cells Supervisor: Prof. Harry van Goor and Prof. Marco Harmsen
11/2016 – 04/2017	Research Internship, Master´s Degree Institute of Transfusion Medicine and Immunology, Medical Faculty Mannheim, University of Heidelberg, Germany Project Title: Hyperglycemia-induced oxidative stress and inflammation on macrophages Supervisor: Prof. Julia Kzhyshkowska

04/2019 - Current	Promotion, Dr. sc. Hum (scientiarum humanarum) Institute of Transfusion Medicine and Immunology, Medical Faculty Mannheim, Heidelberg University. RenalToolBox International Research Training Group Thesis title: The immunomodulatory and pro-regenerative capacity of mesenchymal stromal cells and their therapeutic use for kidney disease
-------------------	--------------------------------------------------------------------------------------------------------------------------------------------------------------------------------------------------------------------------------------------------------------------------------------------------------------------------------------------------------------------------

9 SCIENTIFIC OUTPUTS

9.1 Publication

Rendra E, Uhlig S, Moskal I, Thieleman C, Klüter H, and Bieback K. Mesenchymal stromal cells-derived secretome attenuates cisplatin induced inflammation *in vitro* modifying the interplay between proximal tubular epithelial cells and macrophages. *Submitted to Stem Cell Research and Therapy*.

Rendra E, Torres-Crigna A, Daniele C, Sticht C, Cueppers M, Kluth MA, *et al.* Clinical-grade human skin-derived ABCB5+ mesenchymal stromal cells exert modulatory functions on mRNA expression in a cisplatin-induced kidney injury murine model. *Submitted to Frontiers in Immunology*.

Calcat-i-Cervera, S., **Rendra, E.**, Scaccia, E. *et al.* Harmonised culture procedures minimise but do not eliminate mesenchymal stromal cell donor and tissue variability in a decentralised multicentre manufacturing approach. *Stem Cell Res Ther* **14**, 120 (2023). <https://doi.org/10.1186/s13287-023-03352-1>.

Rendra E, Scaccia E, Bieback K. Recent advances in understanding mesenchymal stromal cells. *F1000Res.* 2020 Feb 27;9:F1000 Faculty Rev-156. doi: 10.12688/f1000research.21862.1.

Rendra E, Riabov V, Mossel DM, Sevastyanova T, Harmsen MC, Kzhyshkowska J. Reactive oxygen species (ROS) in macrophage activation and function in diabetes. *Immunobiology.* 2019;224(2):242-253. doi:10.1016/j.imbio.2018.11.010.

Yuniadi Y, Kusnadi Y, Sandhow L, **Rendra E**, *et al.* Progenitor Hematopoietic Cells Implantation Improves Functional Capacity of End Stage Coronary Artery Disease Patients with Advanced Heart Failure. *Cardiol Res Pract.* 2016;2016:3942605. doi:10.1155/2016/3942605.

9.2 Posters or Oral Presentations

September 2021	Mannheim Institute of Innate Immunoscience Retreat 2021, Mannheim <i>The role of mesenchymal stromal cells in the interaction of proximal tubular epithelial cells and macrophages in acute kidney injury</i>
November 2021	Forschungseminar-German Red Cross, Frankfurt <i>The role of mesenchymal stromal cells in the interaction of proximal tubular epithelial cells and macrophages in acute kidney injury</i>
April 2022	RenalToolBox Annual Meeting, Hybrid (Liverpool and Online) <i>The role of mesenchymal stromal cells in the interaction of proximal tubular epithelial cells and macrophages in acute kidney injury</i>
September 2022	55. Jahrestagung der Deutschen Gesellschaft für Transfusionsmedizin und Immunhämatologie e.V. (DGTI), Mannheim

	<i>The role of mesenchymal stromal cells in the interaction of proximal tubular epithelial cells and macrophages in acute kidney injury</i>
--	---------------------------------------------------------------------------------------------------------------------------------------------

10 ACKNOWLEDGEMENTS

I am filled with deep gratitude as I begin to express my heartfelt thanks to all the remarkable individuals who have contributed to the success of my research journey. Their unwavering support and dedication have been instrumental in shaping the outcomes of this project.

First and foremost, I extend my sincere appreciation to my supervisor, Prof. Karen Bieback, for her invaluable guidance, expertise, and unwavering support throughout this project. Her insights and dedication have played a pivotal role in shaping my research journey.

I would like to acknowledge the exceptional collaboration and cooperation of Eleonora Scaccia, especially throughout the RenalToolBox projects. I wish you all the best for her remaining experiments and the rest of your PhD.

I am immensely grateful to Stefanie Uhlig, who has been a steadfast source of support even through my most challenging days at the lab. Working alongside such a talented and passionate individual, often referred to as the "Mother of FACS," has been a privilege for us all. I will also always cherish the time we spent together inside and outside of lab.

To Isabell Moskal, I extend a heartfelt thank you for your valuable help, particularly towards the end of my PhD. Your presence in our lab has been a delightful addition, and I have thoroughly enjoyed spending time with you.

I would also like to express my gratitude to Corinna Thieleman for her support in establishing the protocol for confocal microscopy, and to Susanne Elvers-Hornung for her unwavering moral and technical support throughout my PhD.

A special word of thanks goes out to H el ene, Yen, and Clemens for their support and the enjoyable chats we've had. Additionally, I extend my appreciation to former lab members, Agnese Fiori and Adriana Torres-Crigna, for their guidance in getting started on my PhD and navigating the lab.

I am equally thankful to all the staff members, technicians, and researchers outside our research group who have provided invaluable support and assistance throughout this project. Vladimir Riabov's expertise in immunology and critical thinking have been a constant source of inspiration for me. I am grateful for Bhavin Shah's technical assistance with confocal microscopy and the support of Sandra Kühn, Silke Worwald, Qi Gao, and Ina Schäfer in immunofluorescence and image analysis. My appreciation also goes to Victor Costina for his support with the LUMINEX assay and to Nadine Dietrich and Prof. Benito Yard for providing us with the animal material and a quick course on kidney transplantation. I thank Christina Schmutemeier for her kind assistance in managing the lab.

I must also acknowledge the exceptional collaboration and camaraderie within the RenalToolBox community. My gratitude extends to all the fellows and principal investigators for their extraordinary work and cooperation. It was an honor to be part of this ITN. Special thanks to Arthur Taylor, Prof. Patricia Murray, and Prof. Timothy O'Brien for their administrative and consultative support, especially during the interlab comparison study. I am also thankful to Prof. dr. R. Masereeuw and João Faria for sharing their expertise in the development of our injury model.

My heartfelt thanks to Prof. Harry van Goor and Prof. Marco Harmsen for not only sharing their knowledge but also for their kind encouragement and motivation. To Marije Mossel, thank you for encouraging me to pursue this PhD and for standing by my side through thick and thin. I am grateful to Sabrina Soares for her advice and unwavering support, which has been a constant source of inspiration.

I would like to extend my gratitude to Irene Lazaro Garces and Silvina Romero for their authentic selves. Thank you for always showing up, providing cheerful spirits, and engaging in deep late-night conversations, no matter how random they might be. Muchas gracias!

To Sophia, your kindness and support have meant the world to me, and I will cherish the time we have spent together. To Janggeum Ming, Jia, Andy, Bianca, Helene,

Thomas, Francesco, Sara, Wei, and Diego, thank you for welcoming me to the group and making every moment enjoyable.

I would also like to acknowledge the influence of my late father, who inspired me to venture into the world and step out of my comfort zone. His memory will forever be close to my heart. Special gratitude goes to my mother for her constant support and dedication throughout my life. To my brother, sister-in-law, niece, and aunt-in-law, thank you for your encouragement and understanding during my PhD journey.

Lastly, I am indebted to my partner, Alexandru Visan, for his unwavering encouragement and understanding throughout this PhD journey. Thank you for holding a safe space for me when I need it and for believing in me when I could not. I am deeply grateful that we have grown together through this experience.

To all the staff members, technicians, and researchers whom I may have unintentionally missed mentioning, your contributions, no matter how big or small, have played a crucial role in the completion of my research. Your involvement and dedication have shaped the outcomes of this study, and I am truly grateful for the opportunity to work alongside such talented individuals.

Furthermore, I would like to acknowledge the support and resources provided by the institution and funding agencies that have made this research possible. Their investment in regenerative medicine research has paved the way for groundbreaking discoveries and advancements in the field.

Once again, thank you all for your unwavering support and commitment.

Yours sincerely,

Erika